UNIVERSITY OF SÃO PAULO
POLYTECHNIC SCHOOL

DOUGLAS JOSÉ DO BONFIM

Transient model based lap time simulation of a race car

São Paulo

2023

DOUGLAS JOSÉ DO BONFIM

Transient model based lap time simulation of a race car

Graduation work presented to the Escola Politécnica of the University of São Paulo for obtaining the degree of Mechanical Engineer

Advisor: Prof. Dr. Roberto Spinola Barbosa

São Paulo

2023

Catalogação-na-publicação

Bonfim, Douglas
Transient model based lap time simulation of a race car / D. Bonfim -- São Paulo, 101.
p.

Trabalho de Formatura - Escola Politécnica da Universidade de São Paulo. Departamento de Engenharia Mecânica.

1.VEÍCULOS DE CORRIDA 2.DINÂMICA VEICULAR 3.CONTROLE PREDITIVO 4.CONTROLE ÓTIMO 5.AUTOMOBILISMO I.Universidade de São Paulo. Escola Politécnica. Departamento de Engenharia Mecânica II.t.

ACKNOWLEDGEMENTS

To my family, who have supported and cheered for me throughout my entire life, and who have provided me with every asset to make a positive impact in the world.

To my partner, who has always stood by my side in every moment and continues to inspire me, filling me with excitement for the future.

To the friends I have made along the graduation journey, who have brightened my days and helped create the most cherished memories during my university years.

Thanks.

ABSTRACT

BONFIM, D. J. **Transient-model based lap time simulation of a race car**. 2023. 126p. Monografia (Trabalho de Conclusão de Curso) - Polytechnic School, Universidade de São Paulo, São Paulo, 2023.

Through the meticulous development and implementation of the software, incorporating a sophisticated 14-degree-of-freedom transient model of a race car and a nonlinear model predictive controller, this thesis presents a novel approach to the lap time simulation problem. By comprehensively analyzing vehicle performance and trajectory optimization, it offers valuable insights for achieving a more precise and efficient solution.

The research utilizes a comprehensive model that incorporates vital dynamics such as suspension, tire behavior, aerodynamics, and drivetrain. This intricate model facilitates a detailed understanding of the vehicle's capabilities and limitations, allowing for the estimation of the race car's performance envelope across a wide range of speeds.

To optimize the race car's trajectory, a nonlinear model-predictive controller is employed. This controller engages in an iterative optimization process, refining the trajectory for a complete lap around the race track. The primary objective is to achieve the minimum lap time by dynamically adjusting parameters such as longitudinal and lateral acceleration time histories.

Through the simulation of three distinct vehicle configurations across two varied tracks, a comprehensive analysis of the race car's performance and behavior is conducted. The study explores the effects of different vehicle setups on lap times, handling characteristics, and overall performance, providing insights into the intricate relationship between vehicle configuration, track features, and relative race performance.

The author highlights potential areas for advancement, including adimensionalization of the model, parallelization of the solution process, and the implementation of techniques for quick differentiation of the cost, objective, and state functions.

Keywords:. Race car. Vehicle dynamics. Model predictive control. Optimal control. Motorsport.

RESUMO

BONFIM, D. J. **Simulação de tempo de volta baseada no modelo transitório de um veículo de corrida**. 2023. 126p. Monograph (Conclusion Course Paper) - Polytechnic School, Universidade de São Paulo, São Paulo, 2023.

Através de um cuidadoso desenvolvimento e implementação de software, utilizando um sofisticado modelo transiente de 14 graus de liberdade de um carro de corrida e um controlador preditivo de modelo não linear, esta tese apresenta uma abordagem inovadora para a simulação do tempo de volta. Ao analisar de forma abrangente o desempenho do veículo e a otimização da trajetória, este estudo proporciona percepções valiosas para a obtenção de uma solução mais precisa e eficiente.

A pesquisa utiliza um modelo abrangente que incorpora dinâmicas vitais, como suspensão, comportamento dos pneus, aerodinâmica e trens de força. Esse modelo intricado possibilita uma compreensão detalhada das capacidades e limitações do veículo, permitindo a estimativa do envelope de desempenho do carro de corrida em uma ampla faixa de velocidades.

Para otimizar a trajetória do carro de corrida, um controlador não linear preditivo baseado em modelo é utilizado. Esse controlador é utilizado em um processo de otimização iterativa, refinando a trajetória para uma volta completa na pista de corrida. O objetivo principal é alcançar o tempo de volta mínimo, ajustando dinamicamente parâmetros como aceleração longitudinal e lateral ao longo do tempo.

Por meio da simulação de três configurações distintas de veículos em duas pistas diferentes, uma análise abrangente do desempenho e comportamento do carro de corrida é conduzida. O estudo explora os efeitos de diferentes configurações de veículos nos tempos de volta, características de manuseio e desempenho geral, fornecendo dados sobre a relação intrincada entre configuração do veículo, características da pista e desempenho relativo em corrida.

O autor destaca áreas potenciais de avanço, incluindo a adimensionalização do modelo, a paralelização do processo de solução e a implementação de técnicas para rápida diferenciação das funções de custo, objetivo e estado.

Palavras-chave:. Veículos de corrida. Dinâmica veicular. Controle preditivo. Controle ótimo. Automobilismo.

LIST OF FIGURES

LIST OF TABLES

CONTENTS

1 INTRODUCTION

1.1 Background and motivation

The maximization of vehicle performance is a fundamental objective in the field of automotive engineering. In this context, lap time simulation software plays a crucial role by providing a virtual environment to evaluate and enhance the performance of vehicles on racetracks. By aiding in the prediction of lap times and providing performance metrics, such software can assist in the design and development of high-performance vehicles, leading to improved competitiveness in motorsports and an enhanced understanding of a vehicle's characteristics in real-world scenarios.

The motivation behind this research stems from the continuous quest for better lap time simulation software based on transient vehicle modeling. While existing software solutions have made significant strides in simulating vehicle dynamics, they still suffer from limitations that can affect their accuracy, effectiveness, and practicality. This thesis aims to address these limitations and contribute to the development of advanced lap time simulation software that can better replicate the complexities of real-world racing scenarios.

1.2 Problem statement and objectives

The problem statement for this research revolves around the need for improved transient vehicle modeling techniques, trajectory optimization algorithms, and path-following controllers within lap time simulation software. By developing a comprehensive and integrated framework, the work seeks to create a software solution that can accurately capture the dynamic behavior of vehicles, optimize trajectory planning, and enable precise path following during the simulation of a vehicle traveling on a racetrack.

Based on that, the primary objectives of this thesis are twofold. First, to develop a transient vehicle model that can reliably replicate the intricate dynamics of a racing vehicle. This model will take into account various factors such as tire behavior, suspension characteristics, and aerodynamic forces to create a highly realistic representation of vehicle performance. Second, to design and implement a trajectory optimization algorithm combined with a path-following controller to optimize vehicle paths and enhance lap times within the simulation environment. This integrated approach will enable the exploration of the impact of different parameters and strategies on lap times and overall performance.

1.3 Research contributions and scope

The research contributions of this thesis lie in the development and integration of a comprehensive lap time simulation software framework based on a transient vehicle model. By addressing the limitations of existing software solutions, the work aims to provide a more accurate and realistic simulation environment for vehicle performance evaluation. The results of this research can not only benefit professionals in the motorsports industry but also have broader applications in automotive engineering, enabling more efficient vehicle design, optimization of control systems, and improved safety measures. In addition to that, the results of this work can serve as a base for the development of autonomous racing vehicles.

The scope of this thesis encompasses the theoretical development and implementation of the lap time simulation software framework based on transient vehicle modeling techniques. The research will involve the generation of the transient vehicle model, the establishment of performance envelope generation methods, the development of a nonlinear model predictive trajectory optimization algorithm, and its integration in a path-following controller. Where possible proposed implementations will be evaluated using real-world data and benchmarked against existing real-world data.

In summary, this thesis aims to advance the field of lap time simulation software by developing a comprehensive framework based on a transient vehicle model. By addressing the limitations of existing solutions and integrating advanced techniques, striving to provide a powerful tool for optimizing vehicle performance and enhancing the overall vehicle development process.

2 LITERATURE REVIEW

This section provides a comprehensive overview of lap time simulation and vehicle modeling, offering insights into the existing methodologies, techniques, and limitations in this field. By critically examining the current body of knowledge, the section lays the foundation for the development of the current work. Through an analysis of transient vehicle modeling techniques and lap time simulation algorithms, this literature review aims to identify the research *status quo* and set the knowledge basis for the subsequent sections of this thesis.

2.1 Vehicle modeling methods

The first requirement for a lap time simulation tool is the definition of the vehicle model that is to be used, as it provides a physical and mathematical representation of the vehicle's behavior. Therefore, the choice of the used model requires compromises between accuracy and computational cost, realism and simplicity, and generalization and specificity, among other considerations. Finding the right balance is crucial to develop effective models that accurately represent vehicle motion while being practical and usable in real-world scenarios.

2.1.1 The Quarter-car model

The quarter-car vehicle model is a simplified representation of a vehicle's suspension system that focuses on one corner or quarter of the vehicle. It provides a useful framework for analyzing the dynamic behavior of the suspension and its interaction with the road surface. This model is widely used in various applications related to vehicle dynamics and suspension design [1].

The model consists of two main components: the sprung mass and the unsprung mass. The sprung mass represents the vehicle's body and occupants, while the unsprung mass represents the mass of the wheels, tires, and other components directly connected to the suspension. The two masses are connected through springs and dampers, which represent the compliance and damping characteristics of the suspension system.

Figure 1 – Schematics of quarter car model

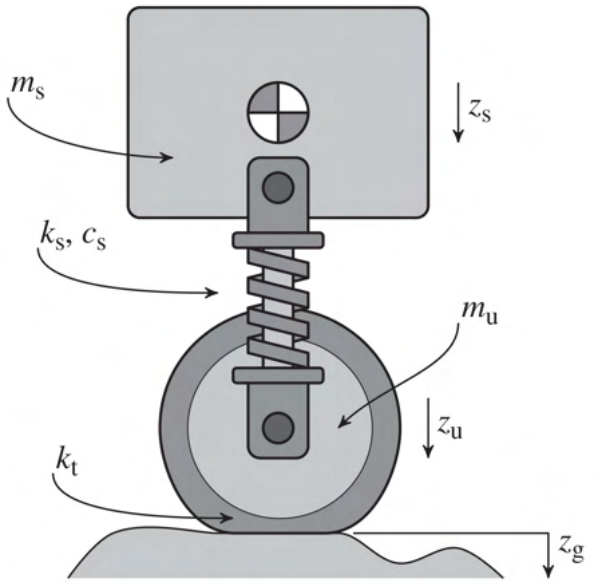

Source: Adapted from [2]

One of the primary applications of the quarter-car model is the analysis of ride comfort. By simulating the response of the sprung mass to road disturbances, engineers can evaluate the effectiveness of the suspension system in isolating occupants from vibrations and impacts. This analysis helps in optimizing suspension parameters, such as spring stiffness and damping coefficients, to achieve a smoother and more comfortable ride or, in case of race vehicles, provide a stable platform for optimal functioning of the aerodynamic package.

The quarter-car model is also instrumental in suspension design and optimization. It allows the assessment of the effects of different suspension parameters and configurations on the vehicle's performance, including ride comfort, handling, and tire contact patch. This information is valuable for selecting appropriate spring and damper rates, optimizing suspension geometry, and tuning the overall suspension setup.

Furthermore, the quarter-car model can serve as a foundation for developing active suspension control systems. By integrating control algorithms and sensors into the model, engineers can design strategies to adaptively adjust suspension parameters in real-time, based on road conditions and driver inputs. Active suspension control systems represent a useful tool to improve ride comfort, handling, and stability by continuously optimizing suspension behavior, depending on the current conditions.

2.1.2 Half-car models

The half-car models, often referred to as the bicycle models, which can be traced back to 1940, stand as one of the earliest and most basic vehicle dynamics models and continues to be utilized in contemporary times [3–5]. Olley's contributions played a crucial role in establishing the fundamentals of modern vehicle dynamics, shedding light on essential aspects like understeer and oversteer tendencies [6]. Segel put forth one of the initial vehicle models for time domain analysis, while McRuer and Klein further delved into frequency domain response during the 1970s [7, 8].

Figure 2 – The bicycle model

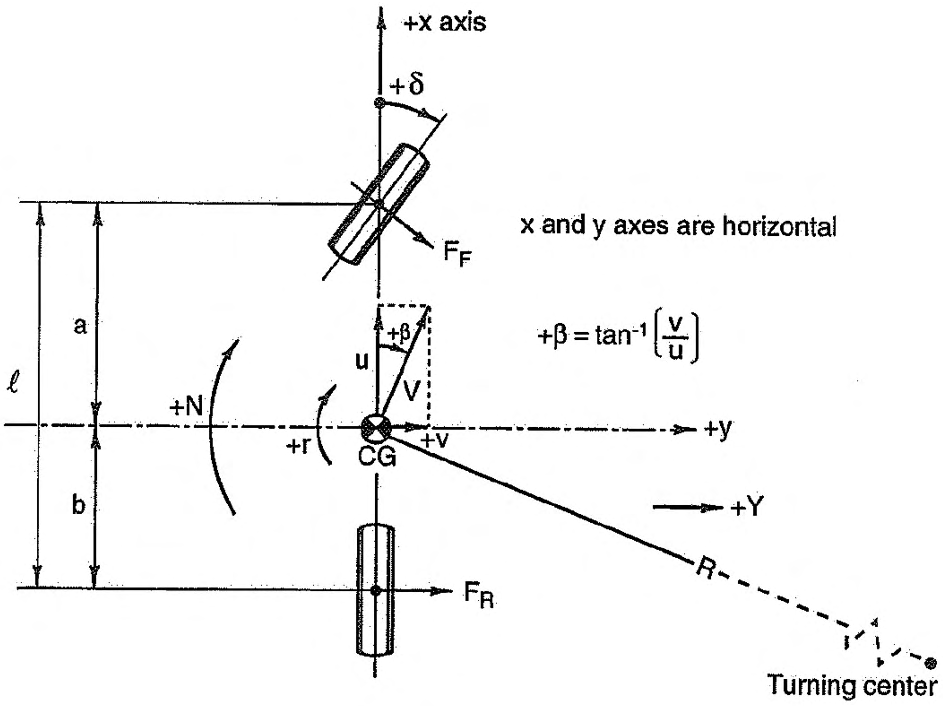

Source: Adapted from [9].

In this model, illustrated in Figure 2, the vehicle is represented as a rigid body linking a front and a rear tire, which simplifies the analysis by ignoring the vehicle's body roll and pitch. The model assumes that the vehicle moves in a plane and considers two main degrees of freedom: lateral motion and yaw motion. The lateral motion refers to the movement of the vehicle perpendicular to its longitudinal axis, and it is described by the lateral position, lateral velocity, and lateral acceleration. Yaw motion, on the other hand, refers to the rotation of the vehicle around its vertical axis and is described by the yaw angle, the yaw rate, and yaw acceleration.

To simulate the dynamics of the bicycle model, various assumptions are made, including:

- No lateral load transfer;
- No longitudinal load transfer;
- No rolling and pitching motions of the body;
- Tires operating in the linear range;
- Constant forward velocity;
- No aerodynamic effects;
- The vehicle is a rigid body, without chassis or suspension compliance effects.

For this model, the input is the front wheel steering angle and the state variables are the yaw angle, the yaw rate, the lateral position, and the lateral velocity of the vehicle. Thereby representing a fourth-order dynamic model.

The single-track model is often linearized to serve as a basis for the linear analysis of a vehicle. In these studies, the linearization process approximates the nonlinear equations of motion using linear equations, which present useful approximations when small angles are considered (for example, at 10°, $\cos\theta \approx 1$ presents only about 2% approximation error). The resulting linearized model is typically represented in state-space form, with state variables and control inputs. The linear stability analysis involves examining the eigenvalues of the system's state-space model. By analyzing these eigenvalues and associated modes, the system's response to small disturbances can be understood.

The linear bicycle model is also used to assess handling qualities and design control strategies. Eigenvalue analysis helps evaluate the response to control inputs, such as rider steering commands, and understand their impact on stability and maneuverability. Based on that, control techniques like PID control, model predictive control (MPC), or linear quadratic regulation (LQR) can be applied to regulate system states and achieve desired stability and performance objectives.

Depending on the desired complexity, the model can be further expanded to include nonlinear tire dynamics, and even to consider the longitudinal motion of the vehicle as a third degree of freedom, in such a way that powertrain and aerodynamic-generated forces can be considered.

2.1.3 The dual-track model

Dual track models, also known as four-wheel models, provide a more comprehensive representation of a vehicle by considering individual forces and motions for all four wheels. These models normally include the effects of vehicle roll, pitch, and vertical motions, as well as tire dynamics and suspension characteristics. Dual-track models are commonly used

for analyzing vehicle handling, stability, and ride comfort. They are particularly valuable in studying vehicle response during aggressive maneuvers and even off-road conditions. The most common twin-track model, and the one that will be further explained, is the 14 Degree-of-Freedom (14-DoF) [10, 11].

Figure 3 – Schematics of 14-DOF full vehicle test model

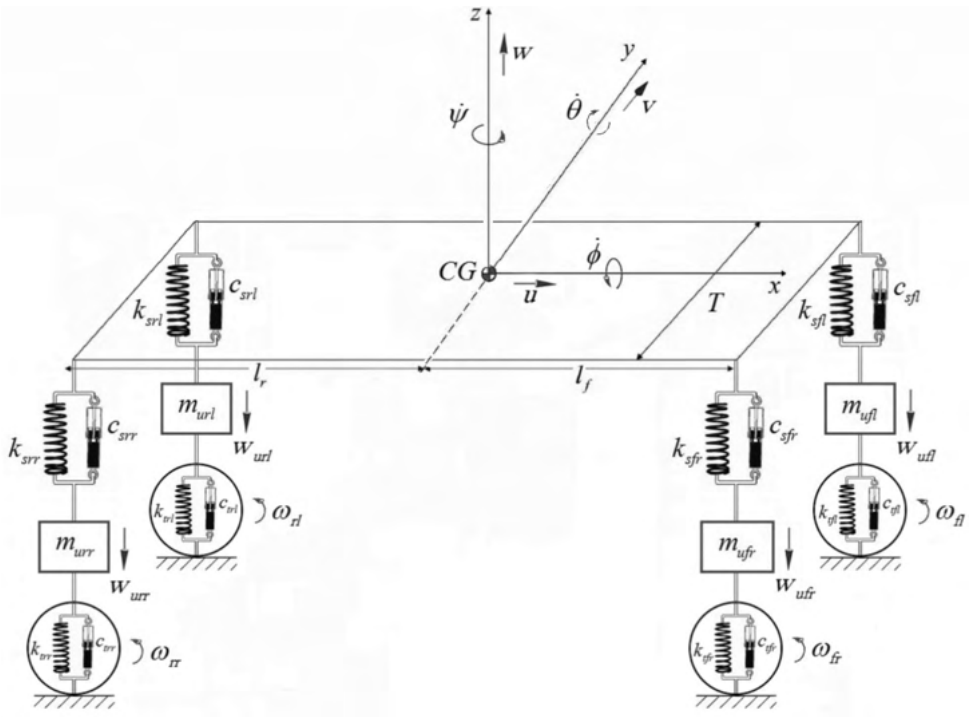

Source: Adapted from [12].

In this model, illustrated in Figure 3, the vehicle is represented as a rigid body suspended at each of its corners by a spring-damper assembly, which links the body to a wheel-tire assembly interacting with the ground. The model assumes fourteen degrees of freedom:

- The longitudinal, lateral, and vertical coordinates of the vehicle's center of gravity in the inertial coordinate system;
- The pitch, roll, and yaw angles of the body in the inertial coordinate system;
- The rotation angle of each wheel about its rotational axis;
- The vertical displacement of each wheel in the vehicle coordinate system.

To simulate the dynamics of such a model, various assumptions are commonly made, including:

- The vehicle is a rigid body, without chassis compliance effects;

- The suspension system exhibits linear spring and damping behavior;
- Complex tire dynamics, such as transient effects are neglected;
- The suspension presents a constant geometry, neglecting changes in camber angle, toe angle, or roll center height due to suspension deflections;
- Detailed powertrain dynamics, such as engine and transmission behavior, are not modeled.

For this model, the inputs are often the steering angle, the accelerator and brake positions, and the state variables are the previously mentioned positions and their time derivatives, thereby representing a twenty-eighth-order dynamic model. Depending on the desired complexity, the model can be further expanded to include nonlinear, transient tire dynamics, consider powertrain dynamics, and even suspension kinematics. The model also serves as a useful tool to perform analysis and development of more complex vehicle control systems such as electronic brake distribution (EBD), traction control system (TCS), and electronic stability control (ESC).

2.1.4 Multibody models

Multibody models offer a comprehensive depiction of a vehicle's mechanical system, accounting for the dynamics of individual components. These models employ rigid or flexible body dynamics and effectively capture the intricate interactions and interconnections between various subsystems by applying classical mechanics equations to each body and solving them collectively. Their wide-ranging applications include the study of vehicle dynamics in areas such as handling, ride comfort, durability, and real-time simulations.

The utilization of computer packages in multibody vehicle simulations enables the analysis and resolution of large problems within multibody systems. These simulations possess the versatility, extending beyond the realm of vehicle dynamics to various engineering industries. In the automotive sector, Hexagon ADAMS (former MSC ADAMS) serves as a commonly utilized software package for simulating subsystems and entire vehicles. It excels in addressing large amplitude non-linear vibration problems such as powertrain isolation and driveline oscillations [13, 14].

A comprehensive multibody model employed for vehicle simulation typically encompasses components such as the body, subframes, suspension arms, struts, anti-roll bars, steering system, engine, drivetrain, and tires.

The primary analysis code of multibody simulation software integrates programs designed for three-dimensional kinematic, static, quasi-static, or dynamic analysis of mechanical systems. These programs function as the fundamental solver, in such a way

that once a model is defined, the core solver automatically assembles and solves the equations of motion.

Figure 4 – Schematics of a multibody model of a suspension

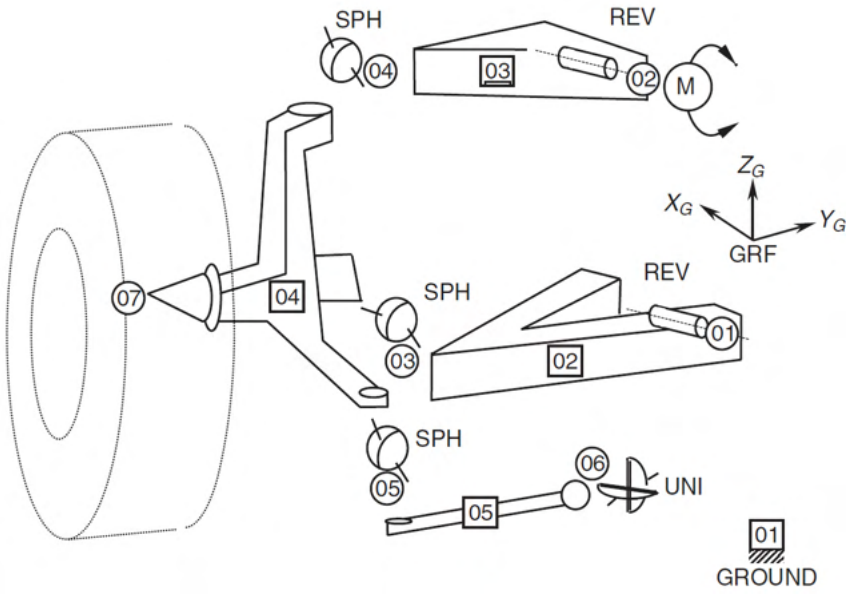

Source: [15]

Note: When used in the rigid body context, the multibody model is essentially a set of rigid bodies linked at specific points through joints that provide the forces that dictate their movement

Despite their higher representativeness, these simulations involve complex computations and require expertise, making them computationally demanding. Numerical representations used in these simulations may introduce inaccuracies, particularly in modeling complex behaviors. Validating and verifying multibody models can be challenging and time-consuming, requiring comparisons with real-world data. Parameter sensitivity and uncertainty in input parameters can affect simulation results, necessitating careful parameter identification and sensitivity analysis.

2.1.5 Use of vehicle models in motorsport

In the context of motorsport, the use of vehicle models in vehicle dynamics analysis and control is highly relevant for improving the performance and handling of racing vehicles. The following exemplifies how these models are applied in the motorsport domain:

1. Performance optimization: by understanding and predicting the dynamic behavior of the racing car. By simulating the vehicle's response to different inputs, such as steering, throttle, and braking, engineers can fine-tune the vehicle setup, suspension parameters, and aerodynamics to maximize performance on the track [16, 17].

2. Vehicle handling and stability: Understanding and improving vehicle handling and stability are crucial in motorsport. These models enable an analysis of the vehicle's stability characteristics, such as yaw stability and response to lateral forces. By examining the eigenvalues and modes of the linearized models, engineers can assess the stability of the vehicle and develop control strategies to enhance its handling qualities, responsiveness, and driver confidence [9, 18, 19].

3. Control system design: the models aid in the design and development of control systems for motorsport vehicles. Control strategies —such as traction control, stability control, and active suspension —can be designed and optimized using the presented models [20].

4. Driver-in-the-loop simulations: providing the integration of driver-in-the-loop (DIL) simulators, which are essential tools for driver training, vehicle development, and race strategy evaluation. With a realistic representation of the vehicle's dynamics, these techniques allow drivers to experience and provide feedback on the vehicle's behavior in a virtual racing environment. This enables iterative development and fine-tuning of vehicle setups and control strategies [21].

5. Race strategy and performance analysis: combined with vehicle performance data, the modeling techniques can be used to analyze and optimize race strategies. By simulating different scenarios, engineers can evaluate the impact of various factors, such as tire wear, fuel consumption, and pit stop timing, on the overall race performance. This analysis helps teams make informed decisions regarding tire choice, fuel load, and race tactics to maximize their chances of success [22, 23].

By leveraging vehicle models in the context of motorsport, teams, and engineers can gain valuable insights into vehicle dynamics, optimize vehicle performance, improve handling and stability, design effective control systems, and make informed decisions during races. These models contribute to enhancing both the speed and safety aspects of motorsport competition.

2.2 Lap time simulation techniques

One valuable use of vehicle dynamics modeling is lap time simulation software, which involves the mathematical modeling and analysis of various factors that influence a vehicle's performance on the track, allowing teams to assess different strategies and make informed decisions.

The utilization of lap time simulation techniques in motorsport is not limited to Formula 1 or professional racing; it extends to other levels of competition and even to the development of road cars. Simulations enable teams to assess the impact of design

changes, test different configurations, and fine-tune vehicle setups in a cost-effective and controlled environment before taking to the track [24].

2.2.1 Deterministic vs. probabilistic approach

One form of categorization of the lap time simulation in motorsport engineering is the deterministic approach as opposed to the probabilistic approach.

The deterministic approach is a method that considers the vehicle's physical characteristics, such as weight, aerodynamics, suspension setup, and tire behavior, along with track-specific data like layout, surface conditions, and elevation changes. By utilizing mathematical equations and algorithms, the deterministic approach predicts the vehicle's performance and lap times under different scenarios, such as varying speeds, cornering forces, and braking points. It enables teams to evaluate the impact of changes in vehicle setup or track conditions on lap times, aiding in the optimization of performance [25–27].

On the other hand, the probabilistic approach acknowledges the inherent uncertainties and variations in racing environments. It incorporates probabilistic models, statistical analysis, and Monte Carlo simulations to account for the variability of factors such as tire grip, aerodynamic performance, and driver behavior. By generating a distribution of possible lap times with associated probabilities, the probabilistic approach provides a more comprehensive understanding of lap time performance under different scenarios [28–30].

Advancements in simulation technology have led to the development of sophisticated lap time simulators that combine both deterministic and probabilistic approaches. These simulators leverage high-performance computing capabilities to rapidly iterate through numerous scenarios, considering various factors simultaneously. They provide valuable insights into vehicle setup optimization, tire management strategies, fuel consumption analysis, and race strategy planning [31].

2.2.2 Quasi-static vs. transient solving algorithms

The present thesis focuses on a deterministic approach based on a specific model considering specified inputs and assumptions. Based on that, it is worth presenting a categorization method inside the bracket of deterministic approaches: the division between quasi-static and transient solving algorithms. These algorithms play a crucial role in solving the equations of motion within the lap time simulation framework.

The quasi-static model-solving algorithms are designed to analyze vehicle behavior under steady-state conditions. They assume that the vehicle's dynamics can be approximated as a series of static equilibrium states throughout the lap. This approximation simplifies the calculations by neglecting the time-varying effects during acceleration, deceleration, and cornering. Quasi-static algorithms are very accurate in scenarios where the

vehicle is in a relatively stable state, such as straight-line acceleration or constant-speed sections while being less accurate for highly-dynamic maneuvers [23, 31, 32].

On the other hand, transient model-solving algorithms capture the dynamic nature of the vehicle's behavior throughout the lap. They take into account the time-varying effects of acceleration, deceleration, and cornering, providing a more accurate representation of the vehicle's response during the lap. Transient algorithms are essential when the lap time simulation involves complex maneuvers, such as cornering, braking, or change of direction, where the vehicle's dynamics change rapidly.

2.2.3 Fixed trajectory vs. optimal trajectory

Another categorization is the method used to determine the trajectory taken by the vehicle on the track. Two common approaches are the use of a fixed trajectory or the use of an optimization algorithm to find the optimal trajectory.

The fixed trajectory approach involves specifying a predetermined path for the vehicle to follow during the lap. This path is typically based on track data, such as the racing line or a reference trajectory. The fixed trajectory is used as a basis for the lap time simulation, and various vehicle parameters and inputs are applied to evaluate the performance along that specific path. This approach provides a straightforward and consistent method for analyzing lap times [32, 33].

On the other hand, the optimization algorithm approach aims to find the optimal trajectory that minimizes the lap time by adjusting vehicle inputs. In this approach, the simulation is run iteratively, and the optimization algorithm explores different combinations of inputs, such as throttle, braking, and steering to find the most efficient path. The algorithm acts to minimize lap time based on predefined optimization criteria, such as minimum energy consumption or minimum lap time. This approach allows for fine-tuning and optimization of vehicle performance to achieve the best possible lap time according to the cost function of optimization [34, 35].

Both approaches have their advantages and applications. The fixed trajectory approach is simpler to implement and provides consistent results for comparative analysis. It is useful for assessing the impact of specific vehicle parameters or conducting sensitivity analyses. On the other hand, the optimization algorithm approach offers the potential for finding more optimal solutions by dynamically adjusting vehicle inputs. It allows for fine-grained optimization and can identify non-intuitive strategies that may lead to improved lap times.

The choice between these approaches depends on the specific goals of the lap time simulation and the available resources. The fixed trajectory approach is suitable for initial assessments and comparative analysis, while the optimization algorithm approach is more

suitable for in-depth optimization and exploring the performance limits of the vehicle.

2.2.4 Commercial lap time simulation software and their limitations

Commercially available lap time simulation tools offer powerful features and capabilities for optimizing performance on the track. Some notable examples include OptimumLap, rFactor Pro, ChassisSim, OpenLapSim, and AVL VSM Race [36–39].

These tools excel in providing a comprehensive analysis of vehicle dynamics, race strategy, and optimization. They allow users to accurately predict lap times under various conditions and fine-tune parameters for optimal performance. With advanced mathematical models, optimization algorithms, and high-fidelity simulations, these tools empower teams and enthusiasts to make data-driven decisions to improve lap times.

While these lap time simulation tools provide significant strengths in lap time optimization, it's important to consider their limitations. Users may need expertise to fully utilize their capabilities and validation and calibration processes are crucial for accurate results. Some tools may require significant computational resources, and complex simulations may result in longer processing times. Additionally, users should evaluate the specific features and capabilities of each tool to ensure they align with their specific needs and requirements. It is worth noting that, in general, these simulation tools may function as black-box systems, limiting the user's access to the underlying models and algorithms, which can limit the versatility of a team to certain detailed studies.

2.2.5 Literature gap addressed by the present thesis

While some existing literature may have briefly touched upon certain aspects of the speed-dependent performance envelope concept, they have not extensively delved into its detailed implementation and integration within the transient vehicle model.[40, 41] The present research aims to bridge this gap by presenting a comprehensive and thoroughly documented approach that explicitly considers the impact of speed on various performance parameters. This includes tire characteristics, such as grip levels and temperature sensitivity, as well as the dynamic behavior of the suspension system and the aerodynamic forces acting on the vehicle.

By offering a more detailed and nuanced understanding of the speed-dependent performance envelope, this thesis contributes to the advancement of lap time simulation software. This knowledge can be leveraged to enhance vehicle performance optimization strategies, aid in the design and development of high-performance vehicles, and improve competitiveness in motorsports. Furthermore, by addressing this research gap, the work opens up new avenues for further exploration and encourages future researchers to build upon and refine its findings.

3 SIMULATION DEVELOPMENT

This chapter outlines the approach and techniques used to achieve the objectives of developing a comprehensive lap time simulation software framework based on a transient vehicle model. It describes the key components of the methodology, including the transient vehicle model, the analysis of vehicle performance, the nonlinear model predictive trajectory optimization, and the integration of these components into a cohesive software solution. By providing a detailed account of the methodology, this section establishes a clear and systematic framework for the subsequent implementation and analysis of the lap time simulation software.

3.1 Transient vehicle model

The foundation of the methodology lies in the development of a transient vehicle model that accurately represents the dynamic behavior of a racing vehicle. This model will take into consideration various factors such as tire characteristics, suspension dynamics, aerodynamic forces, and vehicle mass distribution. By capturing the complex interactions between these components, the transient vehicle model will serve as the basis for generating realistic and reliable simulation results. The model used for this thesis is from the 14-DOF type, as explained in subsection 2.1.3. More specifically, the model described by Schramm [10] was taken as a main reference.

3.1.1 Coordinate system

The coordinate systems used throughout the following deductions are defined by DIN70 000 in the version of January 1994. These are illustrated on Figure 5.

Figure 5 – Coordinate systems according to ISO 8855

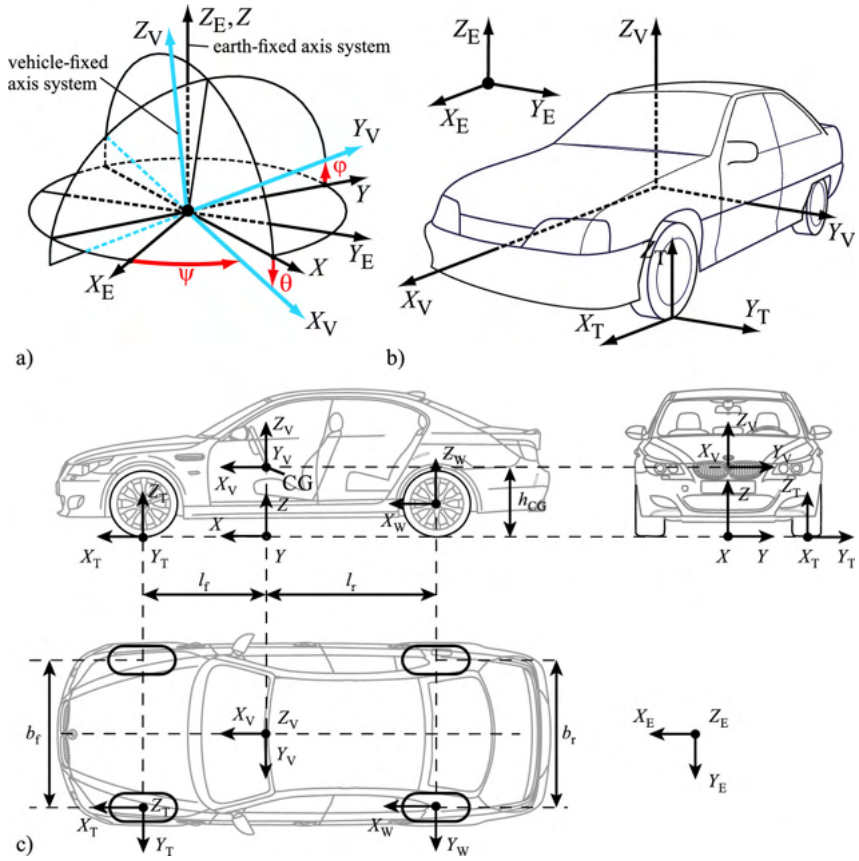

Source: [42]

Note: a) Earth-fixed axis system and horizontal axis system (X, Y, Z)
b) earth-fixed, vehicle-fixed, and tire-fixed axis systems;
c) three-side view of a vehicle with all three axis systems.

The relevant coordinate systems are:

a) **Stationary coordinate system** (X_E, Y_E, Z_E): the coordinate system fixed to Earth fixed to the ground, where X_E and Y_E axes are located in the road plane and Z_E axis points upwards;

b) **Vehicle fixed coordinate system** (X_V, Y_V, Z_V): the coordinate system with an origin in the center of gravity and the X_V pointing to the vehicle's front. The Y_V axis is perpendicular to the longitudinal center plane of the vehicle and points to the left, and the Z_V axis points upward;

c) **Horizontal coordinate system** (X, Y, Z): the coordinate system whose X_E and Y_E are the projections of X_V and Y_V on the ground plane and Z axis points upwards;

d) **Natural coordinate system** (X_N, Y_N, Z_N, not shown): the coordinate system whose origin lies in the vehicle's center of gravity, and in which the X-axis

points in the vehicle's direction of motion —which may be different from the direction the vehicle is pointing —with the Z_N axis pointing upwards.

3.1.2 Model overview

The Table 1 presents an overview of the model's DoFs and the variables that define them.

Table 1 – Overview of the model's DoFs

DoF	**Variable**	**Description**
Chassis displacement	X_E	X-position of the chassis' CG in the stationary CS
	Y_E	Y-position of the chassis' CG in the stationary CS
	Z_E	Z-position of the chassis' CG in the stationary CS
Chassis rotation	ψ	Yaw angle of the chassis
	θ	Pitch angle of the chassis
	ϕ	Roll angle of the chassis
Wheels' displacement	z_{w_i}	Vertical position of the i-th wheel
Wheels' rotation	ω_{w_i}	Rotational velocity of the i-th wheel

Source: Created by the author.

3.1.3 Equations of motion for the chassis

In the mathematical model of the full car, the vehicle's chassis is simplified and represented as a rigid block, suspended at its four corners by the suspension assemblies, and subject to external aerodynamic forces.

By considering the chassis as a rigid block suspended at its four corners, and accounting for the aerodynamic forces and forces transmitted by the suspension system, the mathematical model can be derived using the Newton-Euler approach. This leads to the equations that define the translational motion of the vehicle's chassis, which can be expressed in vector form as:

$$m_v \, \ddot{\mathbf{r}}_\mathbf{v} = \sum_{i=1}^{4} \mathbf{F}_i + \mathbf{G} + \mathbf{F}_w = \sum_{i=1}^{4} \mathbf{F}_i - m_v \, g \, \mathbf{e}_z + \mathbf{F}_w \tag{3.1}$$

In the equation, $\mathbf{F}_i$ represents the forces transmitted from the suspension assemblies to the chassis, while e_z represents the unit vector with the same direction as Z_E. The vector $\mathbf{F}_w$ represents the sum of all the aerodynamic forces on the chassis. Finally, the vector $\ddot{\mathbf{r}}_v$ represents the second time derivatives of the vehicle position in the earth's coordinate system.

Correspondingly, the equations that define the rotational motion of the chassis are defined as:

$$\mathbf{I}_v \dot{\omega} + \omega_v \times (\mathbf{I}_v \omega_v) = \sum_{i=1}^{4} {}_v\mathbf{r}_{S_i} \times \mathbf{F}_i + \mathbf{r}_W \times \mathbf{F}_\mathbf{w} + \mathbf{M}_{ARB,f} + \mathbf{M}_{ARB,r} \tag{3.2}$$

In addition to the previously defined variables, Equation 3.2 contains the position of the aerodynamic center of pressure, $\mathbf{r}_w$; the position of the link between each suspension and the chassis, ${}_v\mathbf{r}_{S_i}$; and the moment generated by the front and rear anti-roll bars, $\mathbf{M}_{ARB,f}$ and $\mathbf{M}_{ARB,r}$.

Moreover, $\mathbf{I}_v$ represents the inertia matrix of the chassis with respect to the vehicle-fixed coordinate system:

$$\mathbf{I}_v = \begin{bmatrix} I_{v,xx} & 0 & 0 \\ 0 & I_{v,yy} & 0 \\ 0 & 0 & I_{v,zz} \end{bmatrix} \tag{3.3}$$

It is assumed that the chassis presents null product moments of inertia, i.e., all of its non-diagonal moments are zero.

3.1.4 Equations of motion for the wheels

In the current work, it assumed that the horizontal tire forces, generated as a result of tire interaction with the road surface, are transmitted directly to the chassis through the suspension system. This assumption is made to simplify the analysis and provide a convenient representation of the car's motion. By considering the suspension as a direct link between the tires and the chassis, the model can focus on the overall behavior of the vehicle without explicitly accounting for the complex dynamics within the suspension components.

However, it is important to consider the vertical movement of the wheels, as it significantly affects the vehicle's handling and ride characteristics. The vertical dynamics of the wheel can be modeled using a simplified representation of the suspension system.

Figure 6 – Free body diagram of one corner of the vehicle

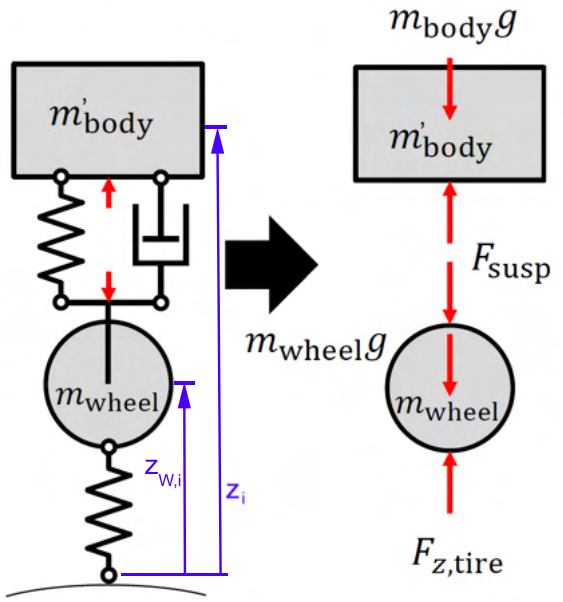

Source: adapted from 43.

In this model, illustrated in Figure 6, the forces acting on the wheel can be divided into two main components: the vertical tire forces $F_z, tire$ and the suspension forces F_susp. The tire forces are generated due to the interaction between the tire and the road surface, while the suspension forces arise from the mechanical properties of the suspension system.

The equation of motion for the vertical movement of the wheel takes into account these forces and their effects on the wheel's acceleration and displacement. It is represented as:

$$m_{w_i}\,\ddot{z}_{w_i} = F_{Z_i,tire} - m_{w_i}\,g - F_{S_i}, \tag{3.4}$$

where m_w represents the mass of the wheel and $\ddot{z}_{w_i}$ denotes the acceleration of the wheel's vertical movement.

In addition to the vertical movement of the wheels, it is important to consider their rotational motion around their own axis. This aspect of the mathematical model provides insights into the wheel dynamics, and more importantly, to the generation of longitudinal forces produced by the tire.

Figure 7 – Moments produced on the at the wheel

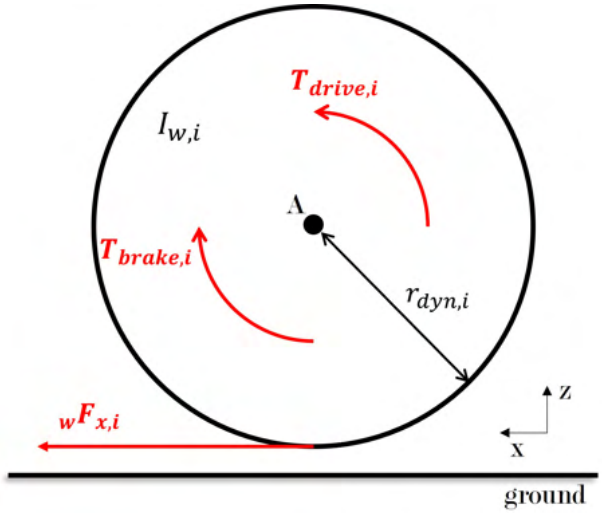

Source: Created by the author.

Note: Only the forces that produce a moment around A are shown: suspension forces and vertical force from the ground are modeled as acting through A.

When applying the Newton-Euler approach, using the wheel center A as a pole, the rotational motion of the wheels can be described by the following equation:

$$I_{w_i}\ddot{\omega}_{w_i} = T_{drive_i} - T_{brake_i} - {}_vF_{x,i} \cdot r_{dyn,i}, \tag{3.5}$$

where I_{w_i} represents the moment of inertia of the wheel around its axis, $\ddot{\omega}_{w_i}$ denotes the angular acceleration of the wheel, T_{drive_i} represents the driving torque applied to the wheel, T_{brake_i} represents the braking torque applied to the wheel, ${}_wF_{x,i}$ represents the horizontal force generated by the tire, projected on its plane of rotation, F_{res_i} represents the rolling resistance generated by the tire, and $r_{dyn,i}$ represents the tire's dynamic radius —assumed constant in this work.

3.1.5 Implementation in Simulink

The mathematical model of the full car was implemented in Simulink. To ensure modularity and ease of understanding, the model was divided into six subsystems: Aerodynamics, Brakes, Drivetrain, Steering, Suspension, and Tires. Each subsystem represents a specific aspect of the car's behavior and is responsible for simulating the corresponding forces, torques, and dynamics.

For detailed information on the implementation of each subsystem, including the equations, parameters, and specific modeling techniques used, please refer to Annex A, where a comprehensive description is provided. This division into subsystems enhances the

clarity and manageability of the Simulink model, allowing for an in-depth analysis of each component's behavior and their collective impact on the overall dynamics of the full car.

The modular nature of the model allowed for the systematic and structured representation of the vehicle's subsystems, making it easier to comprehend and manipulate individual components. This modularity also facilitated future enhancements and modifications to the model, enabling the exploration of additional vehicle configurations and simulation scenarios.

3.2 Analysis of vehicle performance

The implemented model was utilized to conduct a series of simulations encompassing maneuvers aimed at evaluating the longitudinal and cornering limit behavior of the vehicle. These simulations provided valuable insights into the performance boundaries and capabilities of the vehicle under different driving conditions.

The simulations were specifically aimed at replicating the conditions encountered during track time, with a primary focus on extracting the maximum accelerations of the vehicle. By simulating track scenarios, the objective was to push the vehicle to its performance limits and evaluate its capabilities under race-representative conditions.

Due to the availability of data, the vehicle parameters used in the model were taken from a Formula Student[1] vehicle as an example. The parameters of this vehicle serve as a representative example to showcase the capabilities and performance aspects of the car model.

The vehicle parameters, including mass, dimensions, powertrain characteristics, suspension geometry, tire properties, and aerodynamic coefficients, were utilized to create a realistic representation of the vehicle's dynamics. These parameters represent one of the prototypes developed by the university's formula student team. In order to protect the intellectual property of the team, the specific vehicle parameters used in the simulations are not disclosed. Nevertheless, the simulations conducted using these representative vehicle parameters offer valuable insights into the generic behavior of a high-performance race vehicle, allowing for performance analysis and optimization.

It is important to note that while the vehicle parameters are taken from a specific example, the implemented model can be applied to other vehicles by modifying the corresponding parameters to match their characteristics.

[1] Formula Student is an international engineering competition where students design, build, and race single-seat, open-wheel formula-style race cars[44].

3.2.1 Longitudinal performance

The simulation of the acceleration to top speed and subsequent deceleration back to a standstill will serve as the primary tool for determining the longitudinal performance of the vehicle.

The acceleration to top speed simulation involves assessing the vehicle's ability to rapidly accelerate from a stationary position to its maximum achievable speed. By changing factors such as throttle response, gear shifting strategies, engine power curves, and gear ratios, the simulation allows for a detailed examination of the vehicle's acceleration characteristics and its ability to reach and maintain high speeds efficiently.

Additionally, the simulation of deceleration from top speed back to a standstill is equally important in evaluating the vehicle's braking performance and its ability to effectively dissipate the kinetic energy accumulated during acceleration.

By conducting these longitudinal performance simulations, the study of the vehicle's powertrain, transmission, aerodynamics, tire grip, and overall vehicle dynamics can be studied. The simulations provide a thorough understanding of the interplay between various parameters and enable optimization of the vehicle's performance by fine-tuning factors such as engine output, gear ratios, aerodynamic efficiency, and braking system effectiveness.

During this analysis, the following performance indicators will be used:

a) 18 m/s to 25 m/s time

b) 18 m/s to top speed time

c) 25 m/s to standstill time

d) Top speed to a standstill time

e) Longitudinal acceleration vs speed curve considering the accelerating and braking cases)

In the development of the vehicle model, it has been observed that its behavior is not stable at very low speeds. This limitation arises due to the definition of slip angles and slip ratios used in the model. At extremely low speeds, such as during initial vehicle acceleration or when maneuvering in tight spaces, the slip angles and slip ratios become difficult to accurately calculate.

Moreover, this particular speed range often necessitates the engagement of the clutch in traditional vehicles. Since the model primarily focuses on the analysis of race conditions, it is based on a conservative lower speed value of 5 m/s. This choice ensures the reliable and consistent performance of the model within a practical operational range.

3.2.2 Cornering performance

The simulation of a constant-speed, increasing steer maneuver serves as a valuable tool for evaluating the lateral performance of a vehicle. This simulation allows the determination of the maximum lateral acceleration that the vehicle can achieve at a given speed.

This evaluation of maximum lateral acceleration helps optimize the vehicle's handling and performance. By understanding the vehicle's cornering limits, engineers can fine-tune suspension settings, adjust tire characteristics, and develop control strategies to enhance the vehicle's ability to navigate corners at higher speeds.

For this work, the determination of maximum lateral acceleration through this simulation provides crucial information for the trajectory planning and optimization around a given track, as will be explained in section 3.3.

3.2.3 Performance envelope estimation

The estimation of the performance envelope is a critical aspect of the methodology used in evaluating the capabilities of the simulated vehicle. The performance envelope serves as a fundamental representation of the car's limit of adhesion and plays a vital role in determining its lateral and longitudinal peak performance. By using the characteristics of the envelope as the trajectory constraints, the lap time simulation software can later optimize a lap accordingly.

The performance envelope is a graphical representation of the car's maximum available lateral and longitudinal accelerations. Its shape and size are influenced by various factors, including tire characteristics, road surface conditions, and vehicle dynamics. By using it accurately, the lap time simulation software can have condensed information about the interactions that occur between the vehicle's subsystems, as well as between the vehicle and the environment. With that, it can analyze different trajectory options and identify the most efficient path for achieving the fastest lap time.

In this work, the performance envelope will be approximated by two semi-ellipses that join at the x-axis, providing a simplified representation of the vehicle's limit of adhesion. These semi-ellipses are constructed based on the maximum accelerations obtained from the longitudinal and lateral performance evaluations.

The ellipse is defined by the following equation:

$$\begin{cases} \left(\frac{a_y}{a_{lat,max}(v_x)}\right)^2 + \left(\frac{a_x}{a_{acc,max}(v_x)}\right)^2 < 1 & \text{if } a_x > 0 \\ \left(\frac{a_y}{a_{lat,max}(v_x)}\right)^2 + \left(\frac{a_x}{a_{brk,max}(v_x)}\right)^2 < 1 & \text{if } a_x \leq 0 \end{cases} \tag{3.6}$$

Figure 8 – Example of performance envelope for a given speed

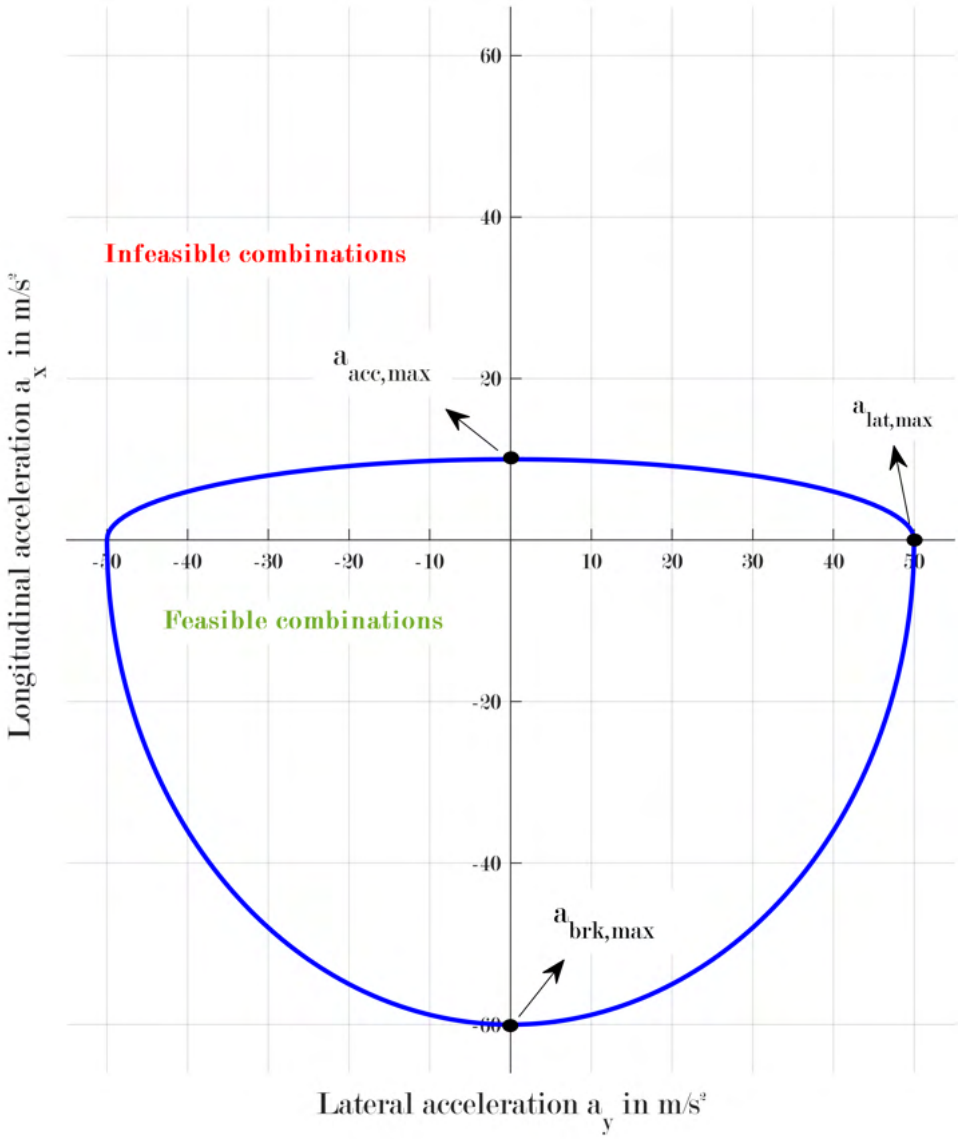

Source: Created by the author.

The graph of the performance envelope in Figure 8 shows the possible combinations of longitudinal and lateral accelerations that can occur at a given speed. The x-axis represents the lateral acceleration of the vehicle, a_y, and the y-axis represents its longitudinal acceleration, a_x. The shape of the ellipse is determined by the values $a_{lat,max}$, $a_{acc,max}$ and $a_{brk,max}$, which are the maximum lateral, forward and braking accelerations, as functions of the vehicle's forward speed, respectively. A given (a_y, a_x) combination is only possible if it satisfies Equation 3.6.

The performance indicators of a vehicle vary with different speeds, leading to changes in the shape of the acceleration envelope. Because the maximum forward acceleration tends to be limited to engine power, it generally decreases as speed increases, primarily due to two factors: quadratic air resistance and linear internal friction. These factors impede the

car's acceleration capability at higher speeds, eventually reaching zero acceleration at its maximum speed. Additionally, vehicle speed is associated with increased downforce, which follows a quadratic relationship. This results in improved grip for turning and braking maneuvers.

Figure 9 – Example of performance envelope for different speeds

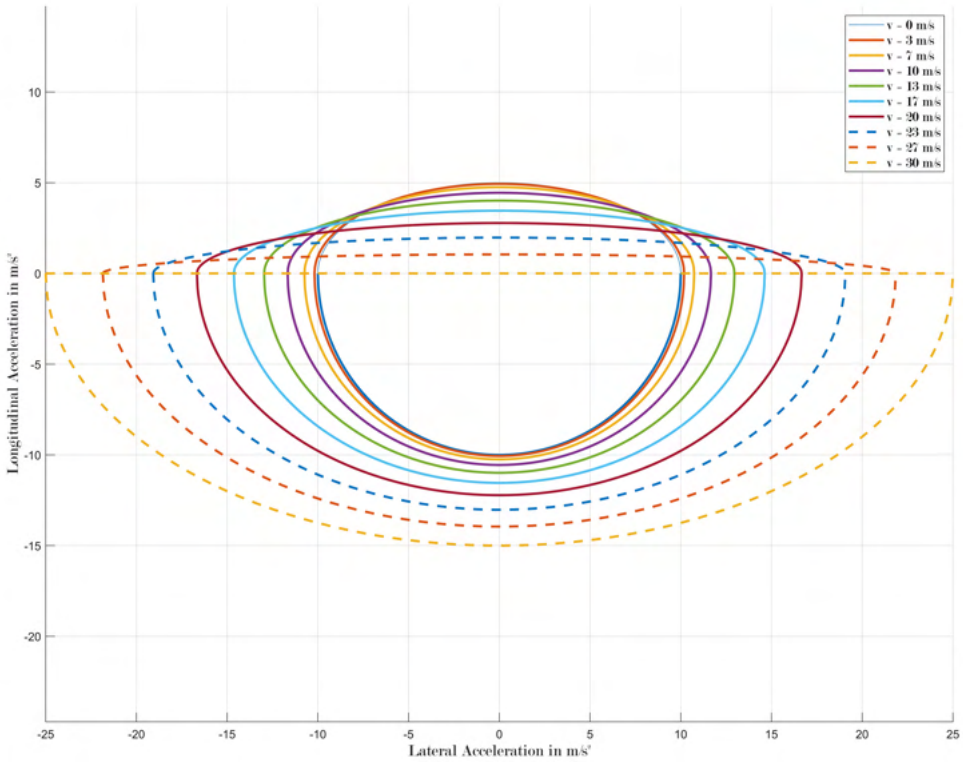

Source: Created by the author.

Figure 9 shows a typical performance envelope evaluated at different speeds. It can be noted that, as speed increases to $v_{max} = 30\text{m/s}$, the part of the envelope representing forward acceleration approaches the x-axis, while the maximum lateral and braking accelerations increase.

Although this approximation simplifies the shape of the envelope, it still captures the essential characteristics necessary for the evaluation of vehicle performance. It allows the lap time simulation software to assess the vehicle's handling limits and make the trajectory optimization. This approach enables the engineer to consider the effect of the vehicle setup on lap time in a simple way since the influence of different suspension, powertrain or aerodynamic configurations will be reflected in the envelope.

3.3 Nonlinear model predictive trajectory optimization

The trajectory optimization algorithm incorporates a nonlinear model predictive controller (NMPC) to enhance performance. To address the computational complexity of

the implemented vehicle model, a simplified point-mass model is employed. This approach still allows for the efficient optimization of the trajectory around a given track by considering the dynamic constraints of the complete model. The combination of the NMPC framework and the point-mass model enables effective trajectory planning for the simulation of racing conditions.

The utilization of the simplified point-mass model strikes a balance between computational efficiency and accuracy. While it may not capture all the intricacies of the actual vehicle dynamics, it provides a practical and effective approximation for trajectory optimization purposes. Furthermore, the algorithm can be used iteratively to refine the planned trajectory in real-time, taking into account the dynamic constraints of the complete model. This opens up possibilities for the coupling of a trajectory-following controller to make the virtual vehicle autonomously travel the track using the optimal trajectory.

The set-up of the minimum time vehicle maneuvering problem, according to the optimal control theory involves the definition of the model equations of motion, the performance measure, the road boundary constraints, and the control bounds. The following sections will elaborate on each definition. However, an important part of modeling the problem is the definition of how a track layout is represented.

3.3.1 Track layout representation

The track layout will be modeled by discretizing the path in equal-length segments and creating a matrix that captures key parameters at each point of the track. The matrix will have rows representing each of these points, and the columns will be dedicated to different attributes of the track. Therefore, a track can be represented by the matrix:

$$\mathbf{T} = \left\{ \mathbf{s} \quad \boldsymbol{\kappa_t} \quad \boldsymbol{\psi_t} \quad \mathbf{X_t} \quad \mathbf{Y_t} \quad \mathbf{w} \quad \frac{\mathrm{d}\mathbf{s}}{\mathrm{d}s} \quad \frac{\mathrm{d}\boldsymbol{\kappa_t}}{\mathrm{d}s} \quad \frac{\mathrm{d}\boldsymbol{\psi_t}}{\mathrm{d}s} \quad \frac{\mathrm{d}\mathbf{X_t}}{\mathrm{d}s} \quad \frac{\mathrm{d}\mathbf{Y_t}}{\mathrm{d}s} \quad \frac{\mathrm{d}\mathbf{w}}{\mathrm{d}s} \right\} \tag{3.7}$$

with each of its elements being a column vector, according to Table 2.

Table 2 – Local track parameters

Variable	Description
s	Distance along the path
κ_t	Local curvature of the path
ψ_t	Travel direction measured in the stationary CS
X_t	X position measured in the stationary CS
Y_t	Y position measured in the stationary CS
w	Local track width

Source: Created by the author.

Note: κ_t is defined as being positive when the variation of ψ_t is positive, and negative otherwise.

Due to the convenience of accessing information about the track's centerline and width through online databases, such as 45 or online map services, the software developed adopts a simplified approach by only taking $\mathbf{X_E}$, $\mathbf{Y_E}$, and $\mathbf{w}$ as track inputs. Using this information, the software discretizes the track by dividing it into segments of a specified length, and, by indirectly deriving the remaining parameters from these inputs, the software avoids the need for explicit data entry or retrieval. However, care must be taken while choosing the segment length, so that the interpolation between the discrete points is accurate enough to represent the track characteristics.

Discretizing the track layout and organizing these attributes into a matrix enables effective analysis and manipulation of the track's characteristics. This approach facilitates the computational handling required in the development of the current lap-simulation software.

3.3.2 The point-mass model

The point-mass model is a simplified mathematical representation used in vehicle dynamics to analyze and predict the path of a vehicle. In this specific case, because the path of the vehicle in relation to a track reference line is considered, the model will also contain states that represent the traveled distance along the track and the distance from its centerline.

The implemented model takes longitudinal and lateral accelerations as inputs and assumes that the vehicle is a point mass traveling along a horizontal plane with a certain velocity vector. The inputs then have the effect of changing the direction or the magnitude of such vector.

Figure 10 – Generic state of the point-mass model

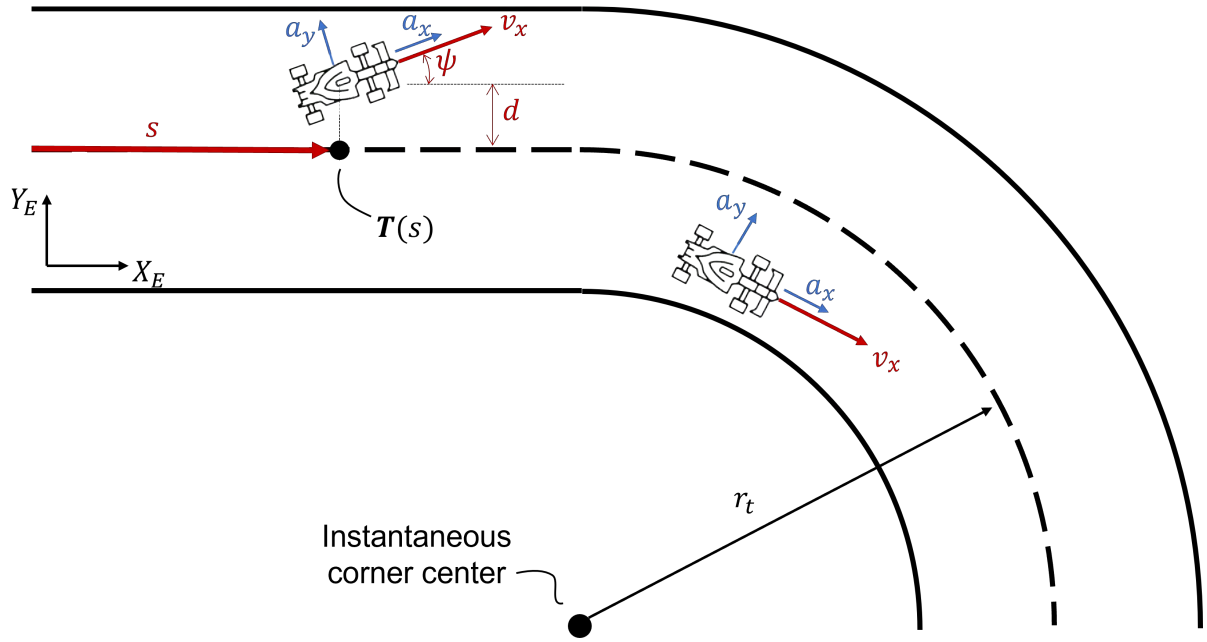

Source: Created by the author.

Figure 10 illustrates a generic state of the model. According to it, the state and input vectors can be defined by:

$$\mathbf{x}(\mathbf{u},t) = \begin{bmatrix} t & \psi & v_x & X_E & Y_E & s_v & s & d \end{bmatrix}^T \tag{3.8}$$

$$\mathbf{u}(t) = \begin{bmatrix} a_x & a_y \end{bmatrix}^T \tag{3.9}$$

where the description of each variable is given in Table 3. Note that, in this model, only ψ, v_x, X_E, and Y_E are sufficient to describe the motion of the vehicle. However, the s and d states must be introduced to account for the vehicle-track interaction.

Table 3 – State variables of the point-mass model

Variable	Description
t	Simulation time
ψ	Yaw angle of the vehicle with respect to the stationary CS
v_x	Longitudinal velocity of the vehicle with respect to the horizontal CS
X_E	Displacement of the vehicle along the x-axis of the stationary CS
Y_E	Displacement of the vehicle along the y-axis of the stationary CS
s_v	Distance traveled by the vehicle
s	Distance traveled by the vehicle along the track centerline
d	Distance from the vehicle to the track centerline
a_x	Acceleration of the vehicle projected in its longitudinal direction
a_y	Acceleration of the vehicle projected in its lateral direction

Source: Created by the author.

Based on equations 3.8 and 3.9, the time derivatives of the states that define the motion of the vehicle can be easily derived:

$$\dot{t} = \frac{dt}{dt} = 1 \tag{3.10}$$

$$\dot{\psi} = \frac{d\psi}{dt} = \frac{a_y}{v_x} \tag{3.11}$$

$$\dot{v}_x = \frac{dv_x}{dt} = a_x \tag{3.12}$$

$$\dot{X}_E = \frac{dX_E}{dt} = v_x \cos\psi \tag{3.13}$$

$$\dot{Y}_E = \frac{dY_E}{dt} = v_x \sin\psi \tag{3.14}$$

$$\dot{s}_v = \frac{ds_v}{dt} = v_x \tag{3.15}$$

For the variables that correlate the vehicle motion with respect to the track, namely s and d, a more complex geometric derivation is needed. For that, an auxiliary variable will be introduced: the time-distance scaling factor S_{cf}, which in accordance with Ref. Casanova can be defined as:

$$S_{\mathrm{CF}} = \frac{dt}{ds} \tag{3.16}$$

Figure 11 – Vectorial relations in the point-mass model

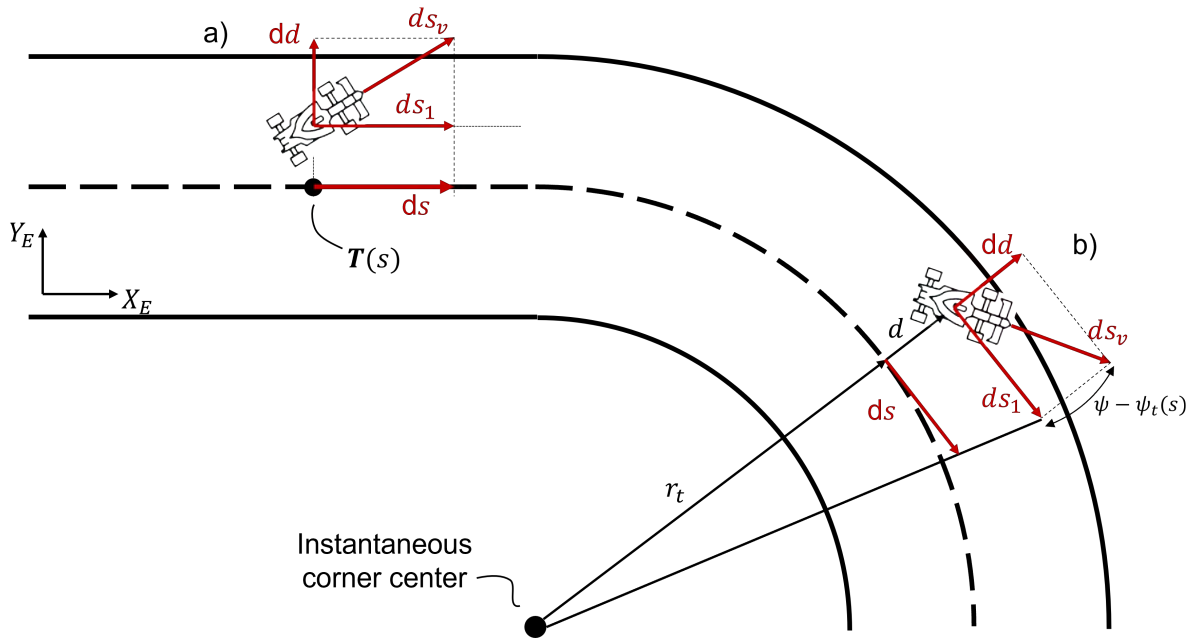

Source: Created by the author.

2

Using Figure 11 let's first consider the vehicle is in a straight section of the track (situation a), but traveling in a direction that is not tangent to the path. The increment of the distance traveled by the vehicle is defined by:

$$\mathrm{d}\vec{s}_v = [\mathrm{d}X_E \quad \mathrm{d}Y_E]^T, \tag{3.17}$$

which can be projected onto the unit vector $\hat{e}_\psi = [\cos\psi \quad \sin\psi]^T$ tangent to the reference path at the current point:

$$\mathrm{d}\vec{s}_1 = \left(\mathrm{d}\vec{s}_v \cdot \hat{e}_\psi\right) \cdot \hat{e}_\psi = (\mathrm{d}X_E \cos\psi_t + \mathrm{d}Y_E \sin\psi_t)\ [\cos\psi \quad \sin\psi]^T, \tag{3.18}$$

in this case, it can be seen that $\mathrm{d}\vec{s} = \mathrm{d}\vec{s}_1$.

However, when the vehicle is in a curved section of the track (situation b), traveling a certain distance parallel to the path centerline does not mean that the distance increment is traveled along the path. This is shown in Figure 10, where a section with constant curvature is shown. For the vehicle to go from section A to section B, it has to travel a longer distance, the farther from the corner center it is. This difference can be calculated by:

$$\frac{\mathrm{d}s}{\mathrm{d}s_1} = \frac{r_t}{r_t + d} \Rightarrow \mathrm{d}s = \frac{r_t}{r_t - d}\mathrm{d}s_1, \tag{3.19}$$

where $r_t = {\kappa_t}^{-1}$ is the corner radius.

Combining equations 3.18 and 3.19, the increment in the distance traveled along the track centerline can be defined as:

$$\mathrm{d}s = \left(\frac{r_t}{r_t + d}\right)\left(\mathrm{d}\vec{s}_v \cdot \hat{e}_\psi\right) = \frac{r_t \cdot (\mathrm{d}X_E \cos\psi_t + \mathrm{d}Y_E \sin\psi_t)}{r_t - d} \tag{3.20}$$

Considering temporal increments:

$$\dot{s} = \frac{\mathrm{d}s}{\mathrm{d}t} = \frac{r_t \cdot \left(\dot{X}_E \cos\psi_t + \dot{Y}_E \sin\psi_t\right)}{r_t - d} = \frac{1}{S_{\mathrm{CF}}} \tag{3.21}$$

Now substituting equations 3.13 and 3.14:

$$\dot{s} = \frac{r_t \cdot (v_x \cos(\psi)\, \cos(\psi_t) + v_x \sin(\psi)\, \sin(\psi_t))}{r_t - d} = \frac{r_t\, v_x\, \cos(\psi - \psi_t)}{r_t - d} \tag{3.22}$$

Analyzing Equation 3.22, it is evident that, if the vehicle trajectory is perpendicular to the track, i.e., if $\psi - \psi_t = \frac{\pi}{2} + k\pi$, with $k \in \mathcal{Z}$, the increment in distance traveled along the path is zero and the time-distance scaling factor tends to infinity ($S_{\mathrm{CF}} \to \infty$). The importance of that will be explained later.

Finally, the distance d from the vehicle to the track's centerline can be calculated as:

$$d = (Y_E - Y_t)\cos\psi_t - (X_E - X_t)\sin\psi_t, \tag{3.23}$$

and its time derivative can be written as:

$$\begin{aligned}\dot{d} \;=\; & \sin\psi_t \left(\frac{\mathrm{d}X_t}{\mathrm{d}s}\,\dot{s} - v_x\,\cos\psi + (Y_t - Y_E)\,\frac{\mathrm{d}\psi_t}{\mathrm{d}s}\,\dot{s}\right) + \\ & + \cos\psi_t \left(-\tfrac{\mathrm{d}Y_t}{\mathrm{d}s}\,\dot{s} + v_x\,\sin\psi + (X_t - X_E)\,\tfrac{\mathrm{d}\psi_t}{\mathrm{d}s}\,\dot{s}\right)\end{aligned} \tag{3.24}$$

Note that, to derive Equation 3.24, the equations 3.13 and 3.14 were used. Besides that, the chain rule was used to determine that:

$$\frac{\mathrm{d}X_t}{\mathrm{d}t} = \frac{\mathrm{d}X_t}{\mathrm{d}s}\,\frac{\mathrm{d}s}{\mathrm{d}t} = \frac{\mathrm{d}X_t}{\mathrm{d}s}\,\dot{s}, \tag{3.25}$$

Now isolating the terms that depend on $\dot{s}$ in Equation 3.24:

$$\begin{aligned}\dot{d} \;=\; & \dot{s}\,\sin\psi_t \left(\tfrac{\mathrm{d}X_t}{\mathrm{d}s} + (Y_t - Y_E)\,\tfrac{\mathrm{d}\psi_t}{\mathrm{d}s}\right) + \dot{s}\,\cos\psi_t \left(-\tfrac{\mathrm{d}Y_t}{\mathrm{d}s} + (X_t - X_E)\,\tfrac{\mathrm{d}\psi_t}{\mathrm{d}s}\right) + \\ & + v_x\,\sin\psi\,\cos\psi_t - \,v_x\,\cos\psi\,\sin\psi_t,\end{aligned} \tag{3.26}$$

and knowing that $\sin a\,\cos b - \sin b\,\cos a = \sin(a - b)$, and $\dot{s} = \frac{1}{S_{\mathrm{CF}}}$:

$$\begin{aligned}\dot{d} \;=\; & \tfrac{\sin\psi_t}{S_{\mathrm{CF}}} \left(\tfrac{\mathrm{d}X_t}{\mathrm{d}s} + (Y_t - Y_E)\,\tfrac{\mathrm{d}\psi_t}{\mathrm{d}s}\right) + \\ & + \tfrac{\cos\psi_t}{S_{\mathrm{CF}}} \left(-\tfrac{\mathrm{d}Y_t}{\mathrm{d}s} + (X_t - X_E)\,\tfrac{\mathrm{d}\psi_t}{\mathrm{d}s}\right) + \\ & + v_x\,(\sin\psi - \psi_t)\,,\end{aligned} \tag{3.27}$$

with the linear interpolation of the track representation providing $\frac{\mathrm{d}\psi_t(s)}{\mathrm{d}s}$, $\frac{\mathrm{d}X_t(s)}{\mathrm{d}s}$ and $\frac{\mathrm{d}Y_t(s)}{\mathrm{d}s}$, as per subsection 3.3.1.

3.3.2.1 Representation in the state space

Finally, the time derivative of the model's state vector is given by joining equations 3.10-3.15, 3.22 and 3.27:

$$\dot{\mathbf{x}}(\mathbf{x}, \mathbf{u}) = \begin{bmatrix} 1 \\ \frac{a_y}{v_x} \\ a_x \\ v_x \cos\psi \\ v_x \sin\psi \\ \frac{1}{S_{\mathrm{CF}}} \\ \dot{d} \end{bmatrix}, \tag{3.28}$$

with $\mathbf{x}$ and $\mathbf{u}$ defined in Equation 3.8 and Equation 3.9, respectively.

These model equations are an essential component of the NMPC problem as they are used to predict the future behavior of the system based on the current state and input trajectories. By integrating the model equations over p discrete time intervals (i.e., the prediction horizon) using an input trajectory $\mathbf{u}_p$, the NMPC algorithm can predict the trajectory of the model states and, based on a score given by the objective function and on feasibility criteria given by the optimization constraints.

Since in the minimum time Optimal Control problem T is not a constant, an alternative way to express the model equations is to assume the s coordinate as the independent variable of the simulation instead of the time. For that, we can apply the chain rule, in such a way that:

$$\frac{\mathrm{d}\mathbf{x}}{\mathrm{d}s}(\mathbf{x}, \mathbf{u}) = \frac{\mathrm{d}\mathbf{x}}{\mathrm{d}t}\frac{\mathrm{d}t}{\mathrm{d}s} = S_{\mathrm{CF}}\frac{\mathrm{d}\mathbf{x}}{\mathrm{d}t}(\mathbf{x}, \mathbf{u}) \tag{3.29}$$

where the definition of S_{CF} comes from Equation 3.16.

The implications of using Equation 3.28 or Equation 3.29 are discussed in the next section.

3.3.2.2 Consideration about the two different discretization approaches

In the context of the minimum lap time optimization problem, the objective is to "*minimize the total time required to complete a single lap*". Since the lap distance remains constant when considering the track centerline, reducing this time necessitates achieving higher average speeds throughout each of its segments. Consequently, the former statement is equivalent to "*maximize the speed of the vehicle along the track centerline*".

Although equivalent, each statement represents one different approach to the problem. In the first, the independent variable for the simulation at each step is an increment on the distance traveled by the vehicle along the centerline Δs, while in the second, the independent variable is a fixed time increment Δt.

When the time increment is fixed, the distance traveled by the vehicle during each simulation step depends on its speed (as the vehicle's speed increases, it covers a greater distance within each step). Therefore the preview distance, which represents the distance over which future control inputs are planned, is dependent on the vehicle speed. Consequently, when determining this increment, careful consideration is needed to maintain an appropriate lookahead horizon. A longer preview distance is typically useful at higher speeds to account for the increased distance covered during each time step. This ensures that the controller can anticipate and respond to upcoming track features and optimize control inputs accordingly. However, when considering low speeds, it might be less computationally efficient, since the distance covered at each step is small, resulting in more steps to cover one lap, hence more optimization iterations.

On the other hand, when utilizing track distance steps, the preview distance remains fixed regardless of the vehicle speed. This fixed preview distance allows for a consistent number of optimization iterations over one lap, which can speed up the simulation. With that, the prediction horizon must be chosen so that it is long enough for the controller to capture more complicated track features such as corner sequences and chicanes.

Additionally, it is worth noting that when using fixed-time steps, the accuracy of the vehicle dynamics remains constant throughout the simulation, since the step size determines the precision with which the vehicle's state variables are updated at each iteration. In contrast, when employing track distance steps, the accuracy of the vehicle dynamics becomes dependent on the vehicle speed, with a potential decrease in precision at higher velocities.

Upon analyzing the derived equations in subsection 3.3.2, it becomes apparent that the fixed time-step approach exhibits greater numerical stability. This is evident when the vehicle is traveling perpendicular to the track, resulting in a situation where $S_{\mathrm{CF}} \to \infty$. In this scenario, Equation 3.28 maintains finite values, whereas Equation 3.29 yields non-finite values. Based on this observation, the fixed-time approach is deemed more suitable and will be utilized for the present thesis.

3.3.3 The objective function

As previously mentioned, the main goal of the present controller is to "*maximize the speed of the vehicle along the track centerline*". When using the time-fixed approach, this equates to traveling the maximum distance along the track centerline during the prediction horizon $p\Delta t$. Therefore, the objective function is defined as:

$$J = -(s_p - s_0), \tag{3.30}$$

where s_p represents the track-coordinate predicted on an instant $p\Delta t$ in the future and s_0 represents its current value. Depending on the optimization solution used, the algorithm will try to maximize or minimize this objective function. In the case of Matlab Model Predictive Toolbox, used in this thesis, the goal is to have the smallest possible value of J, hence the minus sign in the equation.

3.3.4 The optimization constraints

The two constraints that must be considered for the present problem are the performance envelope —here, the derivation presented in subsection 3.2.3 becomes particularly useful —, and the track boundaries. The first is directly linked to the admissible inputs **u** to the model, while the second can be evaluated directly by looking at the d state of the model.

The mathematical description of such constraints has a crucial role in the computational efficiency of the solving algorithm, as well as in its stability. The main aspects to be considered are that the description must be valid for all possible system states while being computationally simple. In general, it is useful to define differentiable constraint equations, since they allow for gradient-based optimization, which can greatly improve computational efficiency. For the present problem, the used formulation reads:

$$c_i = \begin{cases} \left(\frac{a_{y,i}}{a_{lat,max}(v_{x,i})}\right)^2 + \left(\frac{a_{x,i}}{a_{acc,max}(v_{x,i})}\right)^2 - 1 < 0 & \text{if } a_{x,i} > 0 \\ \left(\frac{a_{y,i}}{a_{lat,max}(v_{x,i})}\right)^2 + \left(\frac{a_{x,i}}{a_{brk,max}(v_{x,i})}\right)^2 - 1 < 0 & \text{if } a_{x,i} \leq 0\,, \\ d_i^2 - w_i^2 < 0 \end{cases} \tag{3.31}$$

where w is the track width and $i \in [1, \cdots, p]$, meaning that the inequalities presented must be true at each of the prediction steps for a solution to be feasible.

Note that, because the two first lines of Equation 3.31 are mutually exclusive, the problem is composed of $2p$ quadratic inequality constraints. Also, each of the inequalities can be evaluated for every $[a_{x,i},\ a_{y,i},\ d_i]$.

3.3.5 The control bounds

To ensure the control variables of the vehicle model remain within physically meaningful ranges, constant control bounds are imposed. These bounds restrict the values of the control variables according to the vehicle capability.[3] Specifically, the longitudinal

[3] The definition of such bounds is presented as a formality since the optimization constraints are more strict than the control bounds.

acceleration is constrained by an upper limit, a_{acc_max}, and a lower limit, a_{brk_min}. Similarly, the absolute value of the lateral acceleration is limited by a_{y_max}.

$$\begin{bmatrix} -a_{brk,max} \\ -a_{lat,max} \end{bmatrix} \leq \mathbf{u_i} = \begin{bmatrix} a_{x,i} \\ a_{y,i} \end{bmatrix} \leq \begin{bmatrix} a_{acc,max} \\ a_{lat,max} \end{bmatrix} \tag{3.32}$$

3.3.6 The NMPC problem statement

Based on the later sections, the task of the nonlinear model prediction is then, for each simulation step, to find a control trajectory $\mathbf{u}_i$, $i \in [1, \cdots, p]$ that maximizes the distance traveled by the vehicle along the track centerline, while not exceeding the track limits nor the vehicle performance envelope. This can be mathematically described as:

$$\begin{aligned} &\min_{\mathbf{u}} \quad J \\ &\text{Subject to:} \\ &\quad \tfrac{\mathrm{d}\mathbf{x}}{\mathrm{d}t} = \dot{\mathbf{x}}(\mathbf{x}, \mathbf{u}), \quad \mathbf{x}(0) = \mathbf{x_0} \quad \text{(Vehicle equations)} \\ &\quad c_i < 0 \qquad\qquad\qquad\quad \text{(Performance envelope and road constraints)} \\ &\quad \mathbf{u}_L < \mathbf{u} < \mathbf{u}_u \qquad\qquad \text{(Control bounds)} \\ &\text{for the prediction horizon} \quad t - t_0 \in [\Delta t, \cdots, p\,\Delta t] \end{aligned} \tag{3.33}$$

3.3.7 Implementing the NMPC in Matlab

The implementation of the nonlinear model controller was accomplished in MATLAB with the aid of the Model Predictive Control (MPC) Toolbox. This toolbox offers a comprehensive suite of functionalities for designing, simulating, and implementing MPC algorithms.

Within the MPC Toolbox, the key component for implementing the controller is the nlmpcmove function. This function plays a crucial role in solving the optimization problem associated with the nonlinear model controller. Leveraging advanced optimization techniques, it enables efficient and effective control action computation.

3.3.7.1 The solution algorithm

The nlmpcmove function utilizes a method known as sequential quadratic programming (SQP) to solve the optimization problem. SQP is an iterative optimization algorithm that combines principles from Newton's method and quadratic programming. It is specifically designed to handle nonlinear optimization problems with constraints.

At each iteration, nlmpcmove approximates the nonlinear model and its constraints by linearizing them around the current operating point. This linearization process simplifies

the optimization problem and enables the use of efficient quadratic programming techniques. Based on the linearized model, the function constructs a quadratic programming problem that aims to minimize a specified cost (or objective) function while satisfying the imposed constraints. Here, the thoughtful definition of the objective and constraint equations becomes useful, since they allow an analytical definition of their jacobian function, which is used together with the linearization to speed-up the quadratic programming problem.

The SQP algorithm then iteratively solves the quadratic programming problem, progressively updating the control inputs to drive the system toward the optimal solution. By iteratively refining the control sequence, nlmpcmove effectively balances the trade-off between system performance and constraint satisfaction.

The application of nlmpcmove's optimization method offers several advantages. It allows for the incorporation of complex nonlinear dynamics and constraints, providing greater flexibility and accuracy in modeling the system behavior. Furthermore, by utilizing SQP, the function efficiently navigates through the control input space, enabling the determination of optimal control actions that optimize the system's performance.

3.3.7.2 Definition of the prediction and control horizons

Choosing the appropriate prediction and control horizons is a critical aspect of designing a successful model predictive control (MPC) system. The prediction horizon determines the length of time into the future over which the system's behavior is forecasted, while the control horizon specifies the steps at which optimal control actions are computed. The selection of these horizons requires careful consideration and has a significant impact on the performance and stability of the MPC controller.

The prediction horizon must strike a balance between capturing sufficient future dynamics to make informed control decisions and maintaining computational efficiency. A longer prediction horizon allows for better anticipation of the track features, allowing for an optimal trajectory even when tight sequences of corners exist. However, an excessively long prediction horizon can lead to increased computational complexity, as more future states and constraints need to be considered during optimization. Additionally, a longer prediction horizon may be unnecessary, since model uncertainties and environmental disturbances might make the actual motion diverge from the predicted, which means that the steps further are almost certain to not occur as predicted.

Similarly, the control horizon plays a crucial role in determining the responsiveness and adaptability of the MPC controller. A longer control horizon allows for more prolonged planning of control actions, enabling the system to optimize its behavior over an extended time period. This can be particularly advantageous in situations where a turn can only be tightened after passing the apex of a corner, for example. However, similarly to the prediction horizon, a longer control horizon may result in using improbable prediction

steps in finding the optimal solution.

This complexity while choosing these horizons was a great driver in the decision of using the simplified point-mass model, since its lesser complexity allows for the choice of longer prediction horizons while not affecting the computational efficiency as much as the complete 14 DoF would.

3.3.7.3 Simulation of the optimal lap

By creating a simulation of the point-mass model and utilizing the nlmpcmove function to define the next control input at each step, it becomes possible to accurately optimize the vehicle's movement along a given track.

Figure 12 – Lap time simulation flowchart

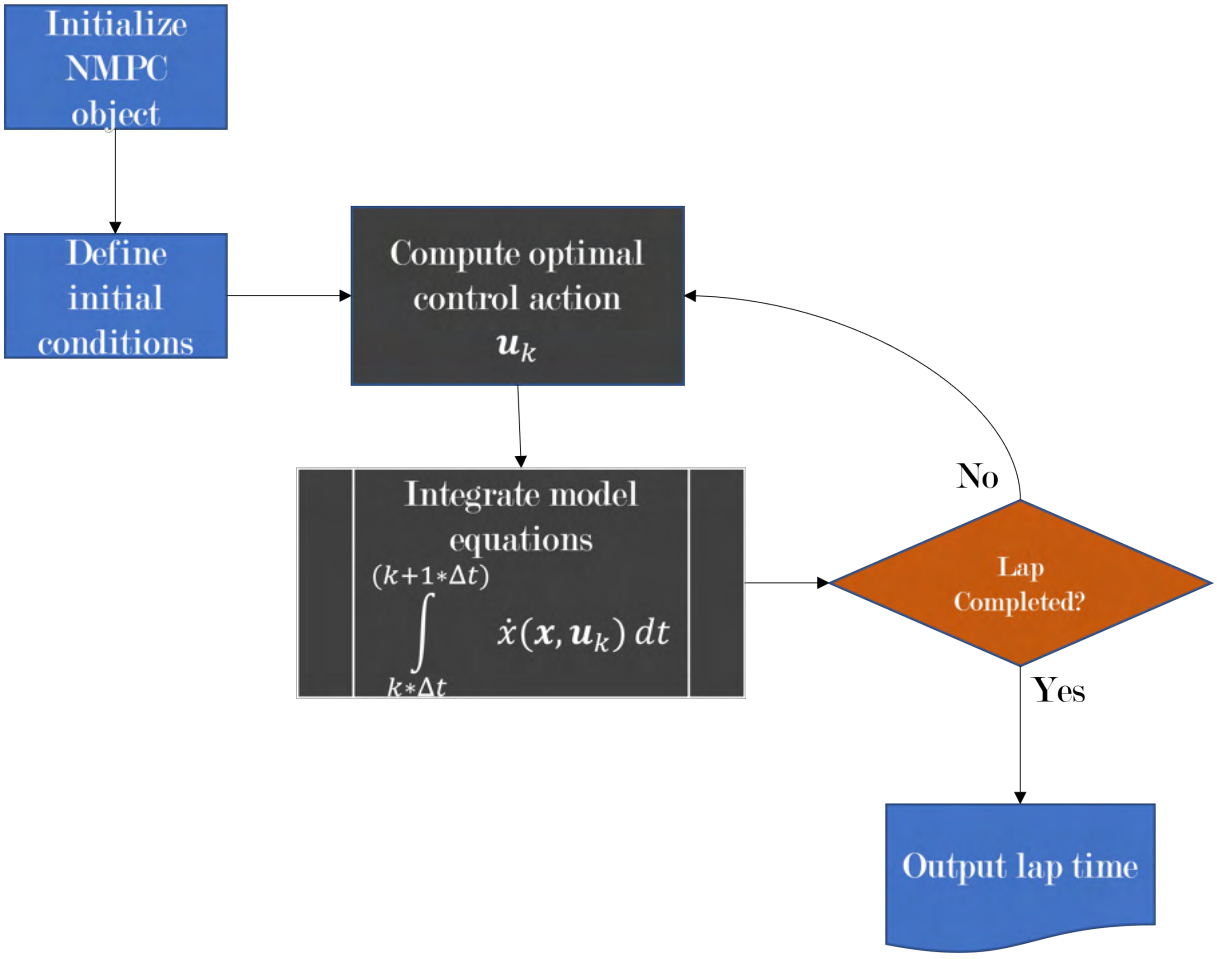

Source: Created by the author.

Figure 12 provides a flowchart with a general description of the implemented code. In the simulation, the nlmpcmove computes the control actions based on the current state of the vehicle and the track features within the prediction horizon. These control inputs

are then applied to the point-mass model, effectively simulating the vehicle's motion along the track.

By iterating this process, simulating step-by-step, the vehicle's position, velocity, and other relevant variables are updated, reflecting its continuous movement along the track. Therefore, an accurate estimation of the lap time is obtained by recording the time it takes for the vehicle to complete a full lap.

For the development of the simulation and for following its current state, a series of interfaces were created using MATLAB.

Figure 13 – Lap time simulation interface

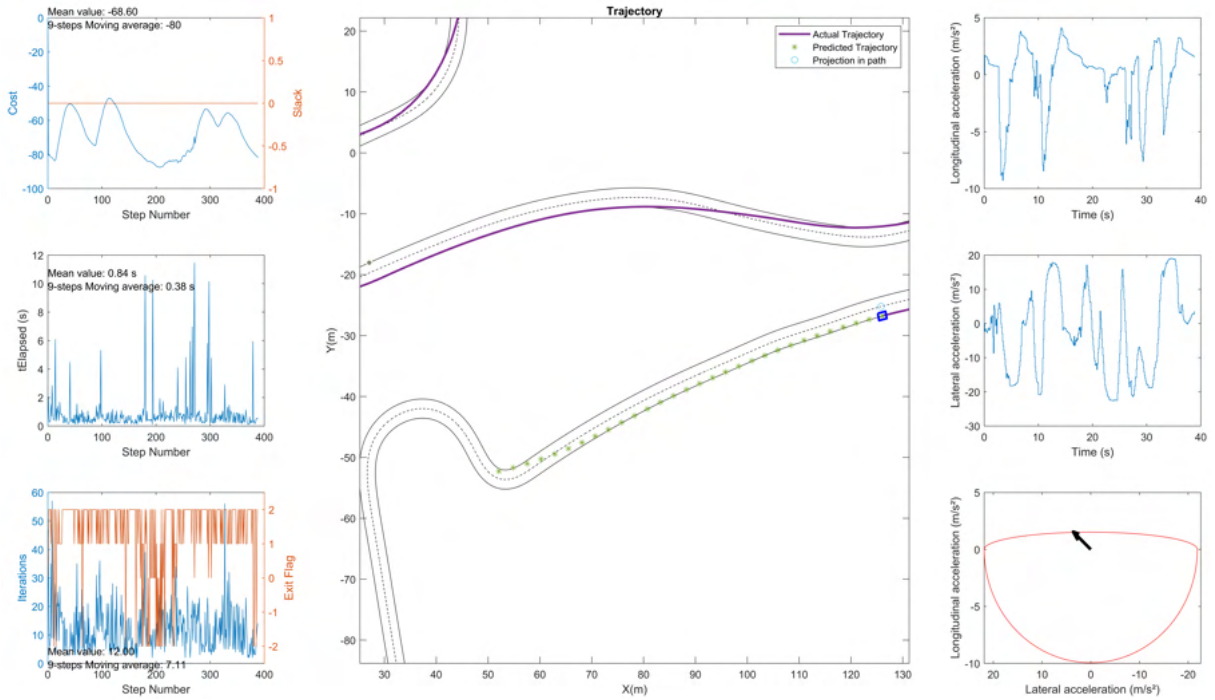

Source: Created by the author.

Figure 13 gives a visual representation of the simulation state at a given time. The graphs to the left show the evolution of parameters such as the value of the objective function, the slack variable, the time taken for the optimization, the number of iterations of the optimization, and the exit flag. [4] The graphs to the right show the time evolution of the inputs, i.e. longitudinal and lateral accelerations, and a GG diagram containing the performance envelope at the current vehicle speed, and a vector showing the last input. Note by the black vector that the algorithm makes use of the full performance envelope by selecting inputs that are near its limit. The center graph shows the past trajectory,

[4] The slack variable is used to soften a constraint, by attributing a penalty to the objective function that is proportional to the value of the violation of the softened constraints. The exit flag is an integer that indicates whether the solver converged or not, and with each convergence criteria.

the predicted optimal trajectory, and the projection of the current position of the vehicle on the track centerline. Note that the predicted trajectory depends on the portion of the track that the algorithm can *see*. The algorithm doesn't know that if the vehicle follows the presented trajectory, it will most likely leave the track after the prediction horizon is traveled.

Figure 14 – Lap time simulation interface (after 8 steps)

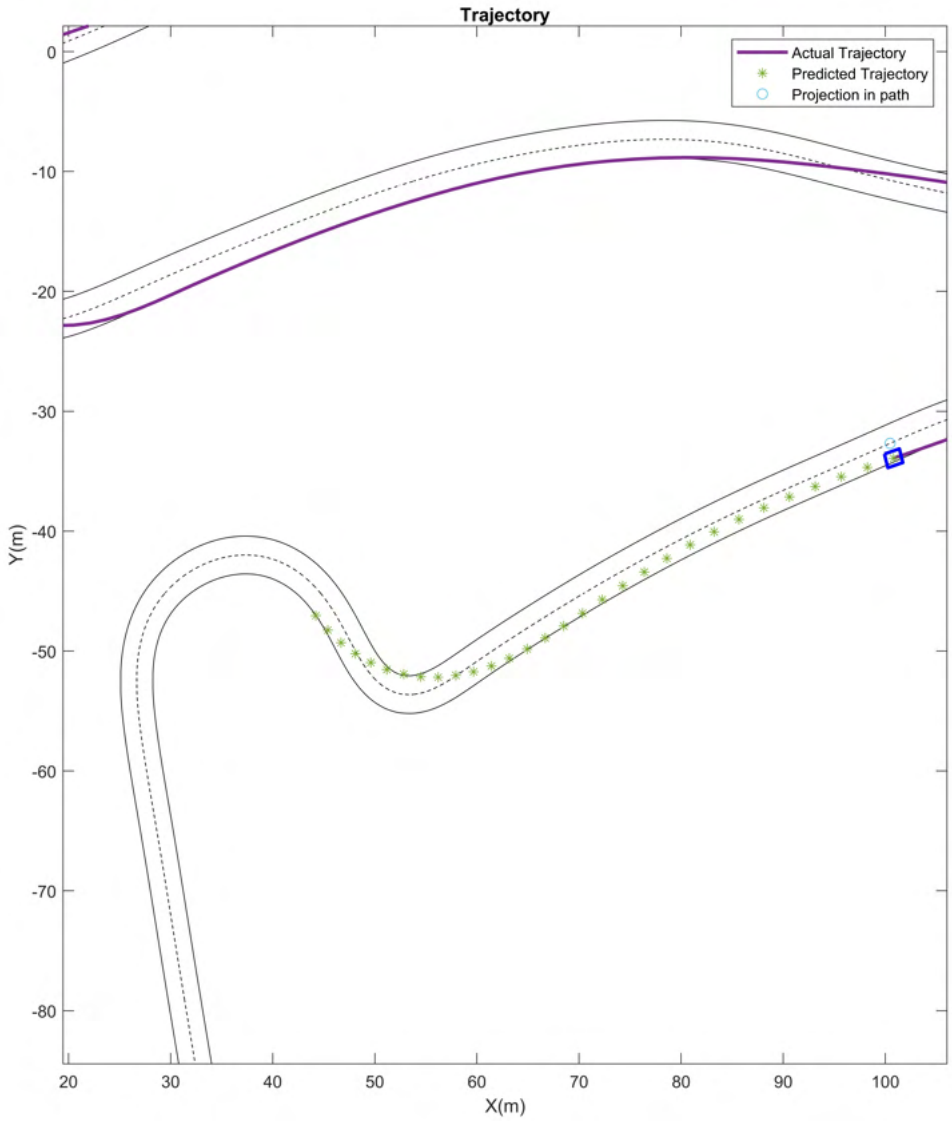

Source: Created by the author.

Figure 14 shows the same simulation after a few simulation steps. It can be noted that the shape of the predicted trajectory has changed significantly. That happened because the algorithm perceived that the previous trajectory would lead to a track excursion, and then, adapted it so track limits were respected, while still with the maximum track coverage during the prediction horizon.

3.4 Software Integration

The methods described in this chapter were implemented in a software framework using Matlab and Simulink. The integration process involved creating interfaces for parameter input, simulation configuration, results processing, and results plotting. The goal was to develop an integrated framework that is easy to set up, operate, and expand by the author in future works.

The software framework was designed to provide a user-friendly experience. It allowed users to input relevant parameters for the transient model and lap time optimization script effortlessly. This enabled customization and experimentation with different vehicle configurations within the simulation environment.

Additionally, the framework included interfaces for simulation configuration, allowing users to define track characteristics, environmental conditions, and other variables necessary for accurate lap time predictions. This reconfigurability helped create simulations that closely resembled real-world scenarios.

The primary objective of the integrated software framework was to provide a tool that is accessible and expandable for the author's future works. The design focused on modularity and extensibility, allowing easy modification or addition of new features, algorithms, or simulation methodologies. This flexibility empowered the author to continue building upon the software framework, advancing lap time simulation and optimization. The following section will present a high-level overview of the system.

Figure 15 – Overview of the Simulink model interfaces

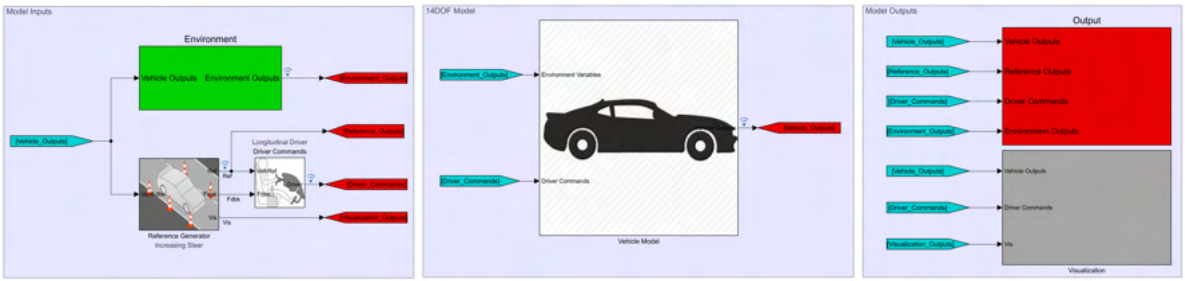

Source: Created by the author.

Figure 16 – Overview of the Simulink model inputs

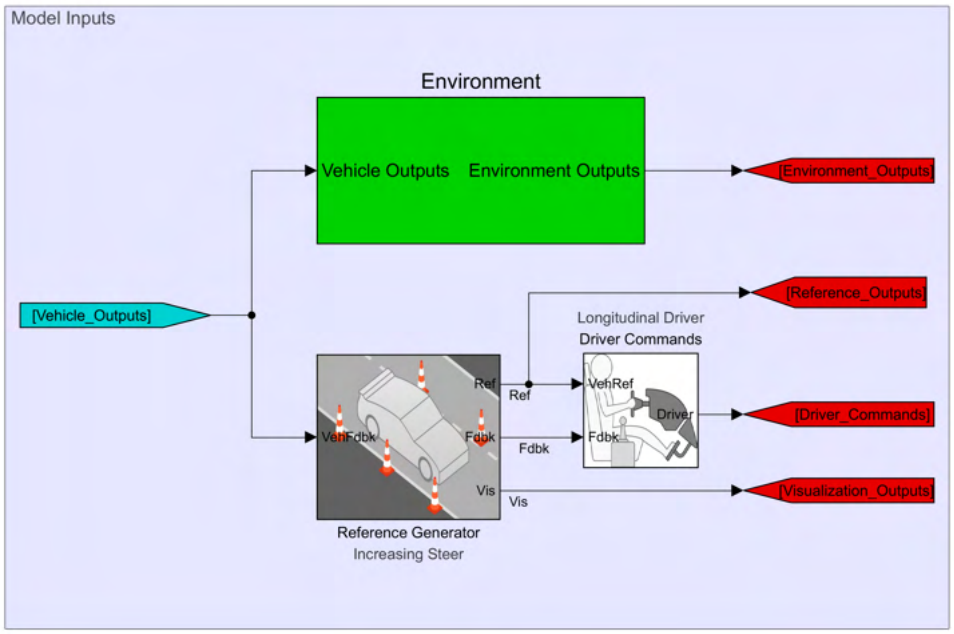

Source: Created by the author.

Figure 17 – Overview of the Simulink model

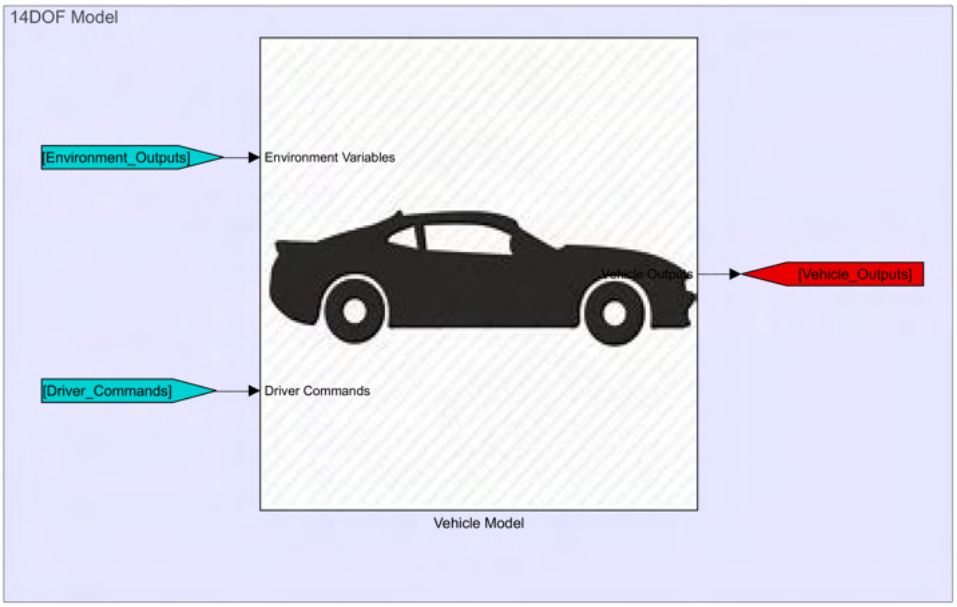

Source: Created by the author.

Figure 18 – Overview of the Simulink model outputs

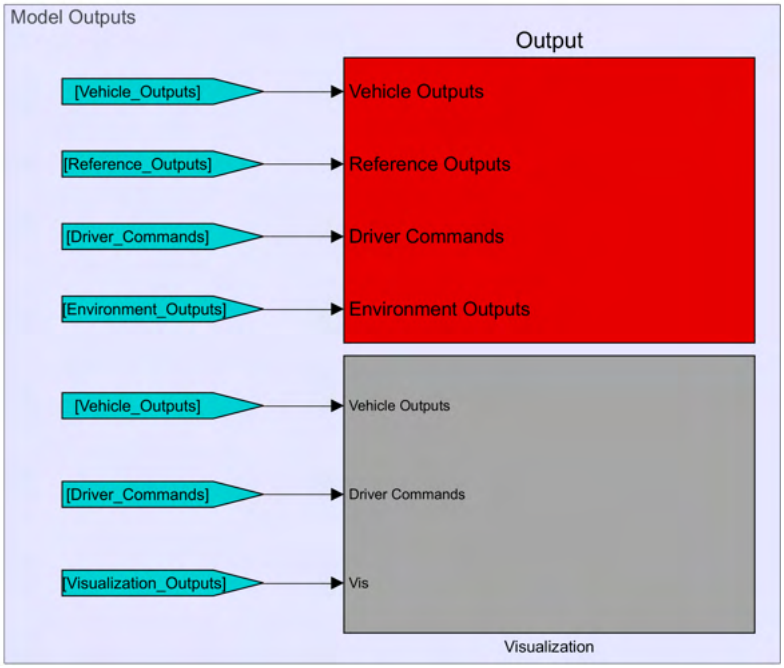

Source: Created by the author.

Figures 16-18 show the high-level inputs and outputs of each model, the signals are separated into five buses:

a) Environment Outputs: contains signals such as wind speed and direction and road profile

b) Reference Outputs: contains the speed, position, or other references that will be used by the driver subsystem

c) Driver Commands: as the name suggests, the commands provided by the driver. Can contain variables such as gear selected, steering wheel angle, and brake and pedal positions

d) Vehicle Outpus: contains that is calculated by the vehicle model itself. It contains the vehicle's state variables, but also many other parameters such tire slip angles, aerodynamic forces

e) Visualization Outpus: the signals that are used by the visualization subsystem to show a schematic representation of the motion of the vehicle during the simulation

In general, users can configure the desired simulation by utilizing the reference generator's mask, as depicted in Figure 19. This mask offers essential functions for reconfiguring the subsystems of the model to suit the intended simulation scenario. To

modify a simulation or any of its parameters, users simply need to open the mask's dialog, select the desired options through the user interface, and execute the model.

Figure 19 – The reference generator

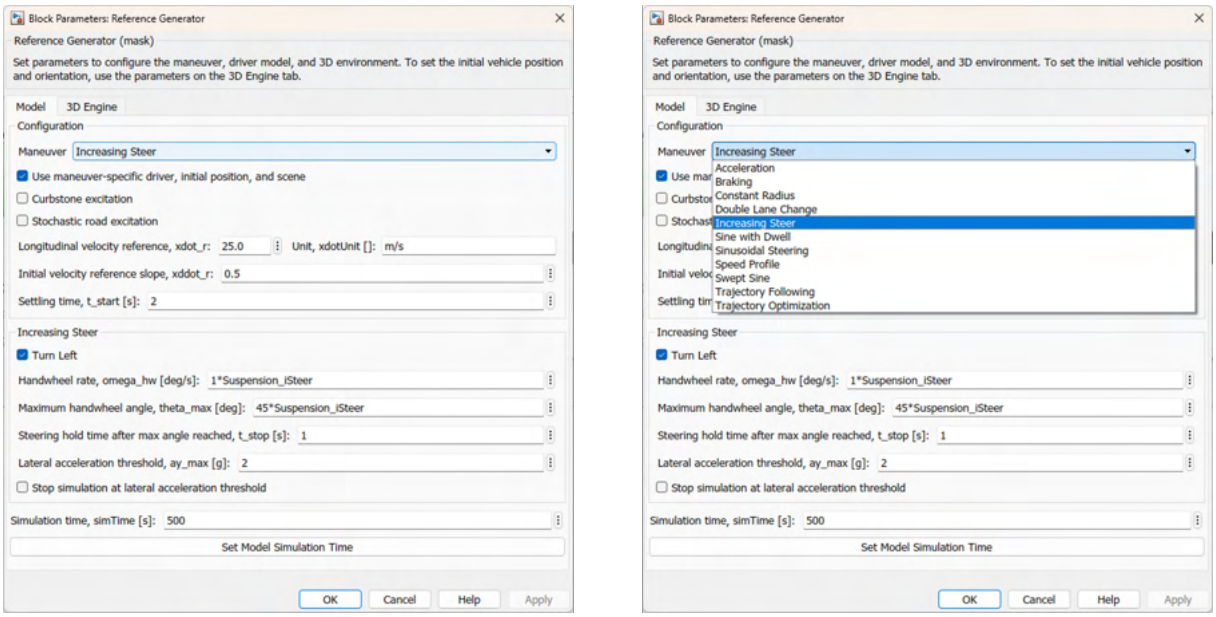

Source: Created by the author.

This block essentially controls a variant subsystem that provides the desired outputs to the system, as seen in Figure 20.

Figure 20 – The reference generator

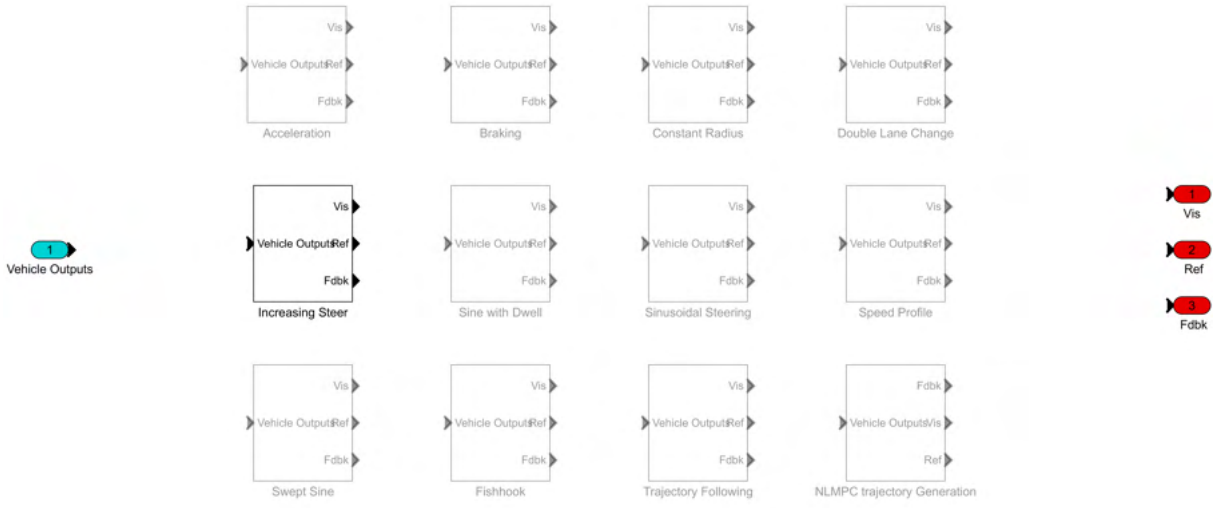

Source: Created by the author.

The subsystem shown in figures 17 implements the model equations, which were defined in section 3.1 and will not be further explained.

4 RESULTS AND ANALYSIS

4.1 Validation of the transient vehicle model

This section presents the validation process of the transient model with the use of data from a formula student vehicle. The validation aims to assess the accuracy and reliability of the model in predicting the vehicle's response in dynamic racing conditions.

As previously mentioned the transient model developed considers various factors that influence a race car's performance during a lap, including aerodynamics, tire characteristics, suspension setup, powertrain dynamics, and driver behavior. To validate the model, a straightforward approach is adopted, which involves comparing the recorded behavior of the real vehicle during testing with the behavior exhibited by the model.

Gathering sufficient data from the vehicle proved challenging due to limited availability. However, efforts were made to collect data from real race car testing sessions. The available data included measurements such as vehicle speed, acceleration, steering angles, and other pertinent parameters. Despite the scarcity of data, capturing the car's behavior in the available racing conditions still yielded a valuable dataset for model validation, in special, the validation of the longitudinal dynamics was very satisfactory. To illustrate that, the following section will show a comparison between the real and simulated vehicles during an acceleration maneuver, and during a braking maneuver.

4.1.1 The acceleration maneuver

The full vehicle was simulated as explained in subsection 3.2.1 and the results were compared with the same maneuver from the real vehicle.

Figure 21 – Acceleration test - real vs simulated car

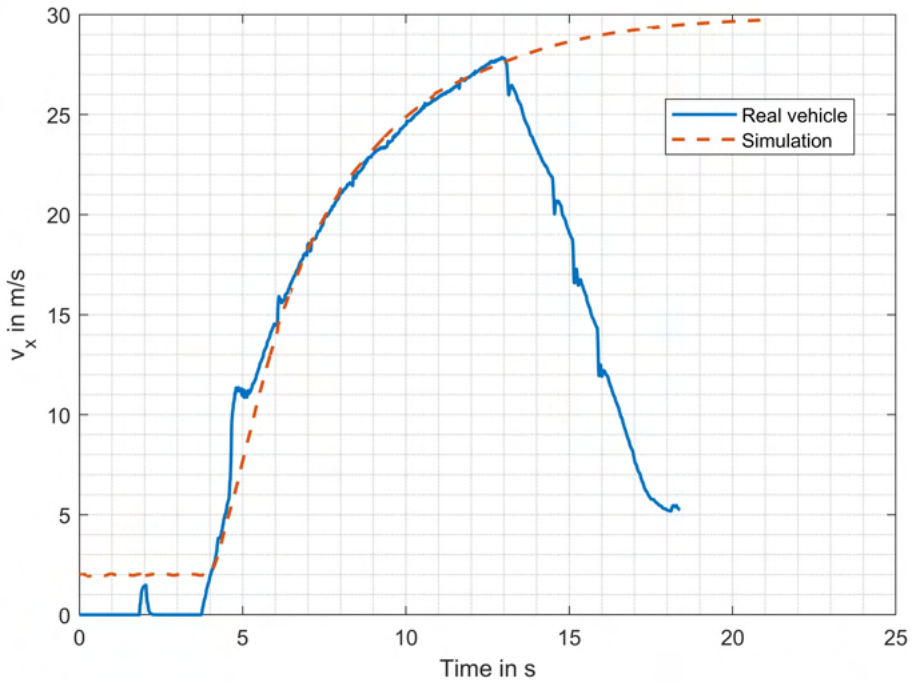

Source: Created by the author.

Figure 21 depicts a comparison between the acceleration maneuver of a vehicle using the model and the recorded data from a real acceleration test. The model demonstrates a high degree of accuracy in representing reality, albeit with a slightly higher deviation during the initial phase of the maneuver.

This divergence can be attributed to the measurement method employed in the test, where the velocity was indirectly determined using Hall effect sensors on the rear wheels. While this approach is sufficiently accurate for small slip ratios, during the vehicle's launch, particularly in first gear, significant wheel slip occurs, resulting in an overestimation of the measured speed.

Conversely, in other sections of the graph, the deviation is minimal, indicating that the model effectively captures the vehicle's maneuver. Furthermore, it is worth noting that although the maximum speed was not attained in the given test, the simulated maneuver predicts a maximum speed of approximately 30 m/s, which was subsequently confirmed by the university's team in other tests.

4.1.2 The braking maneuver

The analysis was extended to include the braking maneuver, where a full-stop scenario was simulated. In this case, the driver initiated maximum braking effort from the vehicle's top speed until a complete standstill, as explained in subsection 4.2.2. The same maneuver was replicated using the model, and the results were compared.

Figure 22 – Braking test - real vs simulated car

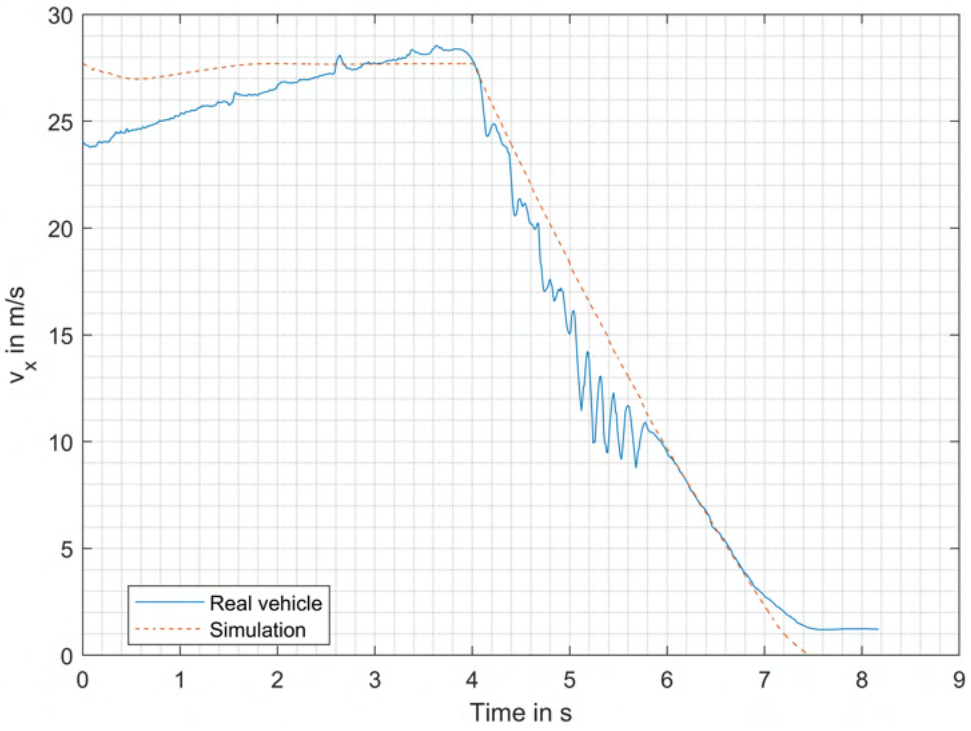

Source: Created by the author.

Figure 22 presents the comparison for the braking case, demonstrating that the model effectively represents the vehicle's behavior during deceleration. Similarly to the acceleration maneuver, the speed measurement method exhibits a notable effect on the observed data. As a consequence of successive downshifts and the interaction between the wheels and the engine, the wheel speed oscillates significantly throughout the braking maneuver. Therefore, besides the speed being underestimated during braking maneuvers, the speed signal oscillates significantly. Nonetheless, the model manages to faithfully capture the overall trend of the curve, indicating its ability to simulate the behavior of the vehicle accurately.

4.1.3 Consideration on the validation of lateral dynamics

Validating the lateral dynamics of the vehicle proved to be a more intricate task due to the unavailability of specific data that could replicate the increasing steering test. Consequently, an alternative approach was adopted, which involved gathering a

comprehensive set of data recorded during timed laps. The focus shifted to examining the relationship between speed and lateral acceleration in track sections known to be constrained by the lateral grip of the vehicle.

By analyzing these data points, it was possible to effectively validate the model's representation of the vehicle's lateral dynamics. The comparison revealed a strong alignment between the model's predictions and the observed behavior during the timed lap. This congruence provided confidence in assuming the validity of the model's depiction of the lateral dynamics of the vehicle, despite the absence of direct replication of the increasing steering test.

Overall, the combined analysis of the acceleration, braking, and lateral dynamics maneuvers provided a comprehensive assessment of the model's performance. The model demonstrates a high level of fidelity in replicating the vehicle's behavior during these critical maneuvers, with minor deviations in specific scenarios explained by the limitations of the measurement methods or the unavailability of specific data. These findings support the confidence in utilizing the model for further analysis and optimization of the vehicle's performance in different driving scenarios.

4.2 Performance envelope generation

With the validated model in hand, the subsequent step involves utilizing it to derive the performance envelope, as mentioned earlier. For that purpose, a set of simulations were conducted to measure the maximum longitudinal and lateral performance of the vehicle: an acceleration test, a braking test, and an increasing steer test.

As an example, this thesis explores three vehicle variants, each showcasing distinct aerodynamic characteristics:

a) **Configuration 1:** The vehicle without an aerodynamic package

b) **Configuration 2:** The vehicle with an aerodynamic package consisting of front and rear wings in its maximum downforce configuration

c) **Configuration 3:** The vehicle with an aerodynamic package consisting of front and rear wings in its minimum drag configuration

Table 4 shows the variables that are affected by each configuration. Here, the simplification that the side force coefficient c_S and the vehicle's yaw moment of inertia I_{zz} are not affected by the changes.

Table 4 – Vehicle configurations

Parameter	**Config 1**	**Config 2**	**Config 3**
Lift coefficient, c_L	0.2	-2.6	-1.7
Drag Coefficient, c_D	0.7	1.46	0.85
Vehicle mass $m_{vehicle}$	266.5 kg	275 kg	275 kg

Source: Created by the author.

Note: The added mass of the aerodynamic package is considered in the analysis.

By carefully evaluating the impact on vehicle mass, coefficient of drag, and coefficient of lift, vehicle designers can make informed decisions about the inclusion and design of an aerodynamic package for their Formula Student car. The following analysis will focus on the performance evaluation of each configuration.

4.2.1 Acceleration performance

The acceleration test aimed to examine the vehicle's behavior during rapid acceleration. To conduct this simulation, the longitudinal driver provided in the Vehicle Dynamics Toolbox from Matlab was utilized.[46] The parameters of the longitudinal driver were appropriately configured to ensure accurate representation. The longitudinal command was given by overriding the controller's outputs from the point where the initial speed was stable at the desired starting value, while the steering command remained fixed at a straight position. Additionally, the gear change behavior was adjusted so that the virtual driver shifted gears at the maximum engine speed of the vehicle.

The simulation began with the vehicle idling in first gear, with the clutch engaged. Subsequently, the throttle was set to 100%. The simulation continued until the specified triggering condition was met, which involved a longitudinal acceleration (a_x) less than or equal to $0.2\,\mathrm{m/s^2} \approx 0.02\,\mathrm{g}$, which was assumed to represent the vehicle's maximum speed.

Figure 23 – Acceleration test results

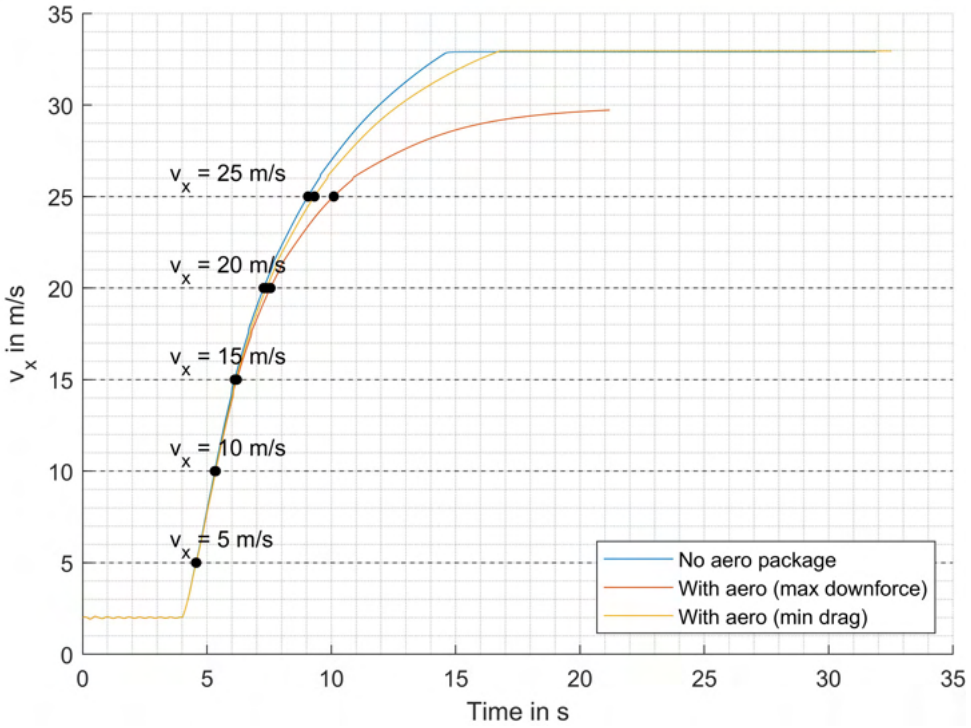

Source: Created by the author.

The simulations provided the graphs shown in Figure 23, from where the results shown in Table 5 were extracted.

Table 5 – Acceleration test results table

Simulation result	**Config 1**	**Config 2**	**Config 3**
Top Speed	33.9 m/s	29.75 m/s	33.9 m/s
$\Delta t_{5 \Rightarrow 10 m/s}$	0.757 s	0.784 s	0.778 s
$\Delta t_{5 \Rightarrow 15 m/s}$	1.553 s	1.627 s	1.596 s
$\Delta t_{5 \Rightarrow 20 m/s}$	2.727 s	2.974 s	2.819 s
$\Delta t_{5 \Rightarrow 25 m/s}$	4.504 s	5.511 s	4.749 s
$\Delta t_{5 \Rightarrow TopSpeed}$	14.683 s	16.642 s	16.861 s

Source: Created by the author.

It can be observed that, for configurations 1 and 3, the vehicle's maximum speed is limited by the gear ratio, which means that, in the highest gear, the engine has enough power to overcome the air resistance until reaching its redline, at 33.9 m/s. However, for configuration 2, the maximum speed is lower, indicating that at 30.1 m/s, all the power produced by the engine is consumed by the air resistance forces. Such a result is reasonable since configuration 2 is the one with the highest drag coefficient.

Another observation is the considerable influence of the aerodynamic package, especially at higher speeds. This can be observed by comparing the discrepancy in ac-

celeration times across different configurations. For $\Delta t_{5\Rightarrow 10m/s}$, the disparity between the configuration without the dedicated aerodynamic package and the one with a minimal-drag aerodynamic package is just 0.018 seconds, which is mainly due to the mass increase of the vehicle. However, for $\Delta t_{5\Rightarrow 25m/s}$, this disparity reaches a substantial 0.234 seconds.

Aside from the values from Table 5, the $a_{x,max}(v_x)$ curves were extracted, which will later be used for the creation of the performance envelopes.

Figure 24 – Acceleration vs speed test results

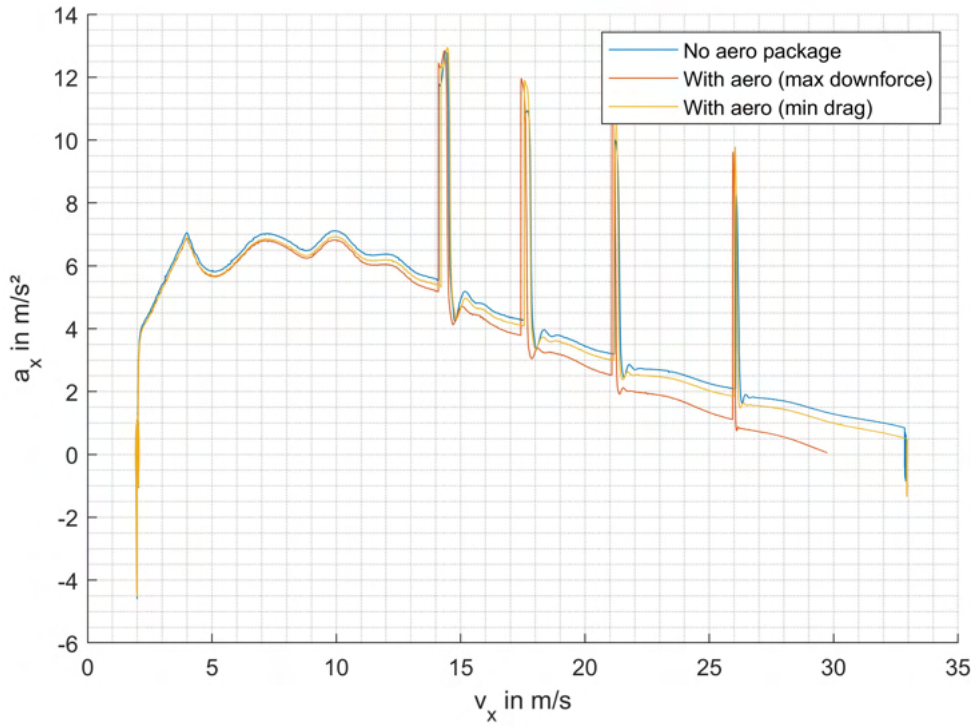

Source: Created by the author.

It is notable that the regions where the vehicle changes gears induce highly transient accelerations on the vehicle. When shifting gears in a vehicle, the engine and transmission speeds become different. As the clutch is dropped after changing gears, the transmission, connected to the wheels, must slow down the engine and, in turn, perceives a forward force as a reaction. This causes a peak of acceleration, representing the abrupt adjustment required to synchronize the engine and transmission speeds. The interplay between the engine, transmission, and wheels during the gear shift process generates this surge of acceleration, showcasing the complex dynamics involved in power transfer within a vehicle.

Here, some post-processing is needed to smoothen the curve so that it serves as input to the lap-time simulation. For that, the acceleration is linearly interpolated between the instants just before and just after the gear shifts, resulting in the following curve:

Figure 25 – Acceleration vs speed test results (smoothed)

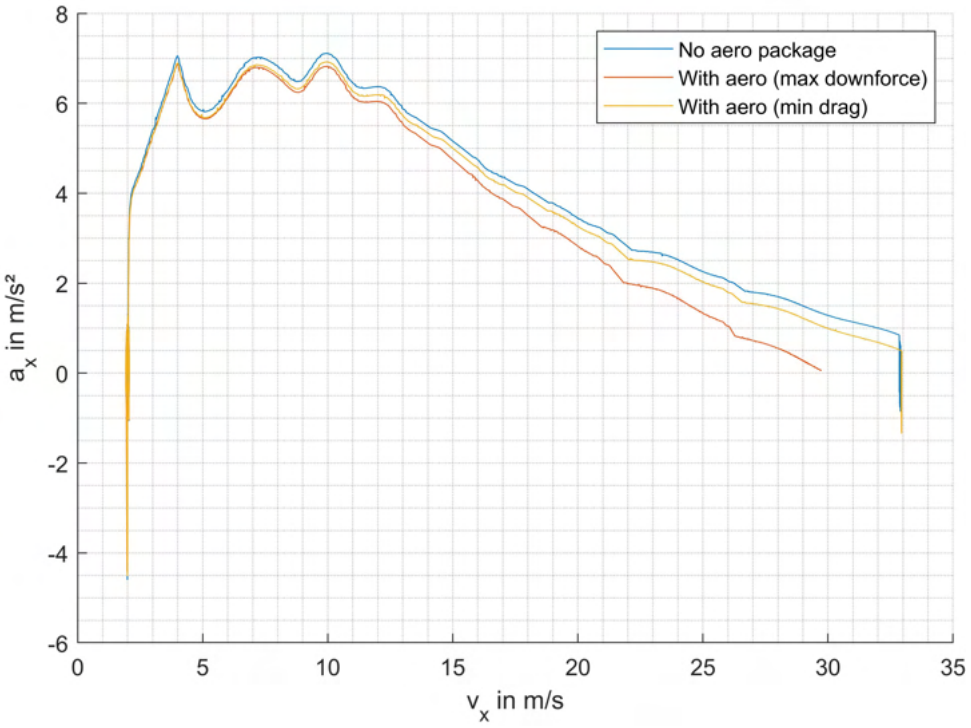

Source: Created by the author.

4.2.2 Braking performance

Similarly, the braking test aimed to assess the vehicle's deceleration capabilities. The model was utilized to simulate different braking scenarios, enabling the measurement of stopping distances and overall braking performance. For this simulation, the same driver model as the previous section was used. However, the downshift speeds were defined as those at which the engine reaches 7000 rpm, this was defined with the use of the acquisition data from a lap of the team's real drivers.

Figure 26 – Braking test results

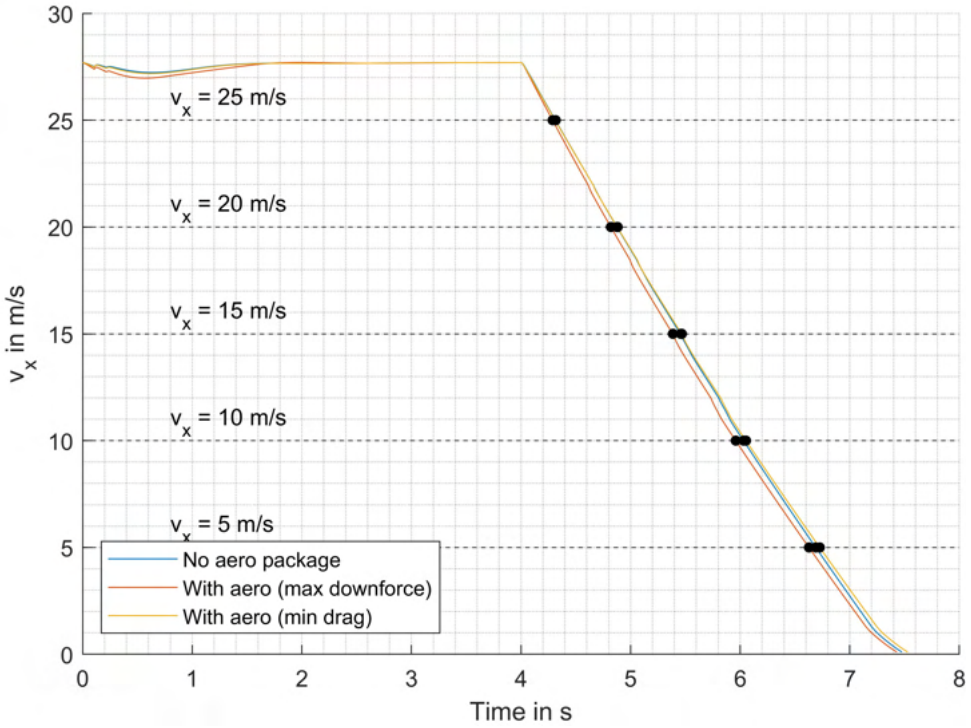

Source: Created by the author.

The simulations yielded the graphs presented in Figure 26, which served as the basis for extracting the results displayed in Table 6.

Table 6 – Braking test results table

Simulation result	**Config 1**	**Config 2**	**Config 3**
$\Delta t_{25 \Rightarrow 20 m/s}$	0.564 s	0.534 s	0.574 s
$\Delta t_{25 \Rightarrow 15 m/s}$	1.14 s	1.097 s	1.158 s
$\Delta t_{25 \Rightarrow 10 m/s}$	1.716 s	1.671 s	1.741 s
$\Delta t_{25 \Rightarrow 5 m/s}$	2.376 s	2.339 s	2.415 s

Source: Created by the author.

In the case of braking, the configurations exhibit a smaller disparity compared to the acceleration. Here, it is worth noting that, although no controller was used to maximize braking, it was observed that the wheels did not exhibit high slip ratios, which would indicate a near-blocking situation. This suggests that, in the presented case, braking is not limited by the tire's grip, but rather by the braking torque exerted by the brake discs. Since the goal of this work is to evaluate the vehicle with the parameters provided by the university's team, the optimization of the braking performance will not be done, but it is clear that the present analysis can be used as a tool for such a task in the future.

Nonetheless, it is still noteworthy that the configuration with maximum downforce

(and maximum drag) initially demonstrates a more pronounced deceleration. One plausible explanation for this phenomenon is the greater drag force exerted by the air, which contributes to enhanced braking performance.

Similarly, the $a_{x,min}(v_x)$ curves were extracted, which will later be used for the creation of the performance envelopes.

Figure 27 – Braking vs speed test results

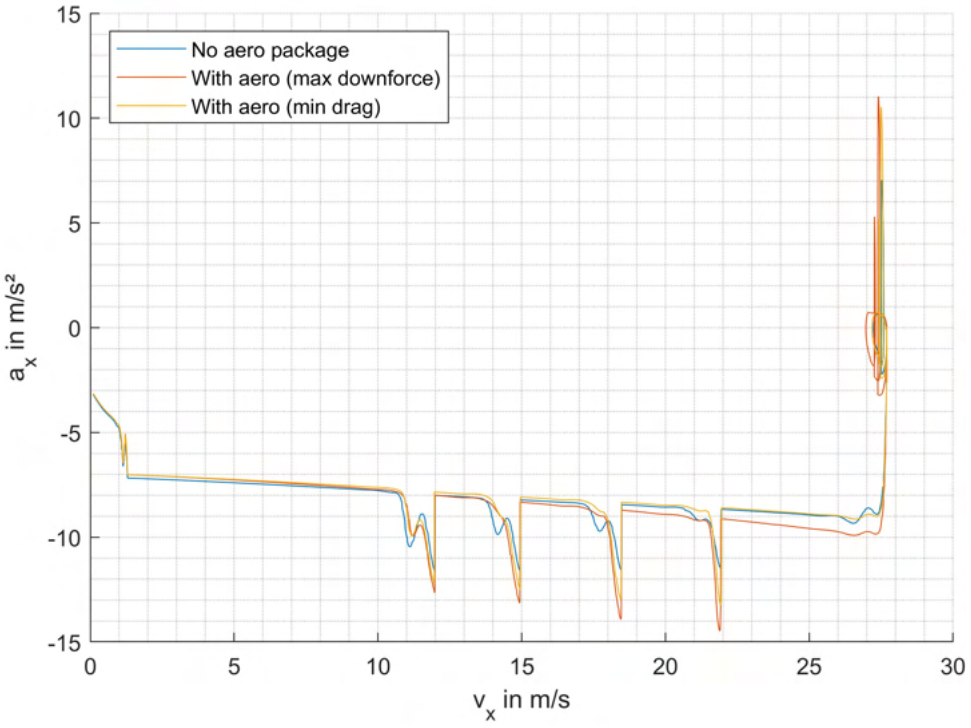

Source: Created by the author.

Note that the apparently complex portion to the right is when the controller is stabilizing the vehicle at the desired initial speed.

Analogously to the acceleration case, the curve was smoothed and the result is as follows.

Figure 28 – Braking vs speed test results (smoothed)

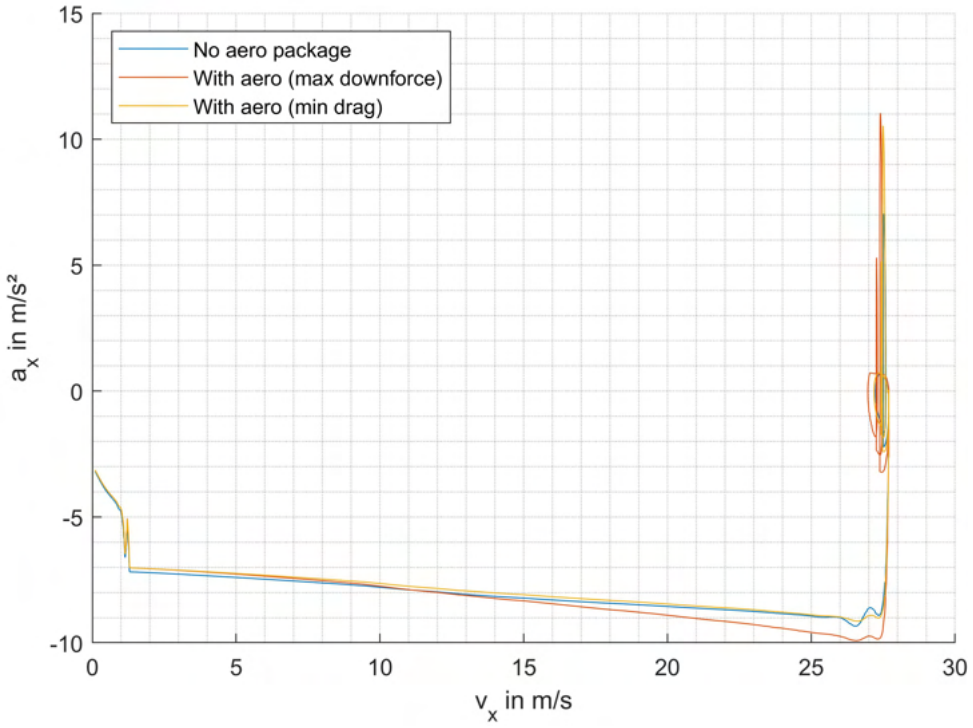

Source: Created by the author.

4.2.3 Cornering performance

Lastly, the increasing steer test was conducted to evaluate the car's lateral performance. The model simulated the vehicle's response to increasing steering inputs, providing valuable insight into its handling, and stability for different speeds. To conduct this simulation, the longitudinal driver provided in the Vehicle Dynamics Toolbox from Matlab was utilized to maintain a constant speed, while the steering wheel angle was slowly increased. The parameters of the longitudinal driver were appropriately configured to ensure accurate representation. Additionally, the gear change behavior was adjusted so that the virtual driver shifted gears at the maximum engine speed of the vehicle.

Each simulation began with the vehicle accelerating to the desired speed, when the target speed was captured, the steering wheel angle started increasing slowly, at such a rate that the wheels would turn 1°/s. This slow increase was done to ensure that the analysis is done in a quasi-static form. The simulation is stopped when the absolute value of the lateral acceleration deviates more than $0.2 m/s^2 \approx 0.02\,\mathrm{g}$ downwards from the maximum obtained in the simulation, i.e., when the software detects that a peak of acceleration has been reached.

The following figures represent the lateral acceleration of the vehicle throughout the test for different speeds. Each figure represents one configuration of the vehicle.

Figure 29 – Lateral performance without aero package

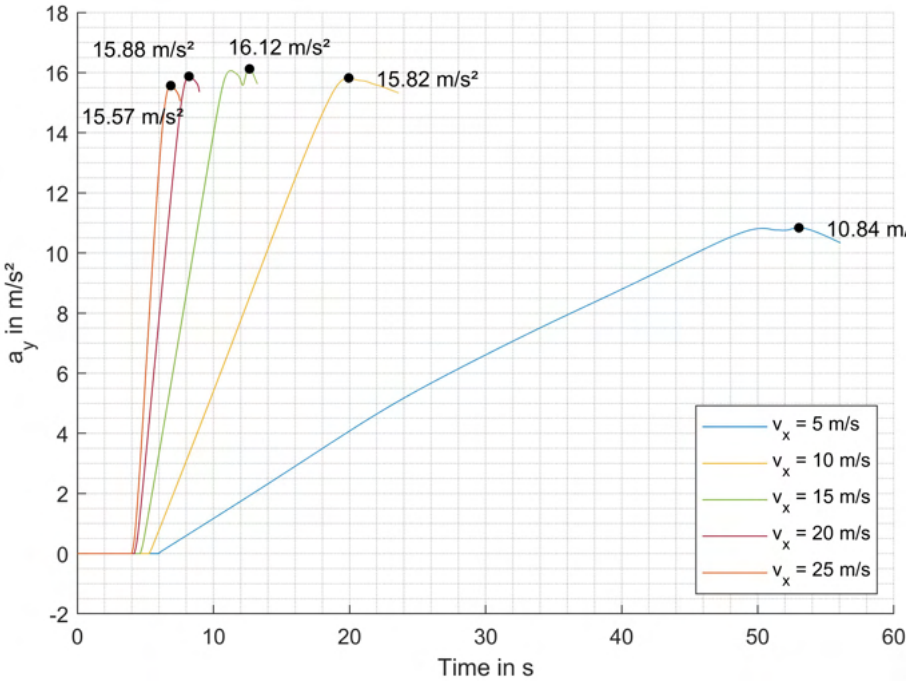

Source: Created by the author.

Figure 30 – Lateral performance with max-downforce aero package

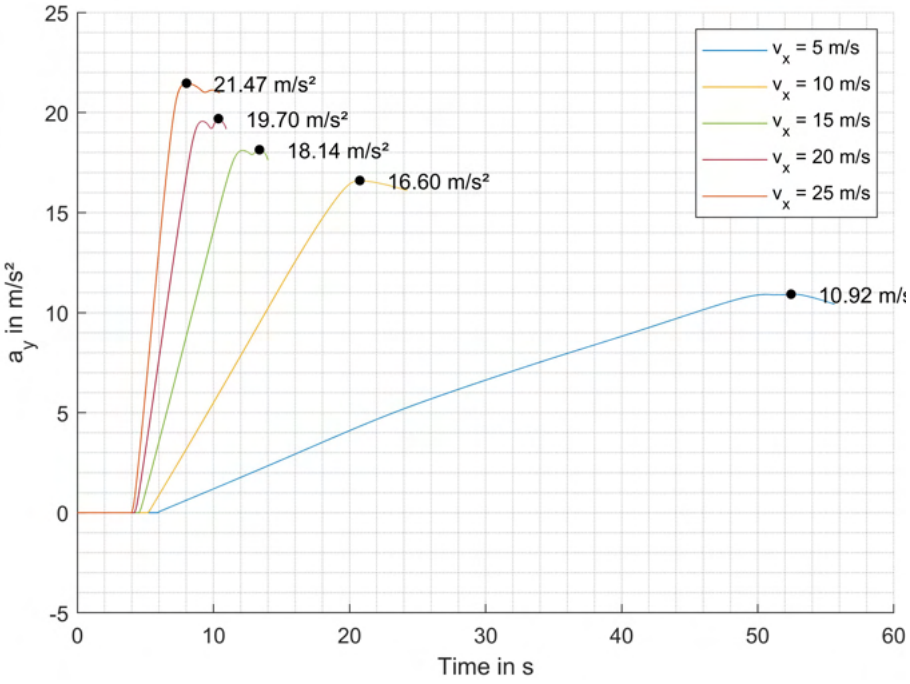

Source: Created by the author.

Figure 31 – Lateral performance with min-drag aero package

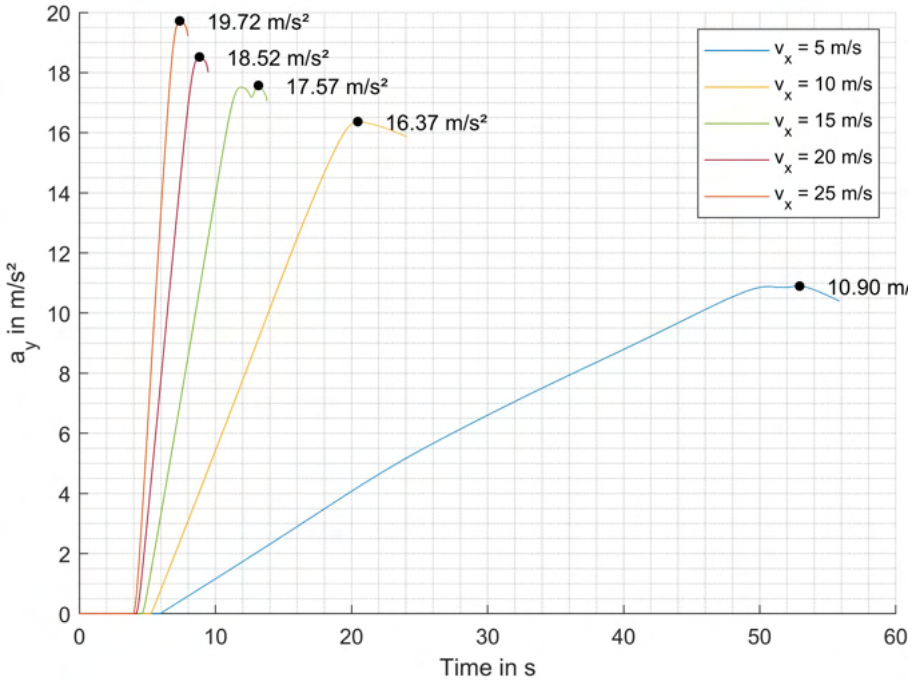

Source: Created by the author.

From the figures 29-31, the following consolidation can be done.

Table 7 – Lateral performance for each configuration

	Maximum a_y in m/s²		
Vehicle Speed	**Config 1**	**Config 2**	**Config 3**
5 m/s	11.37	11.38	11.38
10 m/s	18.90	19.76	19.51
15 m/s	19.52	21.91	21.22
20 m/s	19.35	23.72	22.44
25 m/s	19.08	25.98	23.93

Source: Created by the author.

Finally, these results can be plotted together in a graph to show the differences between the speed sensitivity of the maximum lateral acceleration of the vehicle for the different configurations.

Figure 32 – Lateral acceleration vs speed curves

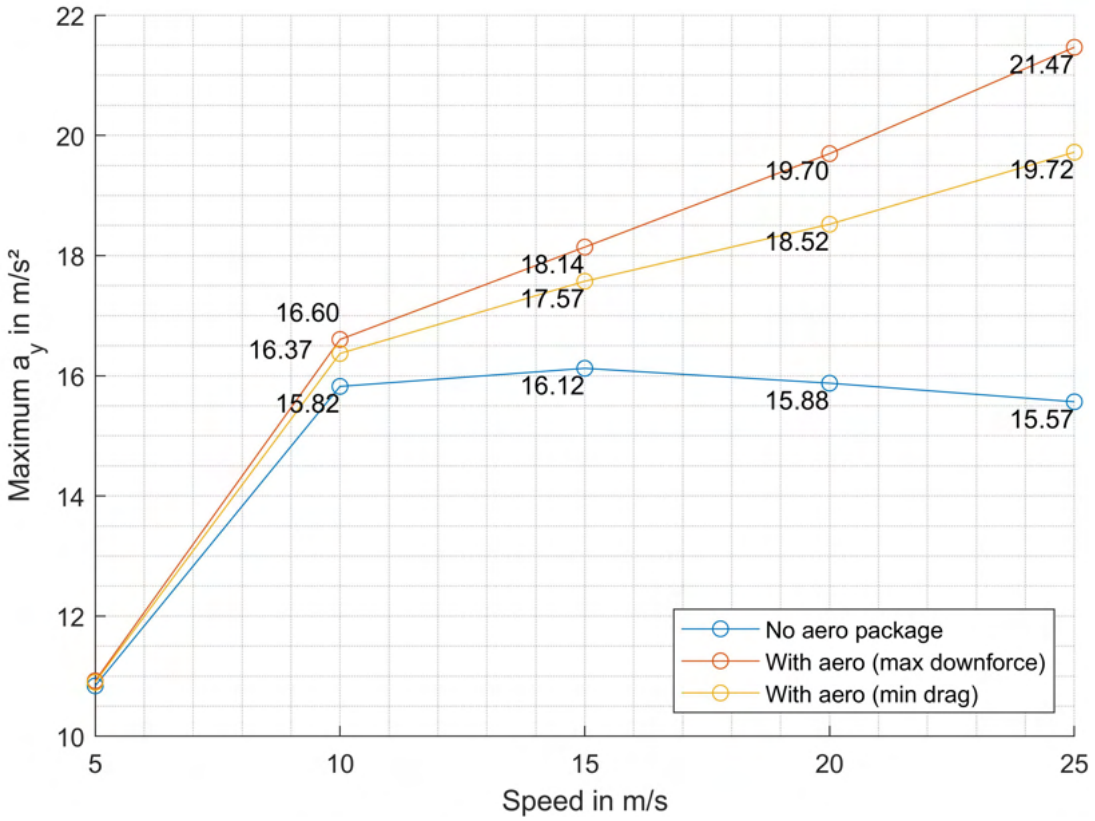

Source: Created by the author.

Here, the difference in vehicle performance is readily apparent. Configuration 2 exhibits superior cornering capabilities at speeds exceeding 5 m/s, highlighting the noticeable impact of a high-downforce aero package even at relatively low speeds. Furthermore, it is evident that the advantage of the high-downforce aero package becomes more pronounced as the speed increases, as expected.

Additionally, it can be observed that the cornering potential of the vehicle without the aerodynamic package diminishes with speed. This occurs due to the upward aerodynamic force experienced by the vehicle, attributed to the positive coefficient of lift associated with this particular configuration.

4.2.4 The evaluated performance envelope

With the $a_x = f(v_x)$ and $a_y = f(v_y)$ curves extracted from previous sections, it is now possible to use the Equation 3.6 to derive the performance envelopes for each configuration. The evaluated performance envelopes are depicted below. For each configuration, both a two-dimensional and a three-dimensional envelope visualization were created. To help visualization, in the 2D cases, the curves representing a few speeds were highlighted while the others appear in black.

Figure 33 – 2D performance envelope (Config 1)

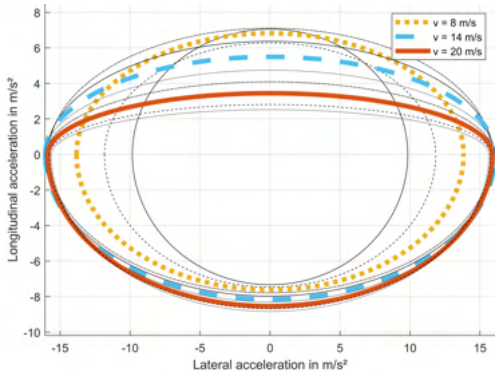

Source: Created by the author.

Figure 34 – 3D performance envelope (Config 1)

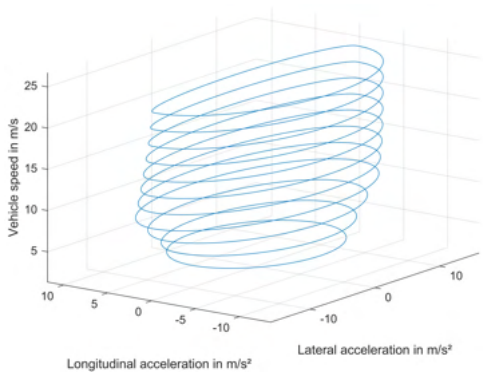

Source: Created by the author.

Figures 33 and 34 show the configuration without a dedicated aerodynamic package. It becomes clear from the graphs that the envelope suffers a loss in lateral acceleration for higher speeds. Note that the curve for $v = 14m/s$, is slightly further outwards in the x-axis than the curve for $v = 20m/s$, which also appears on the 3D plot. As previously mentioned, this is due to the aerodynamic lift forces produced by the vehicle at higher speeds.

Figure 35 – 2D performance envelope (Config 2)

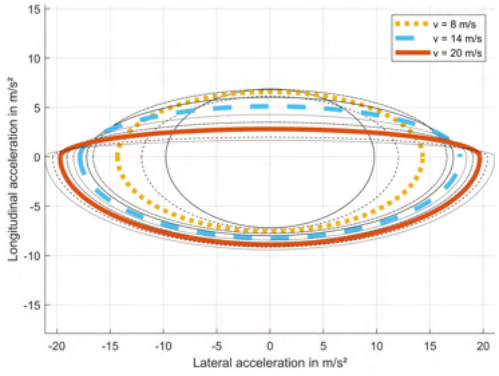

Source: Created by the author.

Figure 36 – 3D performance envelope (Config 2)

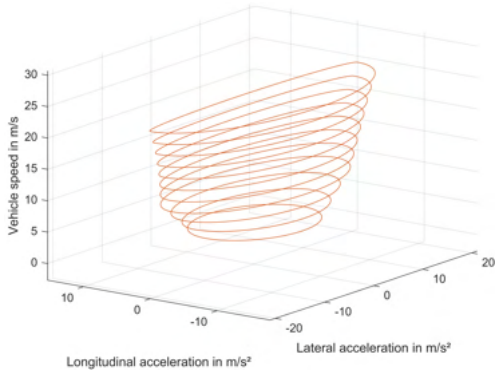

Source: Created by the author.

Figure 37 – 2D performance envelope (Config 3)

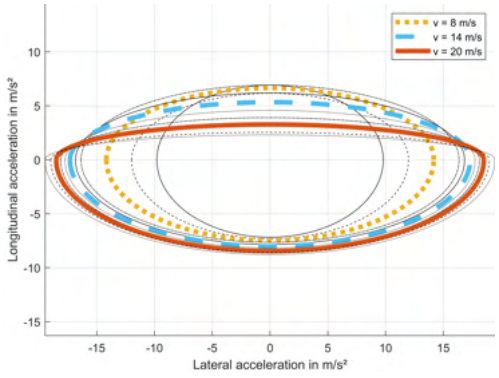

Source: Created by the author.

Figure 38 – 3D performance envelope (Config 3)

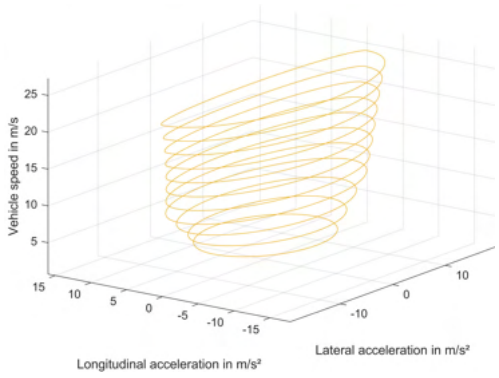

Source: Created by the author.

Figures 35 to 38 show the configurations with a dedicated aerodynamic package. Here, the loss of lateral performance with speed does not occur due to the negative lift produced by the aerodynamic devices. When comparing configurations 2 and 3, the compromise between longitudinal and lateral performance becomes clear: configuration 2 has an envelope that can achieve higher lateral and braking accelerations, but for the same speeds, is able to achieve lower positive accelerations. That comes from the fact that it has a lower coefficient of lift, but a higher coefficient of drag.

In conclusion, the analysis conducted using the performance envelopes of the vehicle has proven to be highly valuable in evaluating the potential differences in performance that can be achieved with a particular configuration. By examining the acceleration, braking, and lateral dynamics envelopes, valuable knowledge about the capabilities and limitations of the vehicle under various driving conditions were gathered.

While the analysis conducted thus far has provided significant insights, it is crucial to remember that the ultimate goal of a race car is to achieve the lowest possible lap time around a given circuit. To accomplish this, trajectory optimization and lap time estimation based on the previous analysis become essential tools in further refining the vehicle's performance.

The upcoming section will delve into the concept of trajectory optimization and how the analysis done until now can be aimed at determining the optimal path and vehicle dynamics to minimize lap times. By integrating the knowledge gained from the vehicle and coupling it with a particular track, the present methodology proves to be a powerful tool.

4.3 Evaluation of the trajectory optimization algorithm

The following section will present the results obtained by applying the methods explained in section 3.3 for the trajectory optimization and lap time estimation around a specific track, leveraging the acquired knowledge from previous analyses to push the bound-

aries of performance while building upon the foundation established by the examination of performance envelopes and their representation of vehicle behavior.

Until this point, the race vehicle has been examined as an independent entity, offering answers about its responsiveness to parameter variations. However, this isolated analysis falls short of providing a definitive determination regarding the optimal combination of parameters to employ. To illustrate this challenge, let us consider the performance envelopes discussed in subsection 4.2.4. Within these envelopes, it remains unclear whether configuration 2's superior lateral performance compensates for its deficiency in forward acceleration. This becomes particularly relevant when navigating tracks characterized by lengthy straights and low-speed corners. To overcome this analysis limitation, the interaction between the vehicle with a particular configuration and a track layout must be considered.

Here, the nonlinear model predictive controller described in section 3.3 will be used. As a recap, this method revolves around simulating the trajectory of the vehicle as it traverses a track. At each simulation step, an optimization algorithm comes into play, aiming to determine the optimal control sequence, which in this case involves the vehicle's longitudinal and lateral acceleration. The goal of this optimization is to maximize the distance covered by the vehicle within a defined horizon.

The optimization process takes into account various factors, including the equations of motion derived from the point-mass model, the track boundaries, and the newly defined speed-dependent performance envelope. The mathematical representation of the problem is as follows:

$$\min_{\mathbf{u}} \quad J$$

Subject to:

$$\begin{aligned} &\tfrac{\mathrm{d}\mathbf{x}}{\mathrm{d}t} = \dot{\mathbf{x}}(\mathbf{x}, \mathbf{u}), \quad \mathbf{x}(0) = \mathbf{x_0} && \text{(Vehicle equations)} \\ &c_i < 0 && \text{(Performance envelope and road constraints)} \\ &\mathbf{u}_L < \mathbf{u} < \mathbf{u}_u && \text{(Control bounds)} \end{aligned} \tag{4.1}$$

for the prediction horizon $\quad t - t_0 \in [\Delta t, \cdots, p\,\Delta t]$

These equations encapsulate the dynamic interactions between the vehicle, the track, and the defined constraints, enabling the formulation of an optimization problem that can be efficiently solved to find the control inputs that yield the optimal trajectory. The problem was implemented using Matlab's Model Predictive Toolbox and the results will be shown in the following sections.

4.3.1 Definition of the tracks to be evaluated

Since the object of analysis is a formula student vehicle, some consideration around the common types of tracks that such a vehicle performs in must take place. Circuits used in Formula Student competitions have specific characteristics designed to test the agility, maneuverability, and overall performance of the participating cars, but in a safe, relatively low-speed environment. The most relevant characteristics of such tracks are:

a) Compact Layout: Formula Student circuits are typically designed on a relatively small area, such as a parking lot or open field. The layout often includes a combination of tight corners, slaloms, chicanes, and short straights. The compact layout challenges the driver'cas ability to quickly change direction and navigate through the course with precision.

b) Variety of Turns: Autocross circuits feature a variety of turns, including hairpin turns, 90-degree corners, sweeping curves, and slaloms. This diversity of turns tests the car's handling capabilities and the driver's skill in finding the optimum racing line to maintain speed and momentum throughout the course.

c) Short Straights: Although autocross circuits mainly consist of corners, there are usually short straight sections incorporated to provide opportunities for acceleration and gear changes. These straights allow cars to briefly reach higher speeds and evaluate their acceleration capabilities before entering the next corner.

The selection of the track layout for evaluating the vehicle was influenced by these specific characteristics. However, to explore the impact of track layout on the optimal vehicle configuration, an alternative track, which deviates from the standard formula student track, will also be taken into account. Therefore, the analysis of vehicle configuration will be done in two different track layouts: a scaled version of the circuit of Zandvoort, which contains a series of tight corners, and a scaled version of the Red Bull Ring, also called Spielberg Circuit, which is known for having long straights, connected by near 90° curves, and a combination of medium to high-speed corners.

Figure 39 – Track layout - Zandvoort Circuit

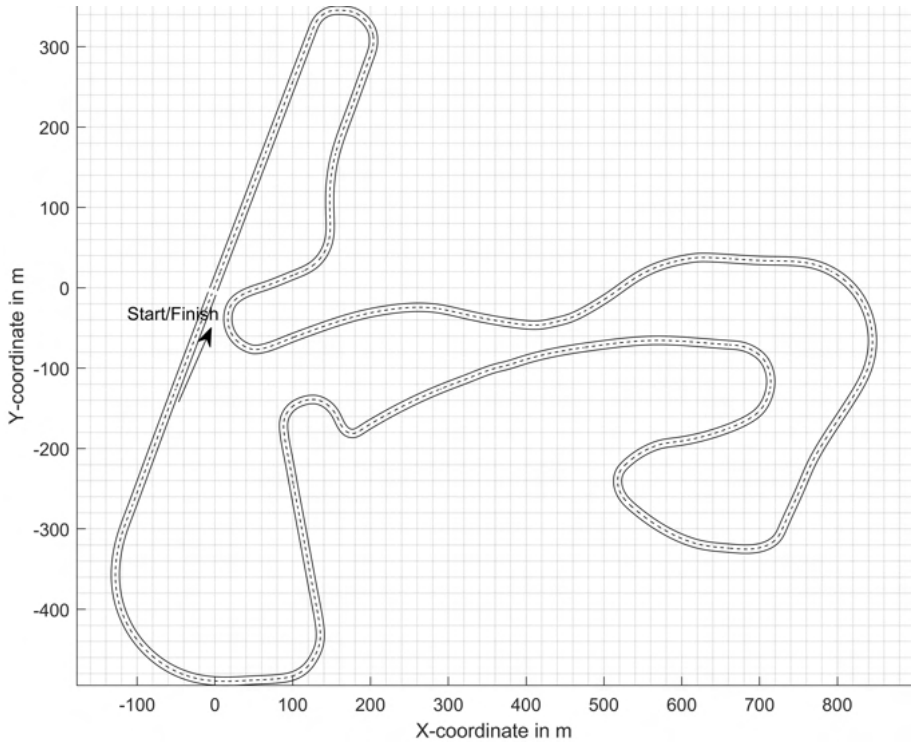

Source: adapted from HEILMEIER, A.[45].

Figure 40 – Track layout - Spielberg

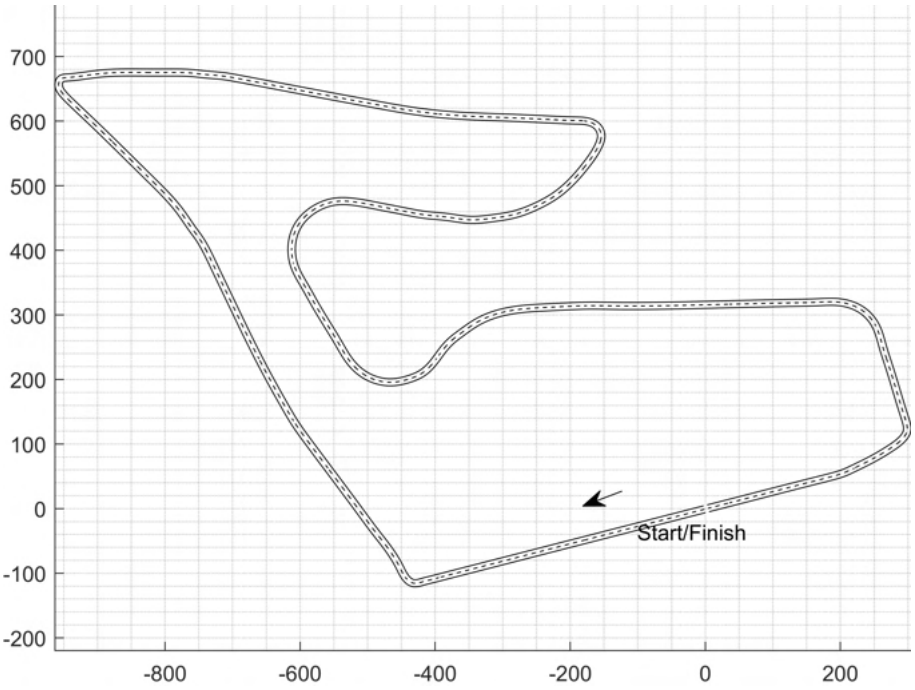

Source: adapted from HEILMEIER, A.[45].

Figure 39 showcases the Circuit of Zandvoort, with its fast straights, demanding

hairpin turns, and technical sequences, the circuit offers a challenging combination of tightly-wound corners. In contrast Figure 40 shows the layout of the Spielberg Circuit. Notice how, in comparison with the previous circuit, it presents long straights and corners that are often traveled at high rates of speed. These two tracks will serve as a basis for the comparison between the configurations mentioned earlier.

4.3.2 Lap time comparison between configurations

Using the method mentioned in section 3.3, the simulation of the lap time was implemented in Matlab. Due to the complexity of the system and the wide range of scenarios, there were instances where the simulation could not yield useful results due to the controller diverging during the solution or taking a very high amount of time. The multitude of variables and constraints made it difficult to find parameters that satisfied all desired criteria for a meaningful solution. In such cases, iterations and fine-tuning of the parameters were necessary. Adjustments and modifications were made to reach a feasible solution. This process demanded careful analysis, experimentation, and often involved collaboration with domain experts for valuable insights.

4.3.2.1 Simulation for the circuit of Zandvoort

The lap time simulation results for the three previously defined vehicle configurations traveling the Zandvoort circuit are presented in this section.

Figure 41 – Speed profile comparison - Zandvoort Circuit

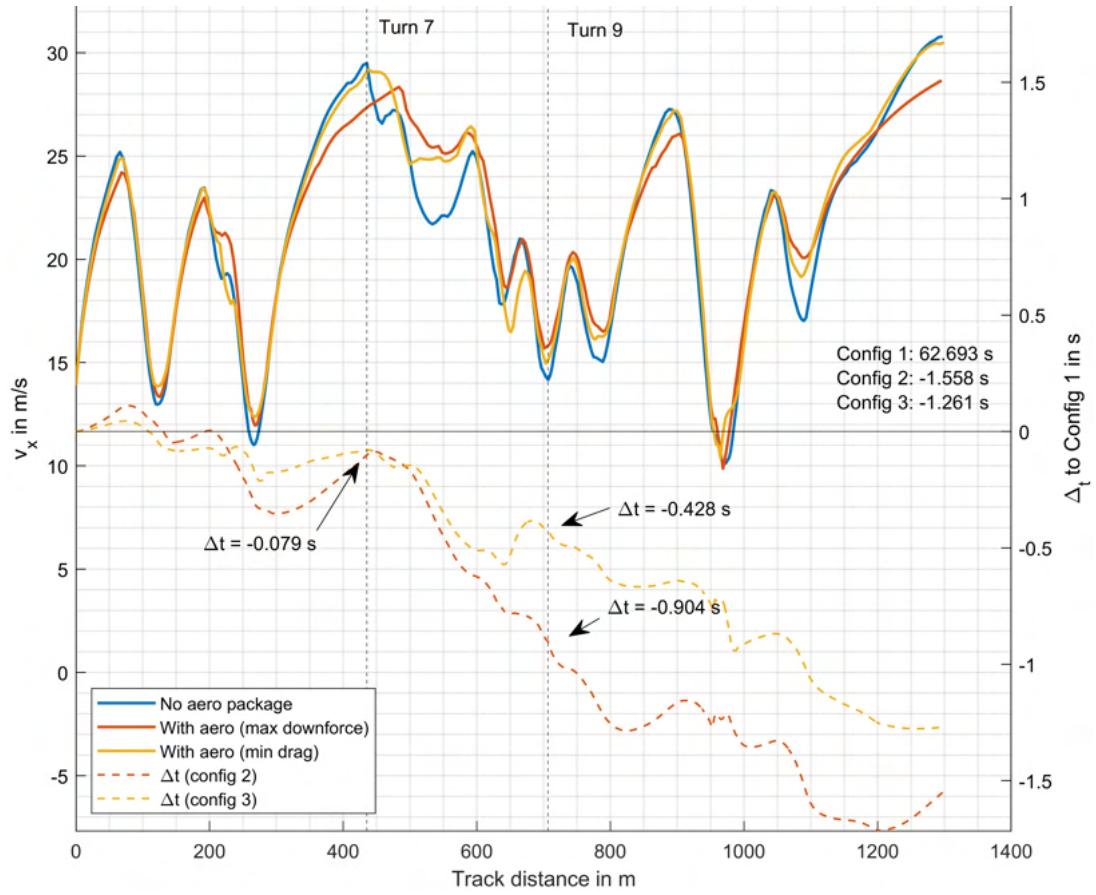

Source: Created by the author

Figure 41 illustrates the speeds achieved by different configurations at various points along the track distance. The solid lines represent the speeds for each configuration, while the dotted lines depict the time difference between configurations 2 and 3 compared to configuration 1 at each point. The time delta lines are particularly intriguing as they indicate whether a configuration is gaining or losing time relative to configuration 1 at a specific circuit location. A downward trend signifies that the corresponding configuration is faster than configuration 1 at that point.

From the graphs, it is evident that section 3.2 provides valuable insights into the vehicle's characteristics. Overall, incorporating an aerodynamic package results in lap time improvements of over 1 second. This advantage primarily stems from the central portion of the lap, which features a higher concentration of corners.

As anticipated, the maximum-aero-downforce configuration exhibits significant gains during cornering but may experience time loss on the straight sections. On the other hand, the minimum-drag-aero configuration gains less time compared to the base configuration around corners but does not suffer significant time loss on the straights.

A notable section where configuration 2 demonstrates substantial time gain is

during turns 7, 8, and 9. Despite entering the corner at a lower speed, the maximum-downforce vehicle can brake later and maintain a higher minimum speed throughout the corner. This results in an impressive time gain of 0.825 seconds across the three corners, which is very significant. In comparison, configuration 3 gains 0.345 s in the same section.

Figure 42 – Trajectory comparison - Zandvoort Circuit

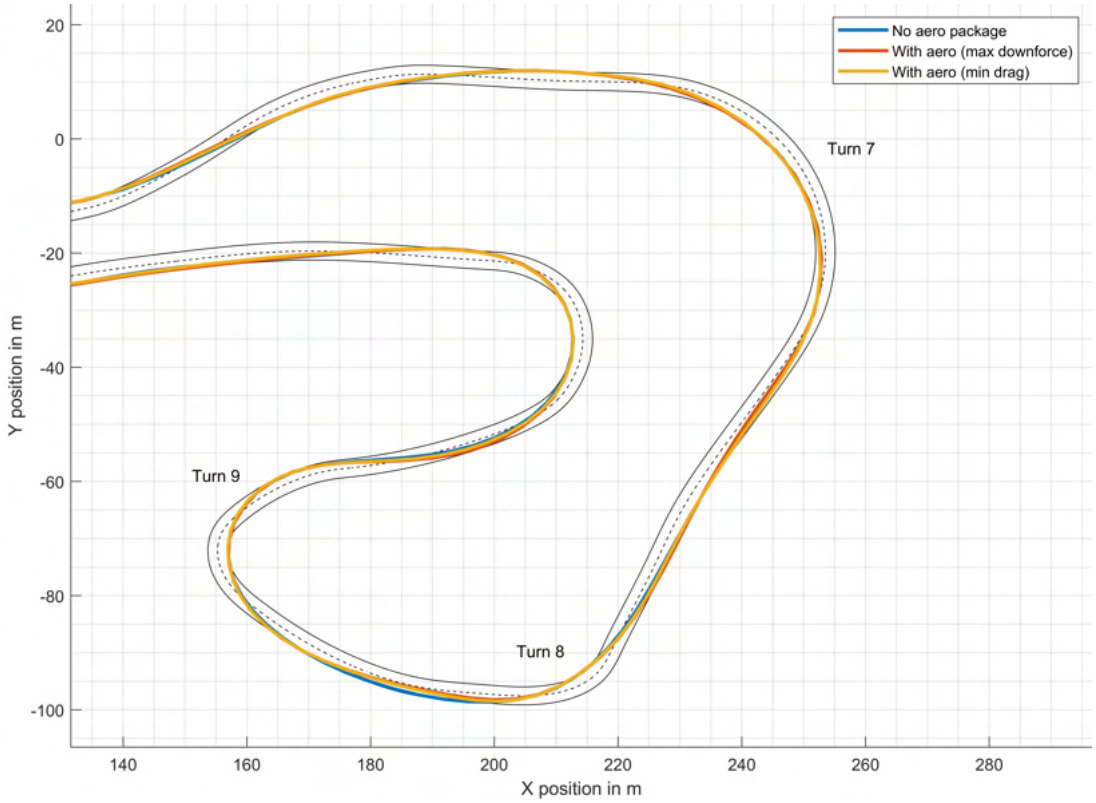

Source: Created by the author.

Figure 42 provides a visual representation of the paths taken by each configuration through the mentioned corner compound. Observing the trajectories, it becomes evident that there is minimal variation among them, suggesting that the discrepancies in section time primarily arise from the ability to attain higher cornering speeds. Nevertheless, an analysis of longitudinal and lateral acceleration profiles can also be valuable to gain further insights into the vehicle's performance.

Figure 43 – Acceleration profile comparison - Zandvoort Circuit

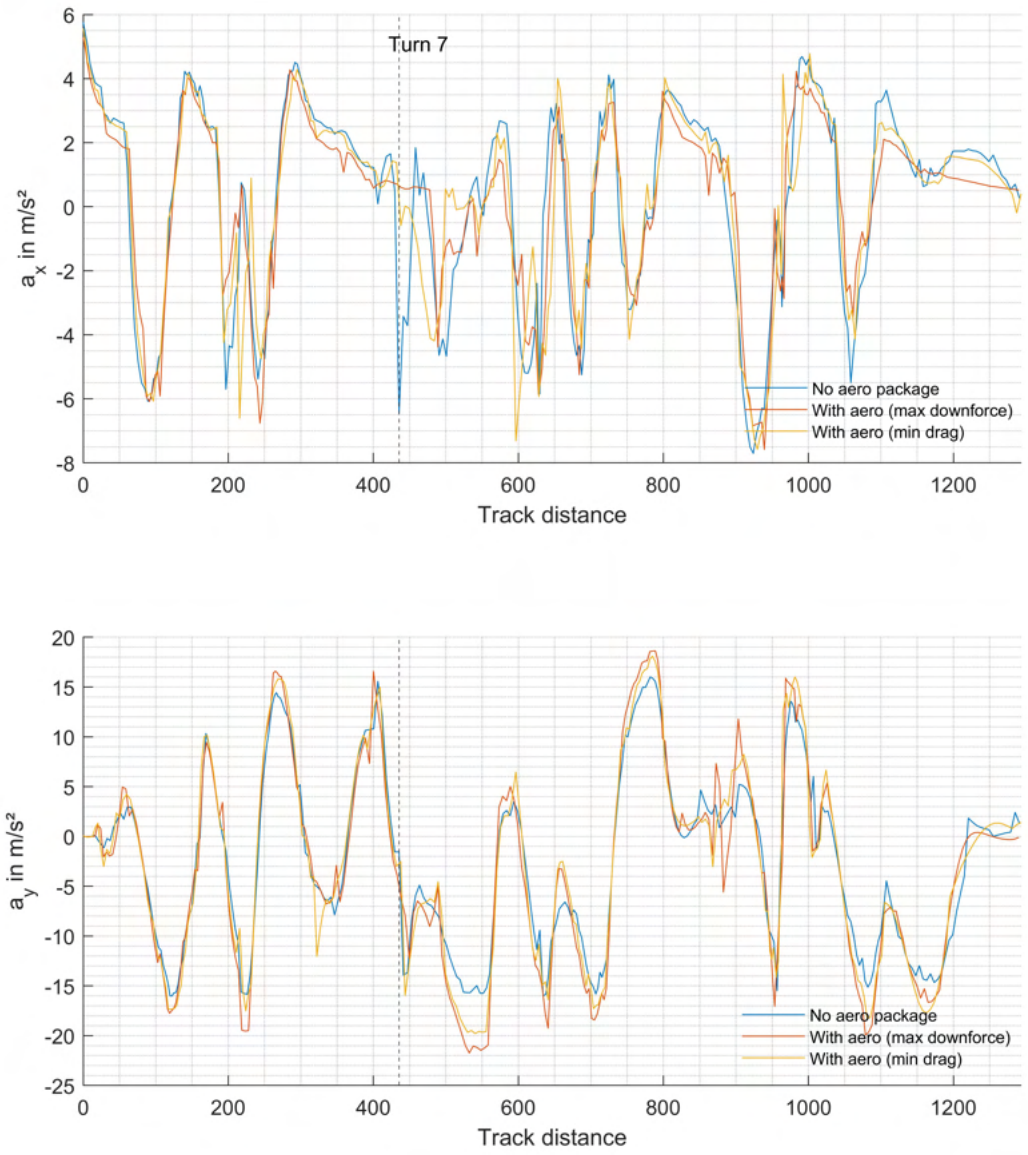

Source: Created by the author

Figure 43 showcases the acceleration plots for the three vehicles. Examining the plot, it becomes apparent that the max-downforce aerodynamic package, with its increased air resistance, leads to lower accelerations for vehicle 2 in the acceleration zones. However, it compensates by demonstrating more intense braking capabilities, particularly from higher speeds, and sometimes even eliminates the need for braking, such as in turn 7. Additionally, configurations equipped with an aerodynamic package exhibit the ability to achieve higher lateral acceleration. This effect is especially pronounced in the high-speed sections, highlighting the significant advantages offered by aerodynamic enhancements.

In conclusion, each configuration exhibits strengths in specific sections of the circuit, and it is the cumulative effect of these relative advantages over a lap that determines the overall speed superiority of a vehicle.

Figure 44 – 3D speed visualization - Zandvoort Circuit

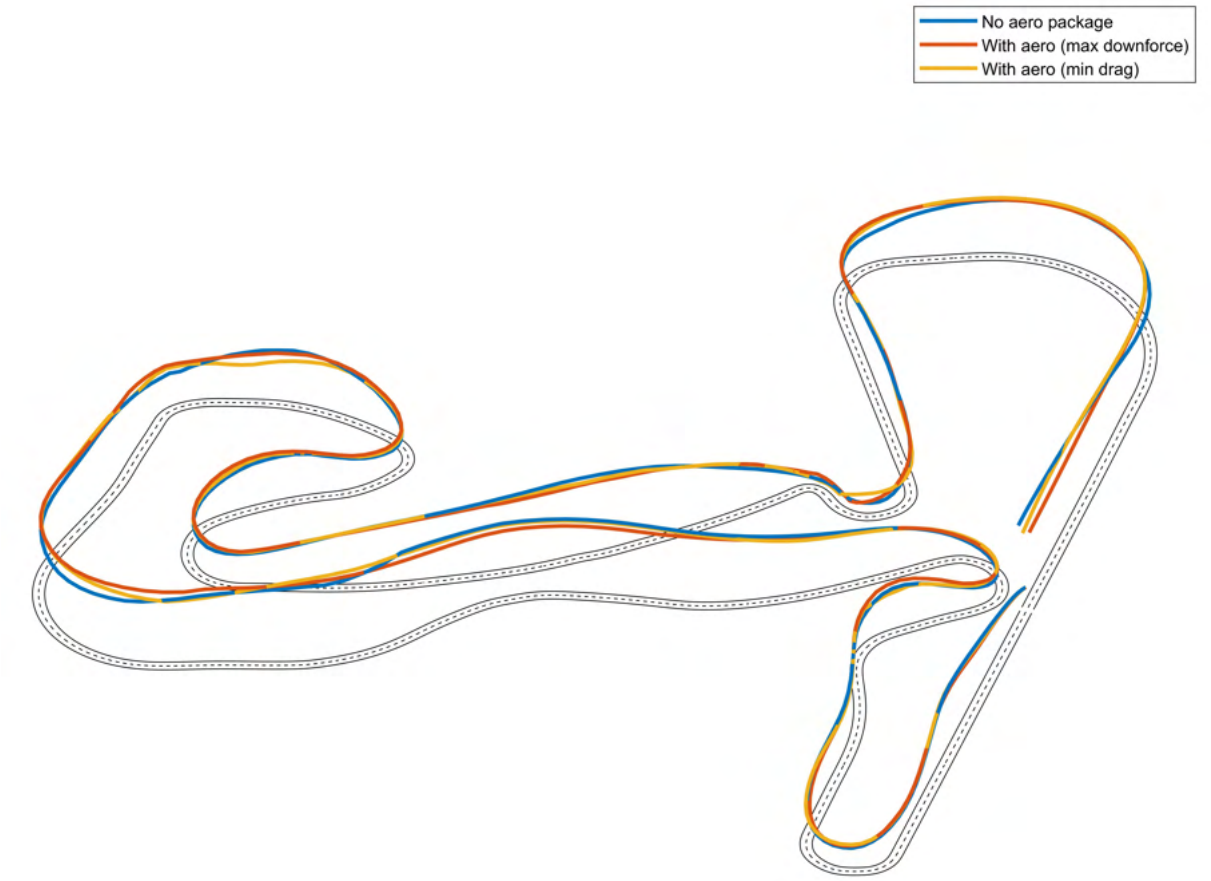

Source: Created by the author

Note: The track layout is presented in gray, in 2D. The higher the curve, the faster the vehicle was at that point of the circuit

To illustrate this point, Figure 44 presents a three-dimensional visualization where the speed of each vehicle is plotted on the vertical axis for different sections of the track. This visualization effectively demonstrates that while configuration 2 showcased an overall higher speed, there are distinct parts of the track where other configurations excel and display the highest speed.

4.3.2.2 Simulation for the circuit of Spielberg

To gain a more general understanding of the performance of the three configurations, it is beneficial to analyze them on a different track layout, for the speed characteristics of a track can significantly impact the relative performance of vehicle configurations. In this

regard, the lap simulation was conducted on the Spielberg circuit for the configurations under investigation. The subsequent results are presented and discussed below.

Figure 45 – Speed profile comparison - Spielberg Circuit

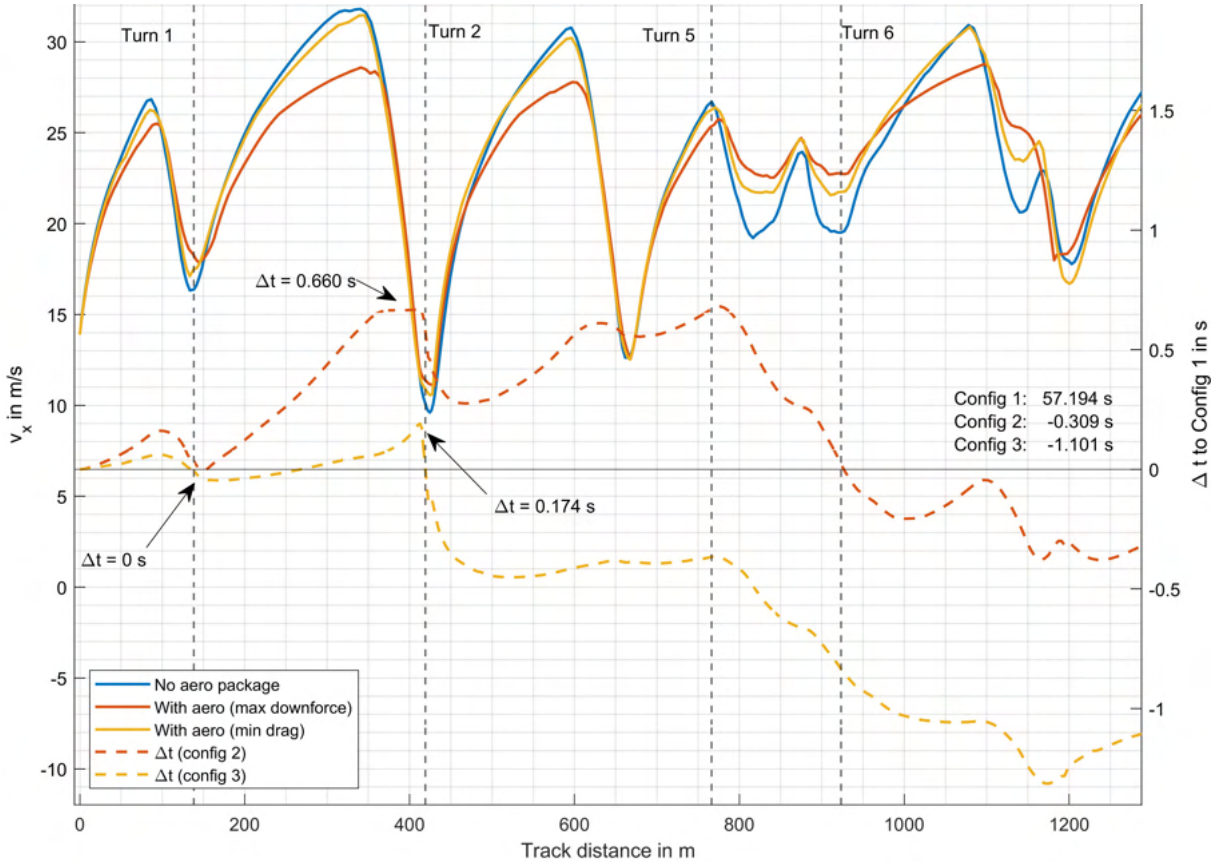

Source: Created by the author

Although the vehicle setups remain the same as in the previous simulation, their characteristics manifest differently when navigating a lap at the Spielberg Circuit. In this context, the same advantageous impact of the aerodynamic package can be seen. Both configurations with aerodynamic enhancements outperformed the non-aero configuration in terms of lap time. However, the differences in lap time are not only smaller but also configuration 3, featuring a lower drag-to-downforce ratio, emerges as the fastest.

As demonstrated earlier, the Spielberg Circuit is characterized by long straights and low-speed 90° corners. In relation to configuration 3, these track features accentuate the weaknesses of configuration 2. Configuration 2 achieves lower top speeds on the straights, resulting in a time loss of 0.66 seconds on the second straight alone. Furthermore, it cannot fully exploit the benefits of its aerodynamic package until the last corners since the first corners are relatively low-speed. In contrast, the min-drag setup of configuration 3 strikes a balance between straight-line speed and cornering capabilities. It experiences lesser time loss to configuration 1 on the straights and is capable of gaining significant time both on

the slow-speed turn 2 and on the high-speed turns 5 and 6.

Figure 46 – Acceleration profile comparison - Spielberg Circuit

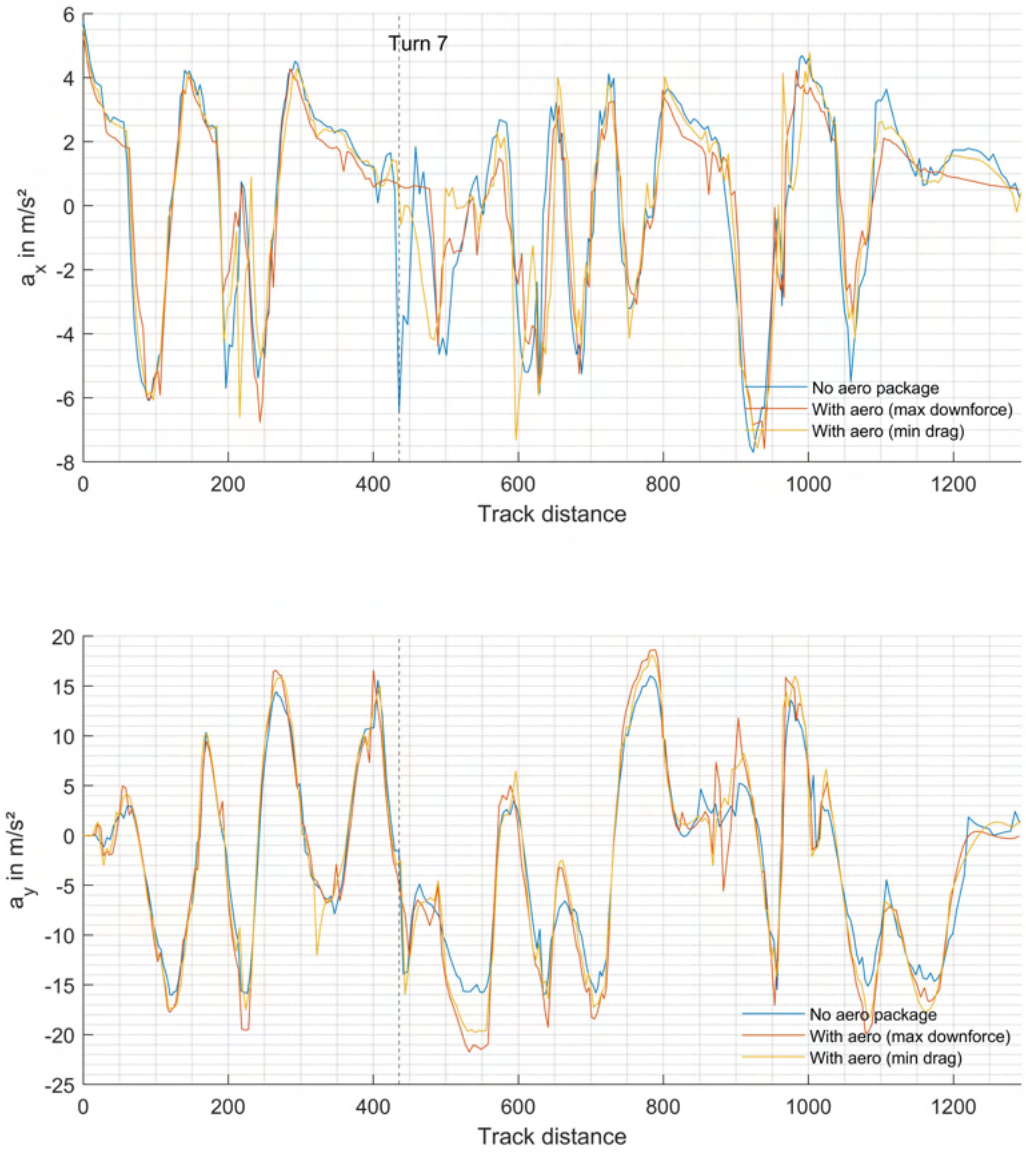

Source: Created by the author

Similar to the observations made for the Zandvoort Circuit, it is apparent that configurations with lower drag excel in achieving faster accelerations out of corners and along the straights. Conversely, configurations with higher downforce demonstrate greater lateral acceleration, particularly at higher speeds. However, in contrast to the previous circuit, the requirement for substantial lateral acceleration remains relatively low until past the halfway point of the track, while a significant demand for forward acceleration

emerges right from the initial parts of the lap.

As previously established, the min-drag-aero setup strikes a balance in performance, proving to be advantageous in both longitudinally dominated and laterally dominated sections of the track. This versatility contributes to its overall superiority in lap time, as it performs well in various aspects across the entirety of the track.

The tridimensional visualization of speed around the track, as depicted in Figure 47, highlights that there is a significant variation in speed during the initial portion of the track (longitudinally dominated), followed by a more flowing section towards the end (lateraly dominated).

Figure 47 – 3D speed visualization - Spielberg Circuit

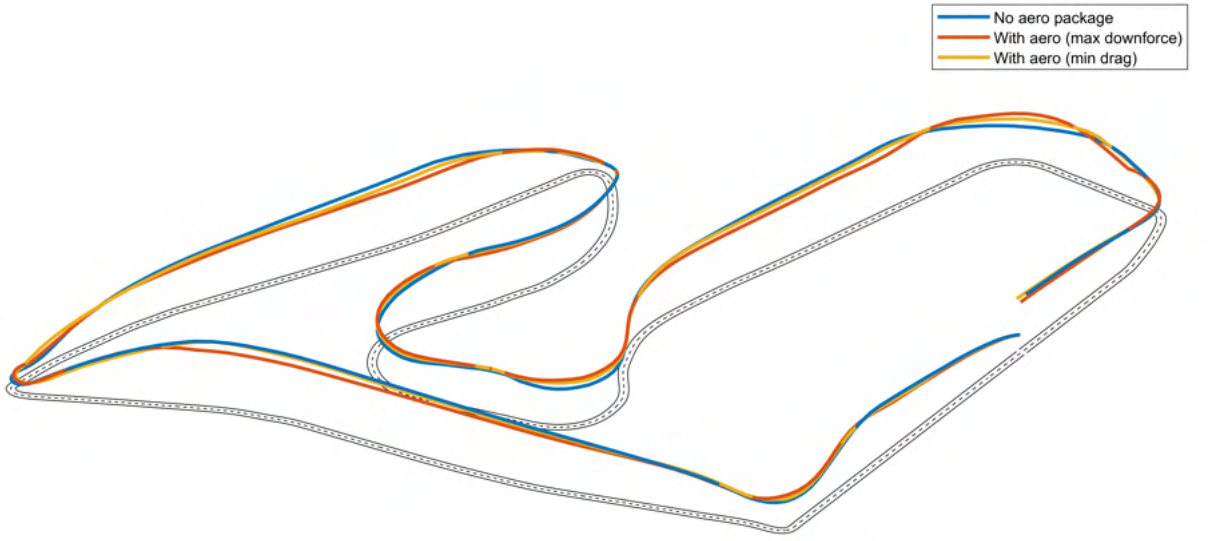

Source: Created by the author

Table 8 provides an overview of the lap times achieved by both configurations for both circuits

Table 8 – Vehicle configurations

	Config 1	**Config 2**	**Config 3**
Zandvoort	62.693 s	61.135 s	61.423
Spielberg	57.194	56.885	56.093

Source: Created by the author.

This analysis was done for a variety of circuits and the results are presented in

4.3.2.3 Considerations about the lap simulation

In conclusion, the lap time simulation and analysis of three different vehicle setups across two distinct circuits have provided valuable insights into their performance characteristics.

In both circuits, it was evident that each configuration demonstrated strengths in specific sections of the track. The overall lap time superiority of a configuration stemmed from the collective impact of its relative advantages across the entire lap. Furthermore, visualizations of speed variations provided additional insights into the track-specific challenges and demands faced by the configurations.

These findings underscore the significance of carefully selecting vehicle setups and aerodynamic packages based on the characteristics of the track. Based on these simulations, a performance engineer would be able to make an informed decision regarding the wing levels of a race car. It emphasizes the need for a balanced approach that optimizes both straight-line speed and cornering capabilities. The results of this chapter contribute to proving that the use of lap time simulation software is of extreme importance when defining vehicle setup for a given track since by definition the minimum lap time is a result of the interaction of the race car with the track.

4.3.3 Considerations about the NMPC method

The latter section emphasized how useful the analysis of the minimum lap time of vehicle can be. In this context, the tool used for the implementation of theses simulations are crucial. In the current example, the nonlinear model predictive Control (NMPC) has emerged as a powerful technique for optimizing the trajectory of the vehicle around a track. By considering the vehicle's dynamics and incorporating constraints such as speed-dependent performance envelopes and track layouts, the method offers the potential for enhanced control and improved performance. However, there are challenges associated with this approach, particularly in ensuring the convergence of the optimization solver. This section will discuss the convergence problem faced by NMPC and explore its implications for vehicle trajectory optimization.

4.3.3.1 The Convergence Problem

One of the primary challenges encountered when using NMPC for vehicle trajectory optimization is the convergence problem of the optimization solver. NMPC involves solving an optimization problem repeatedly at each control interval to determine the optimal control inputs that drive the vehicle along the desired trajectory. However, achieving convergence in a consistent manner can be a complex task due to several factors.

The nonlinear nature of vehicle dynamics and the high dimensionality of the optimization problem pose significant challenges for the solver. These nonlinearities come

from the model used, but mainly from the interaction between the movement of the vehicle in relation to the track. Their presence can lead to multiple local optima, where the solver might get trapped and fail to converge to the global optimum. Besides that, its computational complexity grows exponentially with the number of decision variables and constraints, making the convergence computationally demanding and time-consuming. To overcome the convergence problem associated with NMPC for vehicle trajectory optimization, several different strategies were used.

The first was regarding the initial guess taken by the solver. After successful optimization in one step of the simulation, the predicted, optimal state and control trajectory is available. Therefore, to provide a good initial guess, the solver was initiated with the solution from the previous iterations.

Additionally, when the solver failed to optimize at a given simulation step, which happened when it converged to a non-feasible solution, or when the number of function evaluations was over a threshold, the implemented code checked if the successfully converged solution from a previous step can be used. That was accomplished by, instead of repeating the last acceleration input, applying at the present step, the acceleration inputs that the solver predicted as optimal earlier, extrapolating the missing steps of the optimizing with the use of the state equations.

A substantial part of the work also revolved around defining the correct parameters for the optimization solver and the controller horizons. It was a challenging task that required striking a balance between computational efficiency, solver robustness, and solution performance. Finding the optimal set of parameters for the solver proved to be difficult. Emphasizing computational efficiency too much would yield quick but potentially unreliable solutions. Conversely, prioritizing solver robustness excessively could lead to conservative outcomes that compromised system performance.

Determining the appropriate controller horizons also posed a significant challenge. On one hand, shorter horizons offered faster response times but risked instability or suboptimal results, as well as failing to perform well in long corners, or when a tight corner followed a long straight, which would require a long period of braking, several meters before the corner itself. On the other hand, longer horizons provided more stability and improved vehicle performance, but at the cost of the increased computational burden.

A unique aspect of this work was the requirement for the solver to calculate control inputs not only for the initial steps of the prediction horizon but also for the portion near the end of the horizon, specifically the segment that directly interacts with corners. Unlike typical applications where only the first control steps are calculated, this particular simulation demanded a comprehensive evaluation of control inputs throughout the entire prediction horizon. To mitigate the computational complexity resulting from an excessive number of variables, a strategy was implemented to selectively calculate control inputs

at specific points within the prediction interval while using interpolation to define the remaining control inputs. Crucially, a uniform distance between these decision points was maintained across the entire prediction horizon.

Overall, defining the correct parameters for the optimization solver and the controller horizons presented a formidable challenge. Striving for a balance between computational efficiency, solver robustness, and solution performance required meticulous attention to detail and an understanding of the system dynamics. While some simulations proved challenging, the pursuit of an optimal solution ultimately pushed the boundaries of understanding the system and refined the approach.

5 CONCLUSIONS AND FURTHER WORK

5.1 On the knowledge acquired through the work

The insights gained through this process were multifaceted. Firstly, the process of developing such a comprehensive model necessitated a deep dive into the intricate details of vehicle dynamics, including suspension systems, tire behavior, aerodynamics, and drivetrain characteristics. By modeling these subsystems and integrating them within the Simulink and Matlab environment, the author gained a thorough understanding of the interplay between these components and their impact on overall vehicle performance. The development of a complex, modular, and user-friendly model for vehicle simulation, incorporating subsystem modeling and integration of mathematical models within Simulink and Matlab, proved to be a significant source of understanding and knowledge enhancement for the author in the field of vehicle simulation techniques.

Moreover, the performance envelope analysis allowed for a simple but representative understanding of the limits and capabilities of the race car. It provided crucial information about the car's performance boundaries, ensuring that the optimized trajectory remained within safe and feasible operating limits.

The trajectory optimization utilizing the model predictive controller revealed the sensitivity of lap times to various parameters. It provided insights into the trade-offs between speed, acceleration, braking, and cornering, enabling the identification of key areas for improvement. By analyzing the optimized trajectories, it was possible to uncover optimal racing lines, ideal braking points, and the most effective ways to negotiate corners.

Furthermore, comparing the results obtained from simulating different vehicle configurations shed light on the impact of design choices on performance. It allowed for the identification of the most effective setups for specific tracks or driving conditions. By analyzing the differences in lap times, stability, and handling characteristics between the configurations, valuable insights were gained regarding the effects of aerodynamics, suspension setups, and other vehicle parameters.

5.2 On the limitations of the work

The developed solution faced two primary limitations that posed significant challenges. The first obstacle was the gathering of data for input parameters in the transient model. Acquiring accurate and comprehensive information about the race car's physical properties, suspension characteristics, tire behavior, aerodynamic coefficients, and drivetrain dynamics proved to be a time-consuming and complex task. The accuracy and reliability of the model's outputs were directly influenced by the quality of the input data,

making it crucial to ensure precise parameter values.

Secondly, the MPC developed for trajectory optimization presented notable achievements; however, it still exhibits considerable potential for improvement. Further enhancements can be achieved through careful adimensionalization of the model, which would allow for more generalized applicability and ease of parameter tuning. Additionally, exploring avenues for parallelization of the solution process can significantly enhance computational efficiency, enabling real-time feasibility for more complex racing scenarios. Furthermore, the implementation of techniques for quick differentiation of the cost, objective, and state functions can further refine the performance of the MPC, leading to more precise and responsive trajectory optimization. These avenues of refinement hold promising prospects for elevating the capabilities of the MPC and expanding its effectiveness in race car trajectory optimization.

5.3 On future work

The present thesis opens up several exciting possibilities for future work in the field of race car performance and trajectory optimization. Building upon the foundation laid by the developed solution, there are several avenues to explore in order to further enhance the understanding and capabilities of the software.

One potential area of focus is the development of a more detailed vehicle model. This could involve incorporating advanced suspension kinematics and compliance into the transient model, allowing for a more accurate representation of the car's behavior during dynamic maneuvers. By capturing the intricate interactions between the suspension components and the road surface, a more realistic simulation of the vehicle's handling characteristics can be achieved, leading to improved trajectory optimization.

Another aspect to consider is the refinement of the aerodynamic mapping within the model. By incorporating a more complex and accurate representation of the car's aerodynamic behavior, including the effects of side wind, pitch and height sensitivity, and flow separation, a higher level of fidelity can be attained. This would enable more precise estimation of the performance envelope and further enhance the optimization of the race car's trajectory.

In addition, the developed trajectory optimization software can be leveraged as an outer loop to provide real-time trajectories for autonomous racing vehicles. By integrating the software with an autonomous control system, the optimized trajectories can be used to guide the vehicle's actions on the race track. This would pave the way for the development of autonomous racing algorithms that can adapt and optimize their trajectory based on real-time information, leading to enhanced performance and competitiveness.

Furthermore, the potential exists to refine the model predictive controller (MPC)

with a more sophisticated internal model. By incorporating a more advanced vehicle model to capture the intricate dynamics of the race car, including tire-road interaction and transient behavior, a more accurate and effective MPC can be designed. This would involve delving deeper into nonlinear optimization and control techniques to ensure the controller's ability to handle complex scenarios and optimize the trajectory for minimum lap time.

5.4 Final Conclusions

Through the meticulous development and implementation of the software, incorporating a sophisticated 14-degree-of-freedom transient model of a race car and a nonlinear model predictive controller, this thesis presents a novel approach to the lap time simulation problem. By comprehensively analyzing vehicle performance and trajectory optimization, it offers valuable insights for achieving a more precise and efficient solution.

The utilization of the comprehensive model, encompassing vital dynamics such as suspension, tire behavior, aerodynamics, and drivetrain, facilitated a detailed understanding of the vehicle's capabilities and limitations. This intricate model enabled the estimation of the race car's performance envelope, which encompassed crucial factors such as maximum acceleration, braking, and lateral acceleration across a wide range of speeds.

Building upon the performance envelope as a constraint, a nonlinear model-predictive controller was diligently implemented. By employing a simplified point-mass model of the car, this controller engaged in an iterative optimization process to continually refine the trajectory for a complete lap around the race track, with the primary objective of achieving the minimum lap time. Throughout this iterative optimization, the controller dynamically adjusted parameters such as longitudinal and lateral acceleration time histories to ultimately determine an optimal trajectory.

By simulating three distinct vehicle configurations across two varied tracks, an extensive analysis of the race car's performance and behavior, along with its dependence on track characteristics, was conducted. This meticulous analysis yielded invaluable insights into the effects of different vehicle setups on lap times, handling characteristics, and overall performance. Such insights contribute to a deeper understanding of the intricate relationship between vehicle configuration, track features, and race performance.

The comprehensive integration of the sophisticated model, coupled with the iterative optimization process enabled by the nonlinear model-predictive controller, represents a significant advancement in understanding and optimizing the race car's trajectory. However, it is important to note that this work is not without its limitations and opportunities for further improvement. The developed model predictive controller still possesses potential for refinement, particularly through careful adimensionalization of the model, parallelization

of the solution process, and the implementation of techniques for quick differentiation of the cost, objective, and state functions. These avenues for improvement hold promise for advancing the performance and efficiency of the trajectory optimization process, ultimately leading to even more refined race car performance and lap times.

REFERENCES

1 GILLESPIE, T. **Fundamentals of vehicle dynamics**. [*S.l.: s.n.*]: SAE international, 2021. ISSN 1468601776.

2 MINAKER, B. P. **Fundamentals of vehicle dynamics and modelling: A textbook for engineers with illustrations and examples**. [*S.l.: s.n.*]: John Wiley and Sons, 2019. ISSN 1118980093.

3 RIEKERT, P.; SCHUNCK, T.-E. Zur fahrmechanik des gummibereiften kraftfahrzeugs. **Ingenieur-Archiv**, Springer, v. 11, p. 210–224, 1940. ISSN 0020-1154.

4 AMMON, D. **Modellbildung und Systementwicklung in der Fahrzeugdynamik**. [*S.l.: s.n.*]: Teubner, 1997. ISSN 3519023784.

5 DIEBOLD, L. *et al.* Einspurmodell für die fahrdynamiksimulation und-analyse. **ATZ-Automobiltechnische Zeitschrift**, Springer, v. 108, n. 11, p. 962–967, 2006. ISSN 2192-8800.

6 OLLEY, M. Road manners of the modern car. **Proceedings of the Institution of Automobile Engineers**, SAGE Publications Sage UK: London, England, v. 41, n. 1, p. 523–551, 1946. ISSN 0369-9838.

7 SEGEL, L. Theoretical prediction and response of the automobile to steering control. **Research in automobile stability and control in tire performance, proceedings of the automobile division of the institution of mechanical engineers**, v. 57, p. 26–46, 1956.

8 MCRUER, D. T.; KLEIN, R. H. **AUTOMOBILE CONTROLLABILITY. DRIVER/VEHICLE RESPONSE FOR STEERING CONTROL. VOLUME I. SUMMARY REPORT**. [*S.l.*], 1975.

9 MILLIKEN, W. F.; MILLIKEN, D. L. **Race Car Vehicle Dynamics**. SAE International, 1995. Available at: https://books.google.com.br/books?id=opgHfQzlnLEC.

10 SCHRAMM, D.; HILLER, M.; BARDINI, R. **Modellbildung und simulation der dynamik von Kraftfahrzeugen**. [*S.l.: s.n.*]: Springer, 2010. v. 124.

11 SETIAWAN, J. D.; SAFARUDIN, M.; SINGH, A. Modeling, simulation and validation of 14 dof full vehicle model. *In*: **International Conference on Instrumentation, Communication, Information Technology, and Biomedical Engineering 2009**. [*S.l.: s.n.*], 2009. p. 1–6.

12 ZAREIAN, A.; AZADI, S.; KAZEMI, R. Estimation of road friction coefficient using extended kalman filter, recursive least square, and neural network. **Proceedings of the Institution of Mechanical Engineers, Part K: Journal of Multi-body Dynamics**, SAGE Publications, v. 230, n. 1, p. 52–68, maio 2015. ISSN 1464-4193. Available at: https://doi.org/10.1177/1464419315573353.

13 AB, H. **Hexagon ADAMS Car**. 2023. Available at: https://hexagon.com/products/adams-car?accordId=C1B6F3FAB1E849EA92EEC86D120EBABF.

14 IKHSAN, N.; RAMLI, R.; ALIAS, A. Analysis of the kinematics and compliance of a passive suspension system using adams car. **Journal of Mechanical Engineering and Sciences**, v. 8, p. 1293–1301, 2015. ISSN 2231-8380.

15 BLUNDELL, M.; HARTY, D. **Multibody systems approach to vehicle dynamics**. [*S.l.: s.n.*]: Elsevier, 2004. ISSN 0750651121.

16 BALKWILL, J. **Performance vehicle dynamics: engineering and applications**. [*S.l.: s.n.*]: Butterworth-Heinemann, 2017. ISSN 0128126949.

17 MARCHESIN, F. P. *et al.* High downforce race car vertical dynamics: aerodynamic index. **Vehicle System Dynamics**, Taylor & Francis, v. 56, n. 8, p. 1269–1288, 2018. ISSN 0042-3114.

18 BENINI, C. *et al.* The influence of suspension components friction on race car vertical dynamics. **Vehicle system dynamics**, Taylor & Francis, v. 55, n. 3, p. 338–350, 2017. ISSN 0042-3114.

19 FERNANDES, M. A.; BARBOSA, R. S. Estudos em sistemas de direção veicular. 2005.

20 ROSOLIA, U.; CARVALHO, A.; BORRELLI, F. Autonomous racing using learning model predictive control. *In*: . [*S.l.: s.n.*]: IEEE, 2017. p. 5115–5120. ISSN 150905992X.

21 CIPELLI, M.; SCHIEHLEN, W.; CHELI, F. Driver-in-the-loop simulations with parametric car models. **Vehicle System Dynamics**, Taylor & Francis, v. 46, n. S1, p. 33–48, 2008. ISSN 0042-3114.

22 HEILMEIER, A.; GRAF, M.; LIENKAMP, M. A race simulation for strategy decisions in circuit motorsports. *In*: . [*S.l.: s.n.*]: IEEE, 2018. p. 2986–2993. ISSN 1728103231.

23 MARCHESIN, F. P.; BARBOSA, R. S. Análise de desempenho de veículos do tipo formula. 2012.

24 SHARP, R. S.; CASANOVA, D. A. N. I. E. L. E.; SYMONDS, P. A mathematical model for driver steering control, with design, tuning and performance results. **Vehicle system dynamics**, Taylor & Francis, v. 33, n. 5, p. 289–326, 2000. ISSN 0042-3114.

25 KELLY, D. P. Lap time simulation with transient vehicle and tyre dynamics. Cranfield University, 2008.

26 SIEGLER, B.; CROLLA, D. Lap time simulation for racing car design. **SAE Transactions**, JSTOR, p. 306–314, 2002. ISSN 0096-736X.

27 MASSARO, M.; LIMEBEER, D. J. N. Minimum-lap-time optimisation and simulation. **Vehicle System Dynamics**, Taylor & Francis, v. 59, n. 7, p. 1069–1113, 2021. ISSN 0042-3114.

28 TIMINGS, J.; COLE, D. Robust lap-time simulation. **Proceedings of the institution of mechanical engineers, part D: journal of automobile engineering**, SAGE Publications Sage UK: London, England, v. 228, n. 10, p. 1200–1216, 2014. ISSN 0954-4070.

29 LöCKEL, S.; PETERS, J.; VLIET, P. van. A probabilistic framework for imitating human race driver behavior. **IEEE Robotics and Automation Letters**, IEEE, v. 5, n. 2, p. 2086–2093, 2020. ISSN 2377-3766.

30 BARI, S.; HAIDARI, A. S.; WOLLHERR, D. A fast approach to minimum curvature raceline planning via probabilistic inference. **arXiv preprint arXiv:2203.03224**, 2022.

31 SIEGLER, B.; DEAKIN, A.; CROLLA, D. Lap time simulation: Comparison of steady state, quasi-static and transient racing car cornering strategies. **SAE transactions**, JSTOR, p. 2575–2581, 2000. ISSN 0096-736X.

32 GADOLA, M.; CANDELPERGHER, A.; ADAMI, R. The impact of non-linear aerodynamics on racecar behaviour and lap time simulation. **SAE Transactions**, JSTOR, p. 2380–2386, 2002. ISSN 0096-736X.

33 CAMBIAGHI, D. *et al.* A tool for lap time simulation. **Society of Automotive Engineers, Paper**, n. 962529, 1996.

34 CASANOVA, D. **On minimum time vehicle manoeuvring: the theoretical optimal lap**. 2000. Tese (phdthesis) — Cranfield University, 2000.

35 CASANOVA, D.; SHARP, R. S.; SYMONDS, P. Minimum time manoeuvring: The significance of yaw inertia. **Vehicle system dynamics**, Taylor & Francis, v. 34, n. 2, p. 77–115, 2000. ISSN 0042-3114.

36 OPTIMUMG. **OptimumLap**. 2023. Available at: https://optimumg.com/product/optimumlap/.

37 RFPRO. **RF PRO**. 2023. Available at: https://rfpro.com/de/.

38 CHASSISSIM. **ChassisSim**. 2023. Available at: https://www.chassissim.com/.

39 RACETECH, A. **AVL Racetech**. 2023. Available at: https://www.avlracetech.com/software/.

40 GADOLA, M. *et al.* **A tool for lap time simulation**. [*S.l.*], 1996.

41 CANDELPERGHER, A.; GADOLA, M.; VETTURI, D. **Developments of a method for lap time simulation**. [*S.l.*], 2000.

42 ISERMANN, R. **Automotive control: modeling and control of vehicles**. [*S.l.: s.n.*]: Springer, 2022. ISSN 3642394396.

43 WINNER, H. Skript fahrdinamik und fahrkomfort. Class notes from the Vehicle Dynamics and Confort course at the TU Darmstadt university. 2019.

44 GMBH, F. S. G. **Formula Student Germany**. 2023. Available at: https://www.formulastudent.de/fsg/.

45 HEILMEIER, A.; GEISSLINGER, M.; BETZ, J. A quasi-steady-state lap time simulation for electrified race cars. *In*: **2019 Fourteenth International Conference on Ecological Vehicles and Renewable Energies (EVER)**. IEEE, 2019. Available at: https://doi.org/10.1109/ever.2019.8813646.

46 MATHWORKS. **Vehicle Dynamics Blockset**. [*S.l.*], 2023. Available at: https://www.mathworks.com/products/vehicle-dynamics.html.

47 HUCHO, W.-H. **Aerodynamik des Automobils: eine Brücke von der Strömungsmechanik zur Fahrzeugtechnik**. [*S.l.: s.n.*]: Springer-Verlag, 2013. ISSN 3642579035.

48 BREUER, B. Skriptum kraftfahrzeuge 2. Class notes from the Motor Vehicles II course at the TU Darmstadt university. 2001.

49 PACEJKA, H. **Tire and vehicle dynamics**. [*S.l.: s.n.*]: Elsevier, 2005. ISSN 0080543332.

APPENDIX

APPENDIX A – MODEL SUBSYSTEMS

The model is implemented in Simulink and is comprised of six subsystems: Aerodynamics, Brake, Drivetrain, Steering, Suspension, and Tires. The outputs are state variables that define each of the model's DoFs. In the following sections, the physical and mathematical modeling of each subsystem will be presented. Where suitable, the model's block diagrams will be illustrated.

A.1 Aerodynamics

The drag forces generated by the interaction of the vehicle with the surrounding air are modelled as a function of the relative speed between the air and the vehicle $v_{x,air}$, the angle of incidence β_{air} between the air and the central plane of the vehicle, the vehicle's frontal area A_x, the local air density ρ_{air} and on the non-dimensional drag coefficient c_D that is also a function of β_{air}[47, p. 180]. This function is defined by:

$$F_{x,aero} = \frac{1}{2} \cdot \rho_{air} \cdot A_x \cdot c_D(\beta_{air}) \cdot v_{x,air}^2 \tag{A.1}$$

Analogously, the lateral and vertical aerodynamic forces are modeled with the help of the side force coefficient c_S and the lift coefficient c_L:

$$F_{y,aero} = \frac{1}{2} \cdot \rho_{air} \cdot A_x \cdot c_S(\beta_{air}) \cdot v_{x,air}^2 \tag{A.2}$$

$$F_{z,aero} = \frac{1}{2} \cdot \rho_{air} \cdot A_x \cdot c_L(\beta_{air}) \cdot v_{x,air}^2 \tag{A.3}$$

Note that the frontal area and the longitudinal relative speed are used, regardless of the direction of the evaluated aerodynamic forces. Also, the frontal area and the air density are considered to be constant so that $F_{i,aero} = f(v_{x,air}, \beta_{air})$. For ease of calculation, the aerodynamic forces are assumed to be acting on the vehicle's center of gravity.

Similarly, the aerodynamic interactions create moments around the vehicle's axis that can are modeled as:

$$M_{x,aero} = \frac{l_0}{2} \cdot \rho_{air} \cdot A_x \cdot c_{M,x}(\beta_{air}) \cdot v_{x,air}^2 \tag{A.4}$$

$$M_{y,aero} = \frac{l_0}{2} \cdot \rho_{air} \cdot A_x \cdot c_{M,y}(\beta_{air}) \cdot v_{x,air}^2 \tag{A.5}$$

$$M_{z,aero} = \frac{l_0}{2} \cdot \rho_{air} \cdot A_x \cdot c_{M,z}(\beta_{air}) \cdot v_{x,air}^2 \tag{A.6}$$

Here,l_0 is defined as a reference length of the model, normally the wheelbase length, so that the coefficients c_{Mx},c_{My} and c_{Mz} remain non-dimensional.

The dependencies of the aerodynamic coefficients on the angle of incidence of the air are easily implemented as lookup tables on the Simulink environment. Nevertheless, gathering the necessary data for these tables is not always possible, so it is common to assume that the aerodynamic characteristics of the vehicle are symmetric around its X_vY_v plane and that the coefficients do not depend on the angle β, so that $c_{M,x} = c_{M,z} = 0$ is adopted, and that c_D, c_L, and $c_{M,y}$ are constants. Also, for the generation of the side force $F_{y,aero}$, it was assumed that $c_s = k \cdot \beta$, with k defined in the vehicle parameters, i.e., for a given speed, the side force generated by the aerodynamics is linearly proportional to the angle of incidence of the air.

On the present work's implementation, the outputs from the aerodynamic subsystem are the forces and torques $F_{i,aero}, M_{i,aero}$ with $i \in \{x, y, z\}$, which are applied on the vehicle body.

A.2 Brake System

The brake subsystem is modeled as a linear function that receives the brake pedal position and applies a braking torque to each of the wheels. The applied force is proportional to the maximum respective front or rear braking torques, which are input parameters of the model. Thus, considering the throttle/brake pedal position β_{pedals}, the braking torque to each of the wheels is given by:

$$T_{B,i} = \begin{cases} -\beta_{pedals} \cdot T_{B,i}^{max} & \text{if } 0 > \beta_{pedals} > -1, \\ 0 & \text{if } 0 < \beta_{pedals} < 1. \end{cases} \tag{A.7}$$

For i = {FL, FR, RL, RR}

The brake distribution of the vehicle is given by altering the relationship between the front and rear maximum brake torques.

A.3 Drivetrain

The Drivetrain is composed of four components: An internal combustion engine, a friction clutch, a manual gearbox, and a open differential. Their models are explained below.

A.3.1 Engine

The engine is modeled as a rotating lumped shaft with a mass moment of inertia J_E which is subject to the torque induced by the forces inside the cylinders $T_{E,ind}$; the torque T_{loss} consumed by the engine auxiliaries (air conditioning, alternator, oil pump, water pump, etc.) and by internal engine friction; and the torque transmitted from the clutch T_{clutch}. Therefore, the governing equation is given as:

$$J_E \cdot \dot{\omega}_E = T_{E,ind} - T_{clutch} - T_{loss} \tag{A.8}$$

To determine the engine torque, the model starts by determining the desired torque output. For that, it considers the value of the pedal position β_{pedals} as the desired fraction of the maximum engine power $P_{E,max}$. With that, and the current engine speed, it calculates the desired torque output. To determine if the required torque is feasible, the model compares it to the maximum engine performance data (given as a lookup table or a function) at the current engine speed. Then, the model assigns the minimum value between the desired and the available torque to the variable $T_{E,ind}$. Besides that, the power consumed by the engine auxiliaries is given as a constant input to the model P_{aux}.

It is worth noting that the subsystem only interpolates the desired engine power for $0 \leq \beta_{pedals} \leq 1$.

A.3.2 Clutch

The vehicle is considered to have a mass-less dry clutch. As such, it is modeled as having three states: engaged, slipping, and disengaged. In the engaged state, the angular velocities of the transmission input and the engine are considered equal. In the disengaged state, no torque is transmitted from the engine to the transmission, and their speeds are not coupled. In the slipping stage, the torque transfer between the engine and the transmission is modeled by the following equation:

$$T_{clutch} = T_{cl,0}(\beta_{clutch}) \cdot sign(\omega_E - \omega_{trans}) \tag{A.9}$$

Where $T_{cl,0}(\beta_{clutch})$ is a lookup table containing the slipping characteristics of the clutch for different clutch pedal positions.

A.3.3 Gearbox

The gearbox is modelled as having the transmission ratio i_{tr} of the selected gear, a gear mesh efficiency η_{tr}, a damping torque proportional to the output shaft's speed $T_{d,tr} = d_{tr} \cdot \omega_{tr,out}$ and mass moment of inertia J_{tr}. It receives the torque coming from the clutch T_{clutch}, its output shaft's speed and he selected gear, then it outputs the torque on the output shaft and the rotational speed of the clutch according to the equations:

$$T_{tr} = i_{tr} \cdot \eta_{tr} \cdot T_{tr,in} - \omega_{tr_out} \cdot d_{tr} - \dot{\omega}_{tr,out} \cdot J_{tr} \tag{A.10}$$

A.3.4 Differential

The model contains an open differential that, similarly to the gearbox, is modelled as having the final drive ratio i_{dif}, a gear mesh efficiency η_{dif}, a damping torque proportional to the average output shaft speed $T_{d,dif} = d_{diff} \cdot 0.5 * (\omega_{wheel,left} + \omega_{wheel,right})$ and mass moment of inertia J_{dif}.

The main characteristic of the open differential is that the torque delivered to each of the wheels is always equal. Therefore, the torque throughput to each driveshaft (left and right) is given by:

$$T_{w,i} = 0.5 * [i_{dif} \cdot \eta_{dif} \cdot T_{tr,out} - T_{d,dif} - 0.5 * (\dot{\omega}_{wheel,left} + \dot{\omega}_{wheel,right}) \cdot J_{dif}] \tag{A.11}$$

$$\text{Where} \begin{cases} i = \{FR, FL\}, & \text{if front wheel drive,} \\ i = \{RR, RL\}, & \text{if rear wheel drive.} \end{cases} \tag{A.12}$$

A.4 Steering

The steering system is modeled as a linear steering ratio i_{steer} between the steering wheel angle δ_{strwhl} and the front wheels steering angle δ_W so that:

$$\delta_W = \frac{\delta_{strwhl}}{i_{steer}} \tag{A.13}$$

A.5 Suspension

The suspension is modeled by extending the classic quarter car model to include the forces produced by the anti-roll bars and the anti-dive/anti-squat characteristics. Figure 48 shows the physical model used, consider that the mass m'_{body} is an abstraction of the vehicle chassis, to which the suspension is attached. In reality, the chassis is connected to all corners and couples their movement.

Figure 48 – Free body diagram of one corner of the vehicle

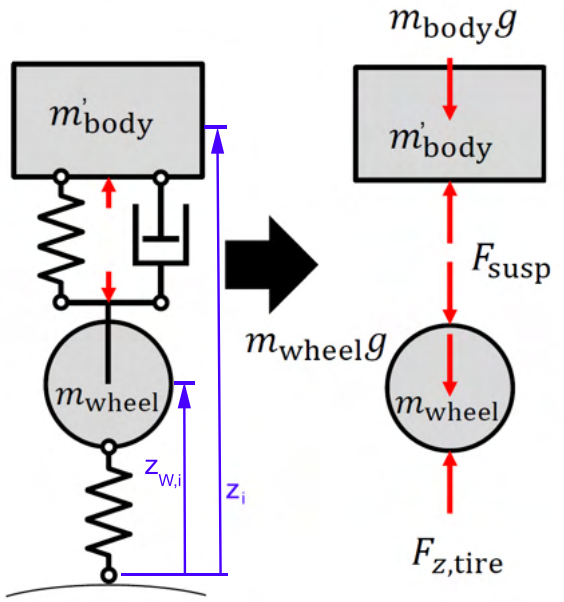

Source: adapted from 43.

The forces from Figure 6 are modelled as follows:

$$F_{susp} = F_{spring} + F_{damper} + F_{ARB,i} + F_{support} \tag{A.14}$$

$$F_{tire} = k_{tire} \cdot (r_{dyn} - z_{W,i}) \tag{A.15}$$

Where

$F_{spring} = k_{spring} \cdot (z_i - z_{W,i})$;
$F_{damper} = d_{damper} \cdot (\dot{z}_i - \dot{z}_{W,i})$;

And

z_i: the vertical displacement of the chassis' corner i;
$z_{W,i}$: the vertical displacement of the wheel i
r_{dyn}: the dynamic radius of the tire.

The forces due to the anti-roll bar $F_{ARB,i}$ and the anti-dive/anti-squat $F_{support,i}$ will be defined in sections subsection A.5.1 and subsection A.5.2.

A.5.1 Anti-roll bar

Figure 49 and the following illustrates both the kinematic relations and the forces created by the anti-roll bar (ARB).

Figure 49 – Kinematic relations of the ARB

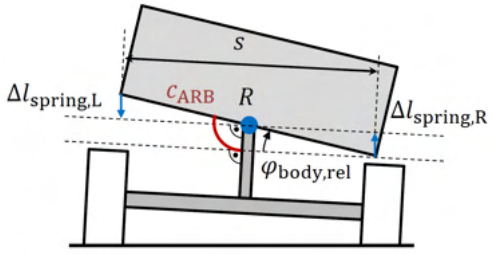

Source: 43.

Figure 50 – Forces created by the ARB

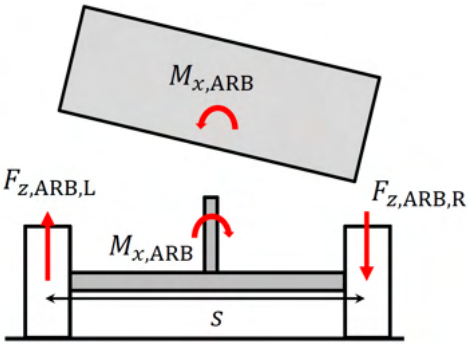

Source: 43.

From the images, it is possible to derive the following equations for the front or rear end :

$$F_{ARB} = \begin{cases} \frac{c_{ARB,axle} \cdot \phi_{body,rel}}{s}, & \text{if on the left side} \\ -\frac{c_{ARB,axle} \cdot \phi_{body,rel}}{s}, & \text{if on the right side} \end{cases} \tag{A.16}$$

Where

$$\phi_{body,rel} = \arctan\left(\frac{(z_{W,left} - z_{body,right}) - (z_{W,left} - z_{body,left})}{s}\right) \tag{A.17}$$

To obtain the force for the different ends of the vehicle (front and rear), the adequate variables z_W, z_{body} and $c_{ARB,axle}$ are used.

A.5.2 Support forces

By positioning the suspension components, such as control arms and linkages, in such a way that the suspension geometry resists compression during braking, anti-dive, anti-squat, or anti-roll characteristics are achieved. This means that a significant portion of the vertical force generated during braking, acceleration, and cornering is directed through the suspension components and not absorbed solely by compression. To consider these features, the combined effect of the forces between the vehicle chassis and its suspension must be considered. For that, the concept of the instant center of a suspension is used. It is defined as the virtual point around which the wheel's center point is rotating. When the instant center is positioned below the ground, the suspension components' geometry causes a force couple that has a vertical component, and depending on the position of the instant center above the ground, this vertical force can increase or decrease chassis roll or pitch movements.

The following sections explain the influence of the position of the instant center (considered fixed in the present thesis) on the "anti" characteristics of the vehicle. In all of them, this position is defined using support angles ϵ.

A.5.2.1 For the acceleration case

The Figure 51 illustrates the forces that act on the vehicle body when it is accelerating (for this part, a rear-wheel drive vehicle is considered).

Figure 51 – Free body diagram of the suspension components during an acceleration maneuver

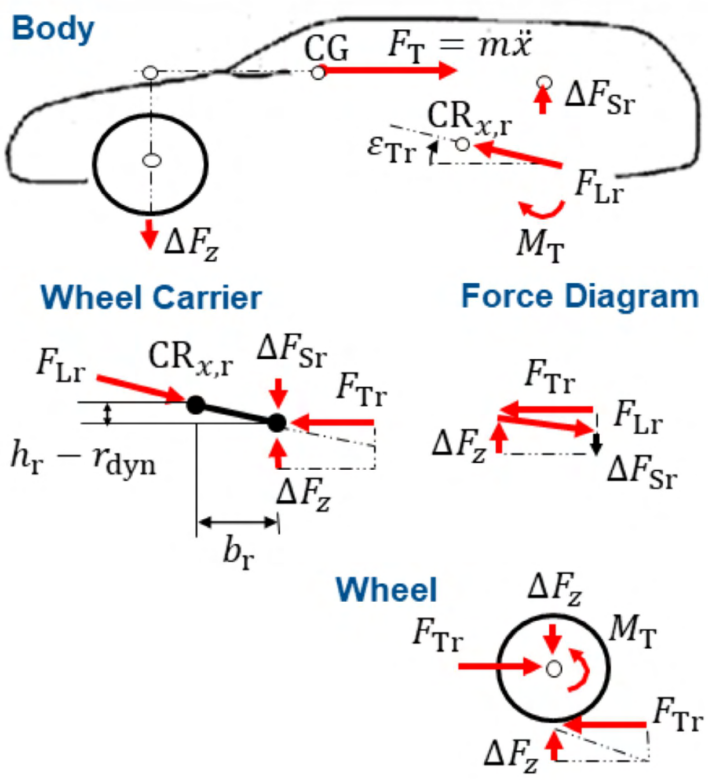

Source: [43]

After some mathematical deduction, it is possible to derive:

$$F_{support,acc} = F_{x,rear} \cdot tan(\epsilon_{tr}) \tag{A.18}$$

where $F_{x,rear}$ is the sum of the tractive forces generated by the rear tires and ϵ_{tr} the support angle as in Figure 51.

For the forward wheel drive vehicle, the angle $\epsilon_t r$ can also be defined, without loss of significance of the Equation A.18, when the coordinate system in which the angle is measured is maintained.

A.5.2.2 For the braking case

The Figure 52 illustrates the forces that act on the vehicle body when it is braking.

Figure 52 – Free body diagram of the suspension components during a braking maneuver

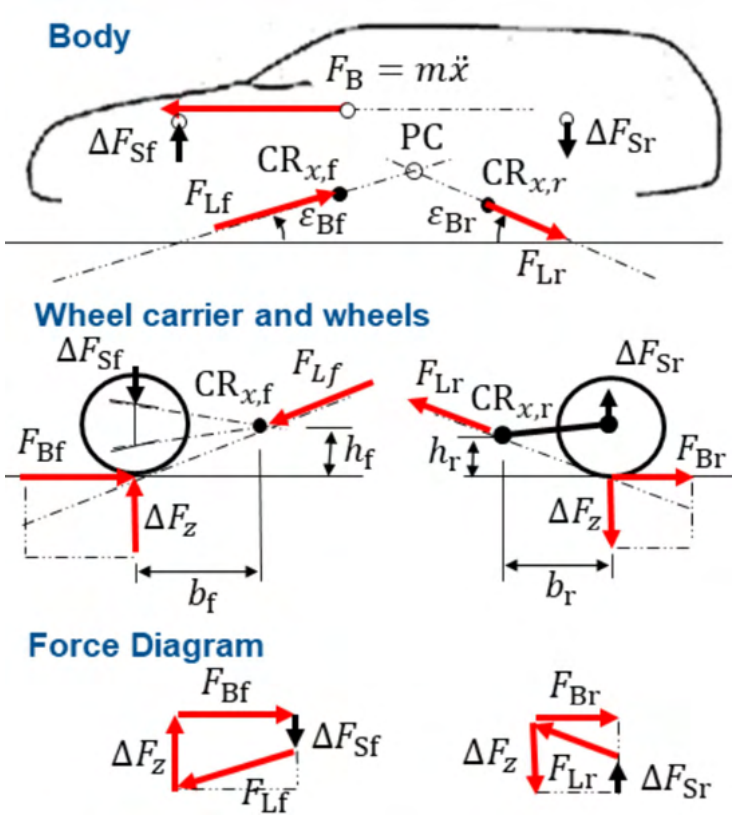

Source: [43]

After some mathematical deduction, it is possible to derive:

$$F_{support,brake} = F_{x,axle} \cdot \tan \epsilon_{br,axle} \tag{A.19}$$

where $F_{x,axle}$ is the sum of the braking forces generated by the tire and ϵ_{br} is the support angle as in Figure 52. Note that now all four wheels are exerting a longitudinal force on the vehicle.

A.5.2.3 For the cornering case

Finally, the support forces induced by lateral accelerations are given on Figure 53.

Figure 53 – Free body diagram of the suspension components during a cornering maneuver

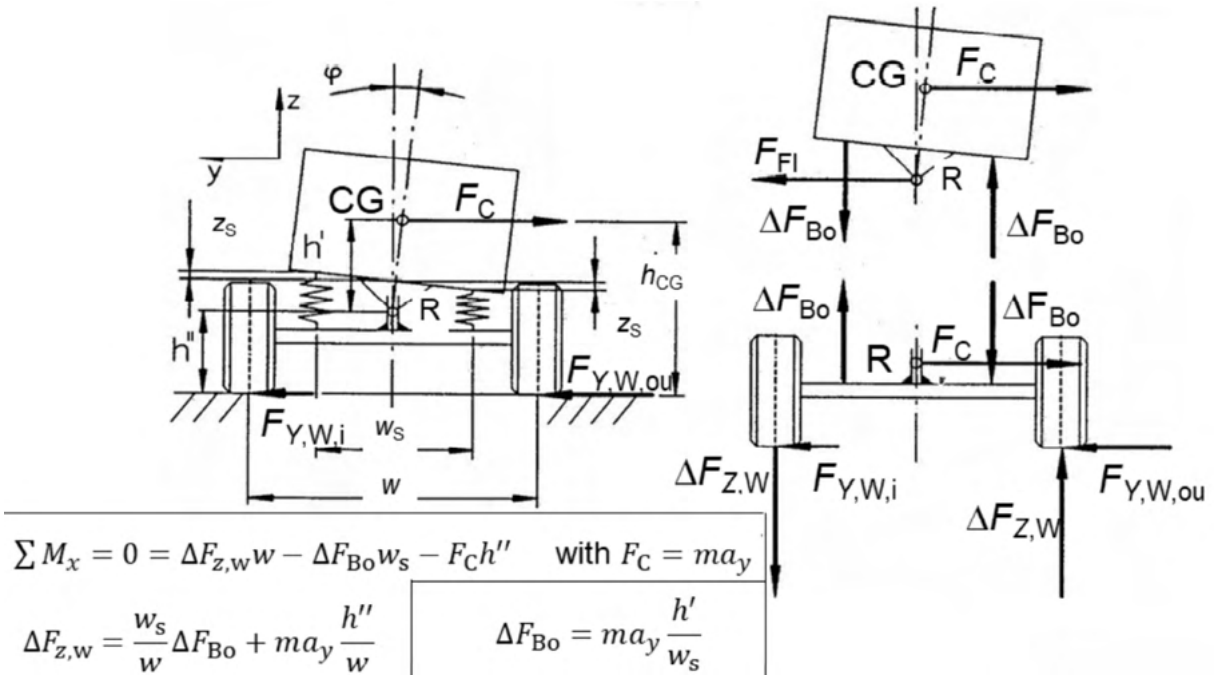

Source: [48]

It is now is possible to deduce the suspension force F_{susp} from Equation A.14 by substituting: $F_{support} = F_{support,acc} + F_{support,brake} + \Delta F_{Bo}$ on it.

A.6 Tire

The modelling used the approach introduced by 49, p. 172: the magic formula.

The following curve was used as an example of tire:

Figure 54 – Example tire curve

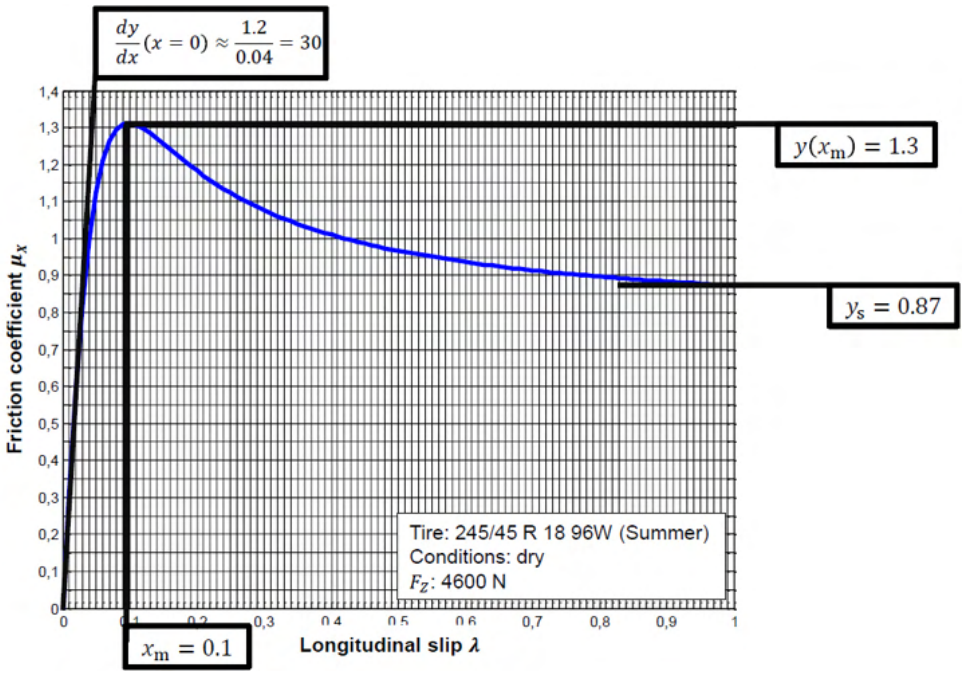

Source: 43

The values gathered from the graph were used to calculate the Magic Formula coefficients:

$$D = \mu(x_m) = 1.3 \tag{A.20}$$

$$C = 1 + \left(1 - \frac{2}{\pi} \arcsin \frac{\mu_s}{D}\right) \approx 1.533 \tag{A.21}$$

$$B = \left[\frac{d\mu}{dx}\Big|_{x=0}\right] / (C\,D) \approx 15.05 \tag{A.22}$$

$$E = \frac{B\,x_m - \tan\left(\frac{\pi}{2C}\right)}{B\,x_m - \arctan(B\,x_m)} \tag{A.23}$$

These values were then input to the equation of the effective force output from the tire:

$$F_{eff} = F_{W,z} \cdot D \sin\left[C \arctan\{Bx - E(Bx - \arctan Bx)\}\right] \tag{A.24}$$

Then, the longitudinal and lateral forces generated by the tire were defined by:

$$F_x = \cos(\alpha_{eff}) \cdot F_{eff} F_y = \sin(\alpha_{eff}) \cdot F_{eff} \tag{A.25}$$

Where

$$\alpha_{eff} = \arctan\left(\frac{\sin\left(\alpha + \frac{c_\gamma}{c_\lambda}\right)}{\frac{\omega_{rot,W}\, r_{dyn} - v_{x,W}}{\max(v_{rot,W}, v, 0.001))}}\right) \tag{A.26}$$

APPENDIX B – LAP TIME SIMULATION FOR VARIOUS CIRCUITS

This appendix presents a comprehensive analysis of the performance of various Formula Student configurations on different circuits.[1] Two key configuration variations were examined:

Aerodynamic Package: The first variation explored the impact of an aerodynamic package on the vehicle's performance. Three setups were evaluated:

a) Without an aerodynamic package

b) With an aerodynamic package set to maximum downforce

c) With an aerodynamic package set to minimum drag

Table 9 – Vehicle configurations

Parameter	Config 1	Config 2	Config 3
Lift coefficient, c_L	0.2	-2.6	-1.7
Drag Coefficient, c_D	0.7	1.46	0.85
Vehicle mass $m_{vehicle}$	266.5 kg	275 kg	275 kg

Source: Created by the author.

Note: The table shows the parameters involved in each configuration. The added mass of the aerodynamic package is considered in the analysis.

The lap times obtained were the following:

Table 10 – Lap times for different aerodynamic packages

Lap times for different aerodynamic packages			
	Config 1	**Config 2**	**Config 3**
Zandvoort	62.693 s	61.135 s	61.423
Spielberg	57.194 s	56.885 s	56.093 s
Interlagos	55.758 s	55.007 s	54.264 s
Hockenheim	59.268 s	58.279 s	57.565 s

Source: Created by the author.

Vehicle Mass: The second variation focused on the effect of 10 kg of added or removed weight on lap times. This comparison aimed to determine whether the development and integration of a new component would yield advantageous results, even though it adds weight to the vehicle. Three setups were evaluated:

[1] Note: all circuits were scaled to 30% of the original size

a) Lighter configuration: vehicle mass of 265 kg

b) Lighter configuration: vehicle mass of 275 kg

c) Lighter configuration: vehicle mass of 285 kg

The lap times obtained were the following:

Table 11 – Lap times for different aerodynamic packages

Lap times for different vehicle masses			
	m = 265 kg	**m = 275 kg**	**m = 285 kg**
Zandvoort	57.516 s	57.832 s	58.142 s
Spielberg	53.285 s	53.660 s	53.976 s
Interlagos	54.739 s	55.061 s	55.277 s
Hockenheim	57.965 s	58.295 s	58.569 s

Source: Created by the author.

B.1 Circuit of Zandvoort

B.1.1 Evaluation of the effect of the mass variation

Figure 55 – Trajectory comparison - Zandvoort Circuit

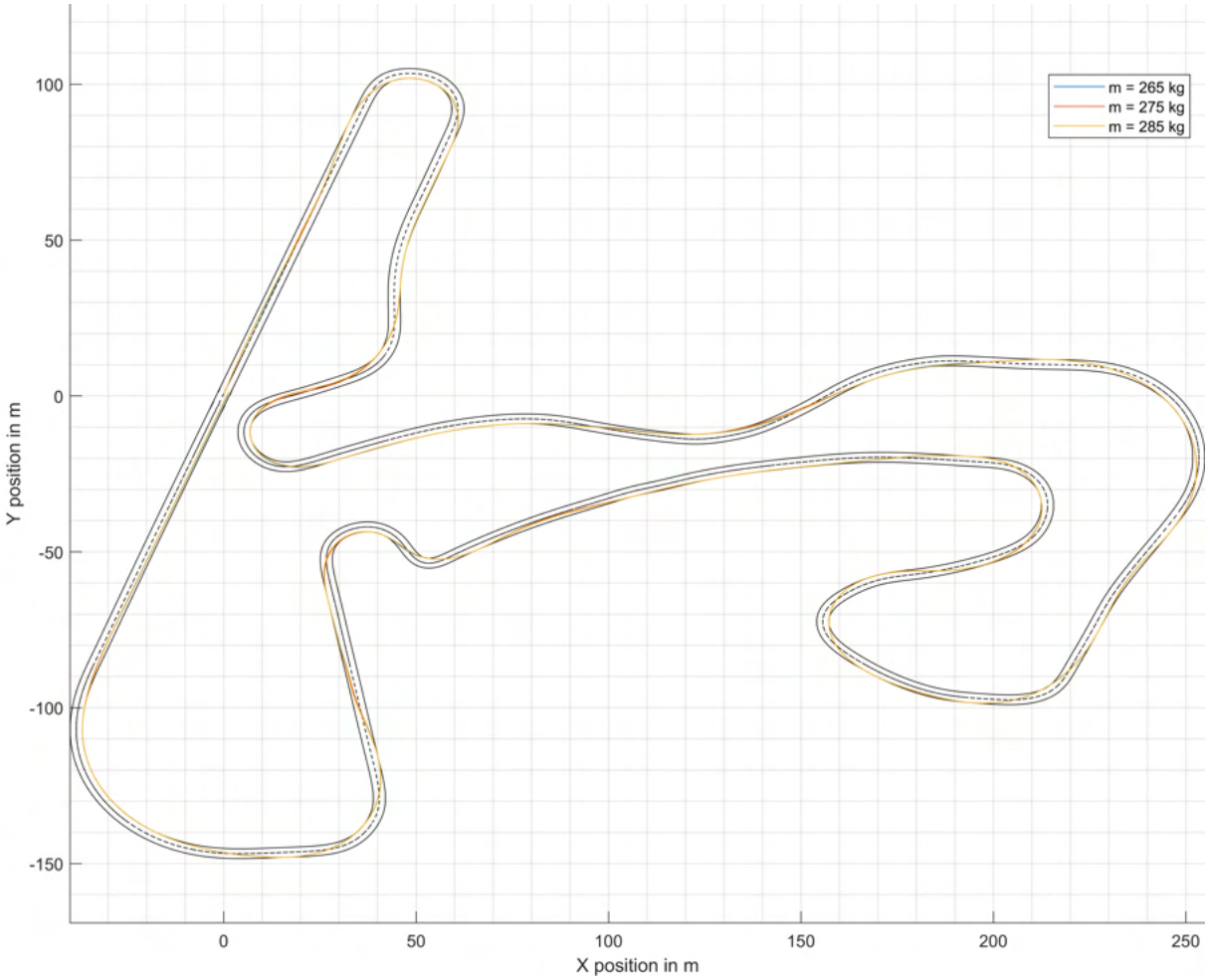

Source: Created by the author.

Figure 56 – Speed profile comparison - Zandvoort Circuit

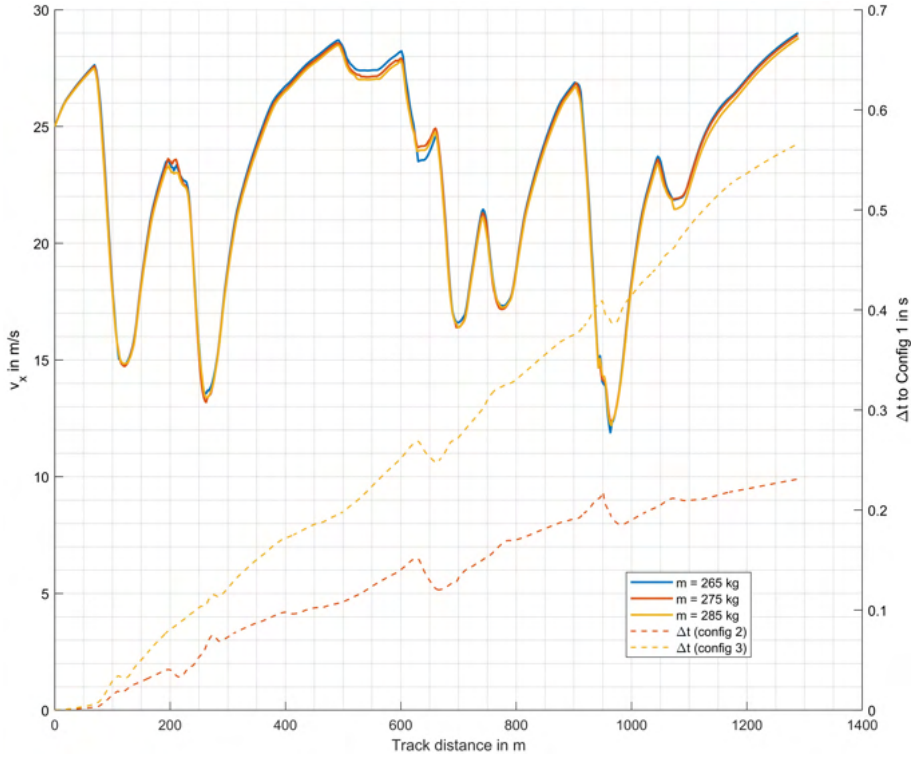

Source: Created by the author

Figure 57 – Acceleration profile comparison - Zandvoort Circuit

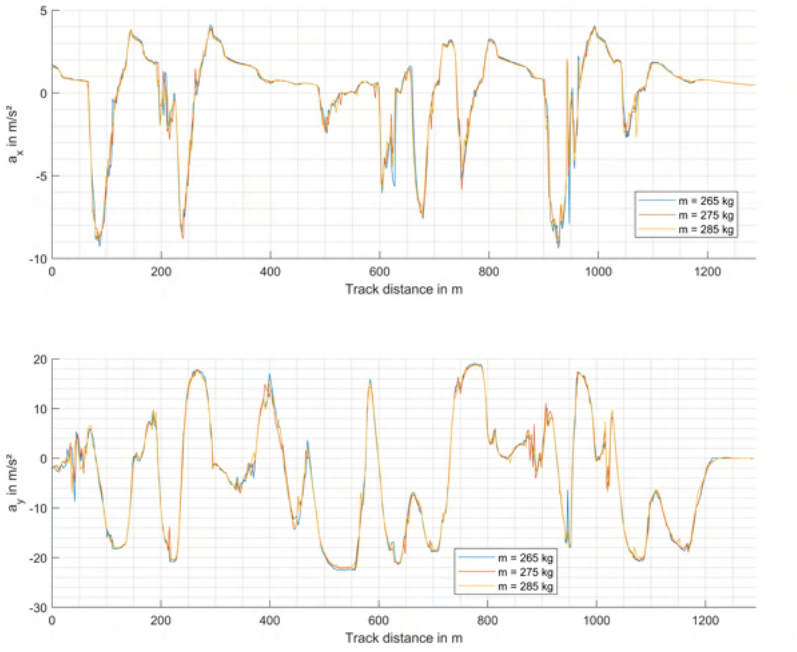

Source: Created by the author

Figure 58 – 3D speed visualization - Zandvoort Circuit

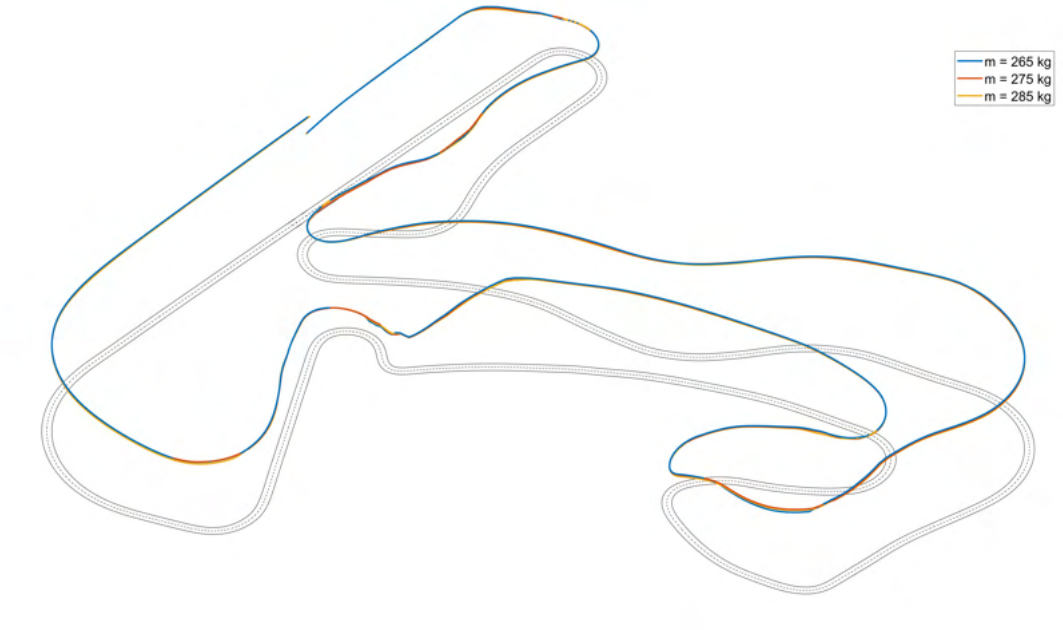

Source: Created by the author

Note: The track layout is presented in gray, in 2D. The higher the curve, the faster the vehicle was at that point of the circuit

B.2 Circuit of Spielberg

B.2.1 Evaluation of the effect of the mass variation

Figure 59 – Trajectory comparison - Spielberg Circuit

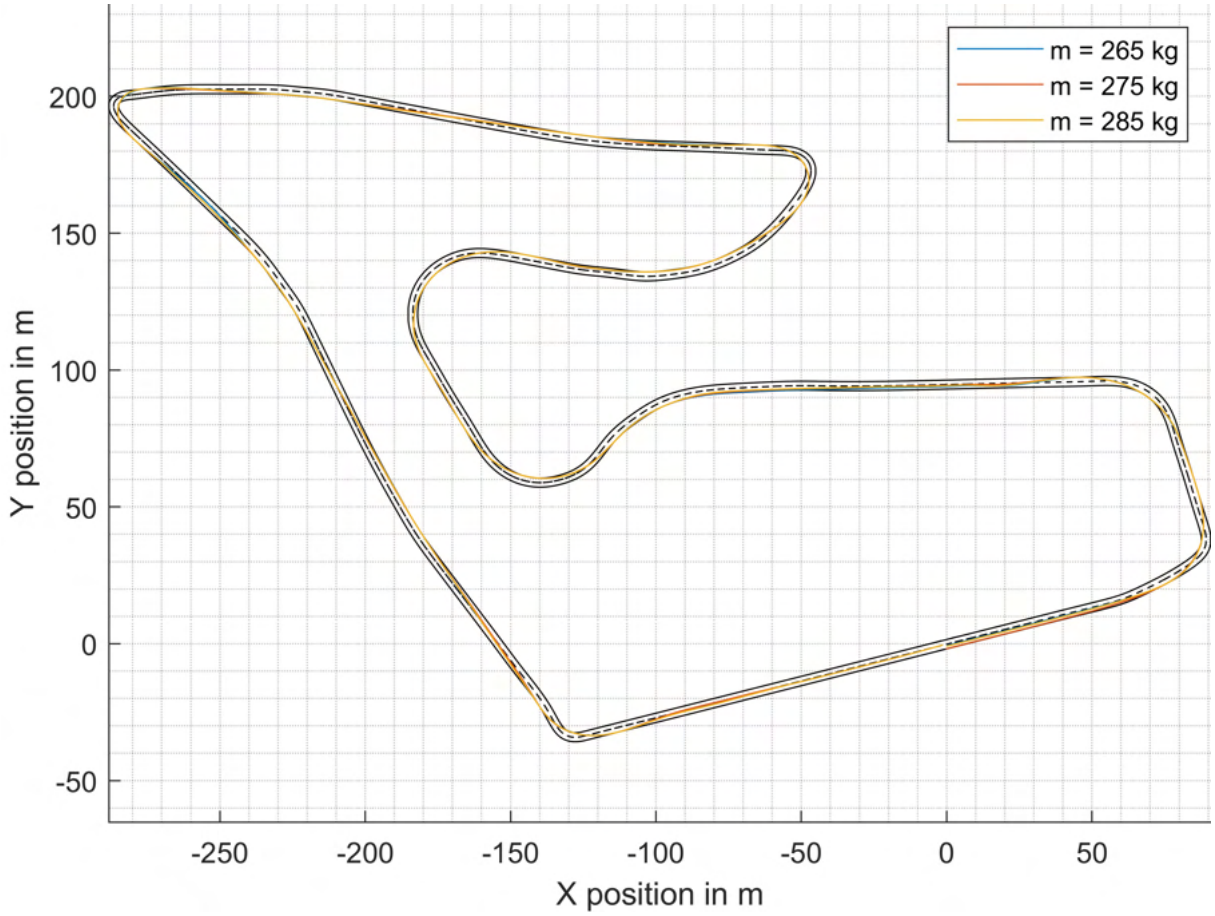

Source: Created by the author.

Figure 60 – Speed profile comparison - Spielberg Circuit

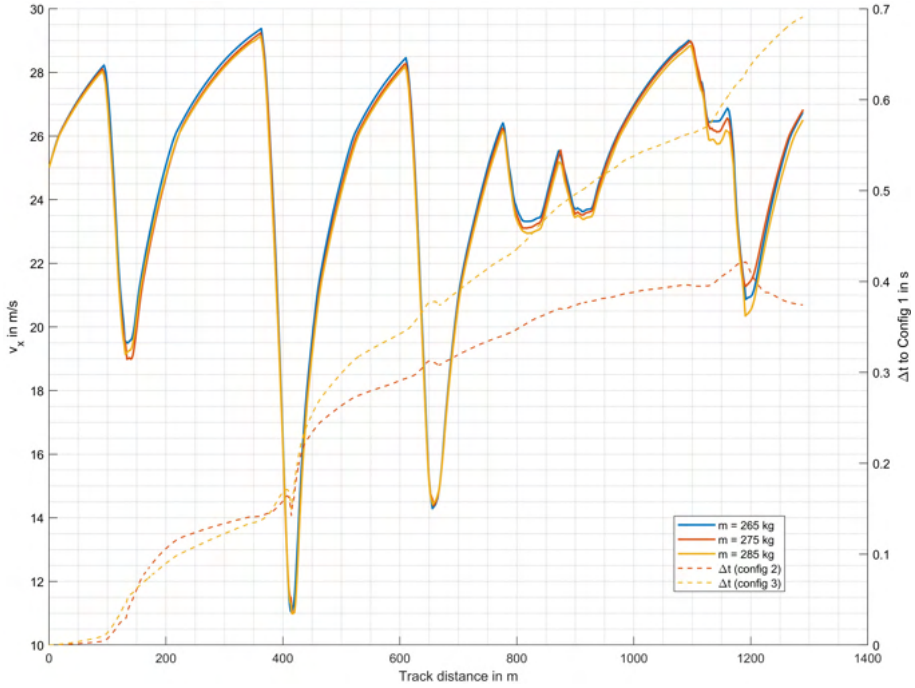

Source: Created by the author

Figure 61 – Acceleration profile comparison - Spielberg Circuit

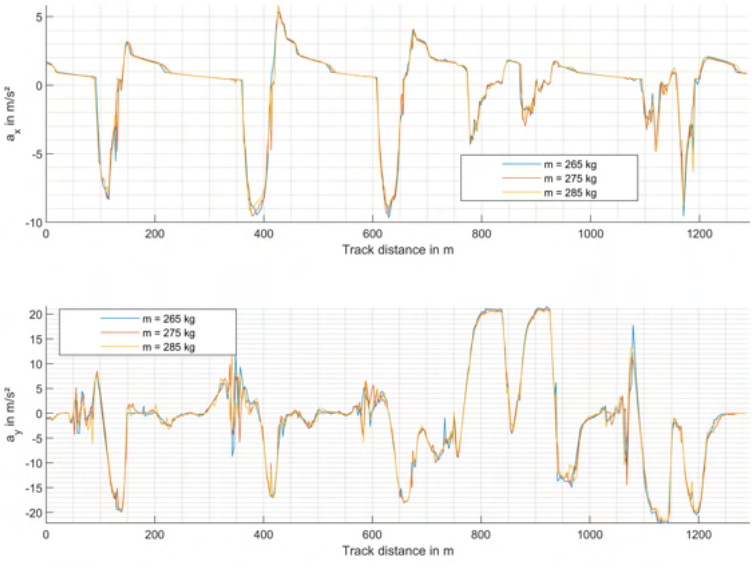

Source: Created by the author

Figure 62 – 3D speed visualization - Spielberg Circuit

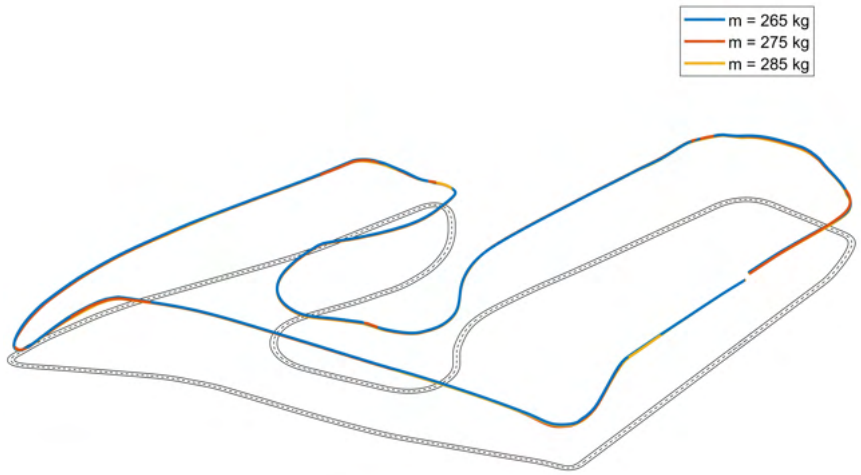

Source: Created by the author

Note: The track layout is presented in gray, in 2D. The higher the curve, the faster the vehicle was at that point of the circuit

B.3 Circuit of São Paulo - Interlagos

B.3.1 Evaluation of the effect of the aerodynamic package - Interlagos Circuit

Figure 63 – Trajectory comparison - Interlagos Circuit

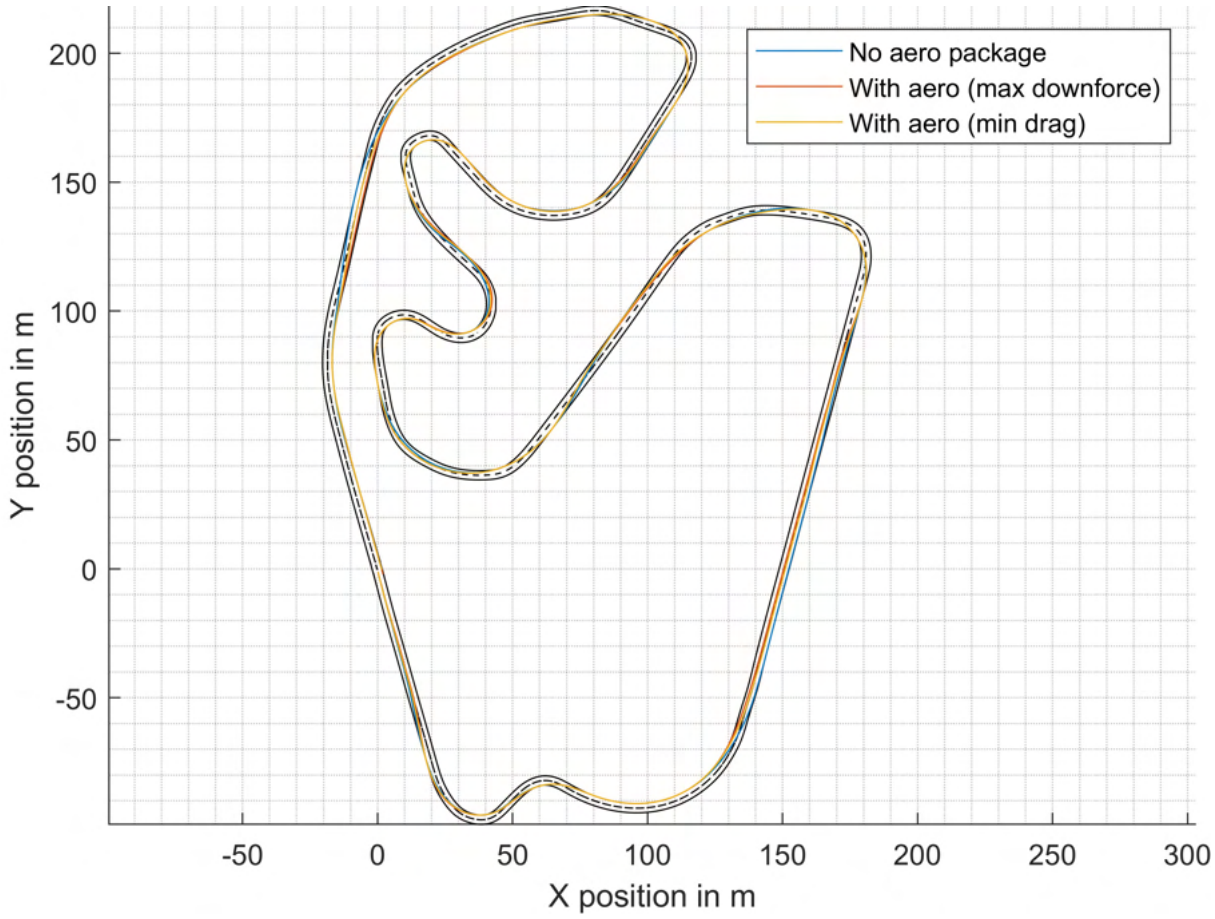

Source: Created by the author.

Figure 64 – Speed profile comparison - Interlagos Circuit

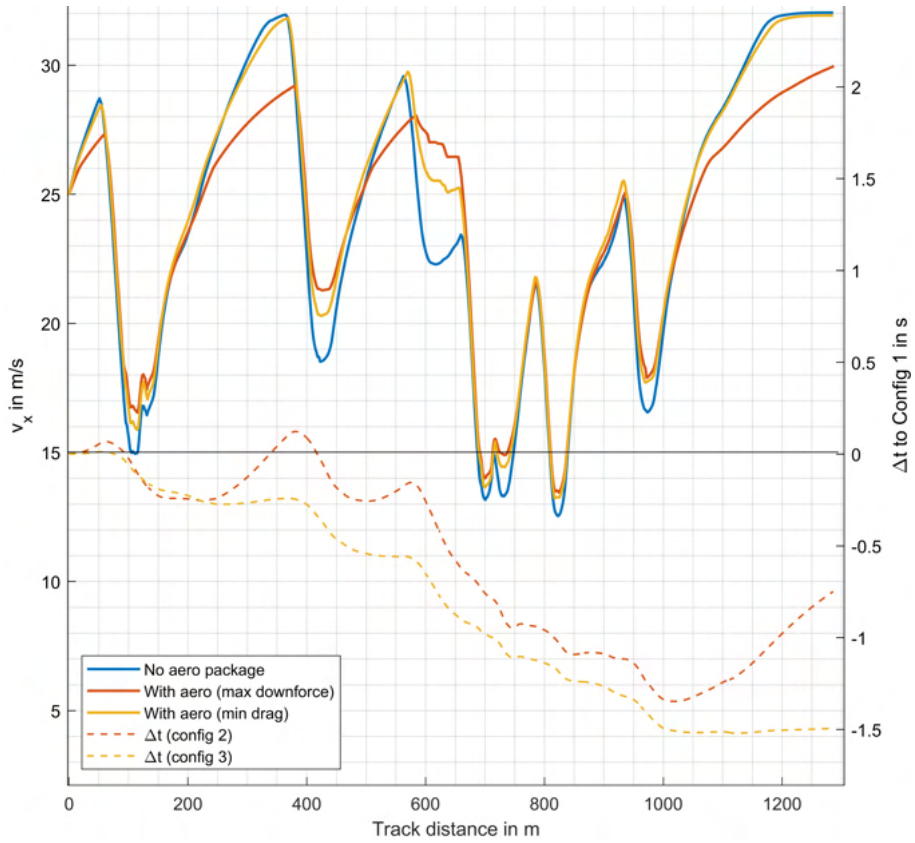

Source: Created by the author

Figure 65 – Acceleration profile comparison - Interlagos Circuit

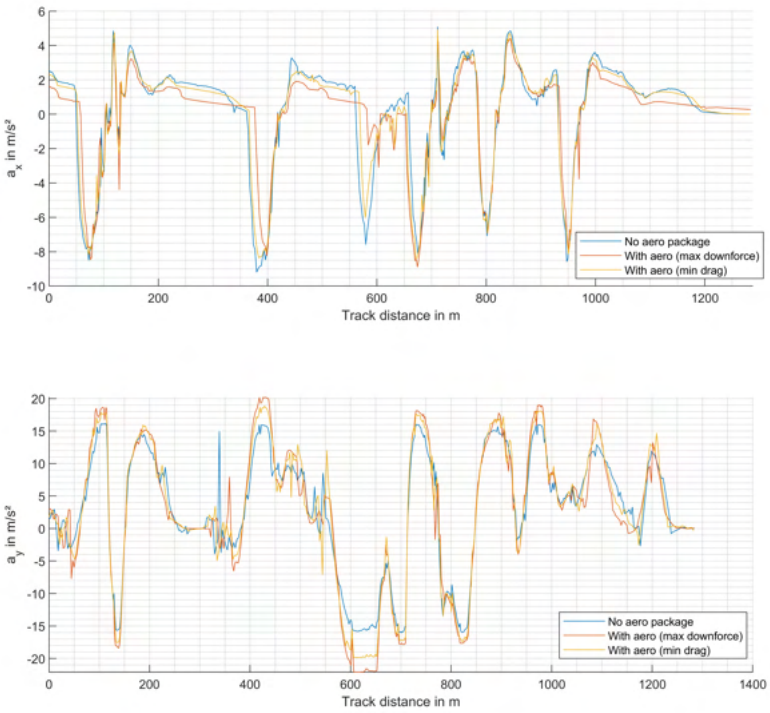

Source: Created by the author

Figure 66 – 3D speed visualization - Interlagos Circuit

Source: Created by the author

Note: The track layout is presented in gray, in 2D. The higher the curve, the faster the vehicle was at that point of the circuit

B.3.2 Evaluation of the effect of the mass variation - Interlagos Circuit

Figure 67 – Trajectory comparison - Interlagos Circuit

Source: Created by the author.

Figure 68 – Speed profile comparison - Interlagos Circuit

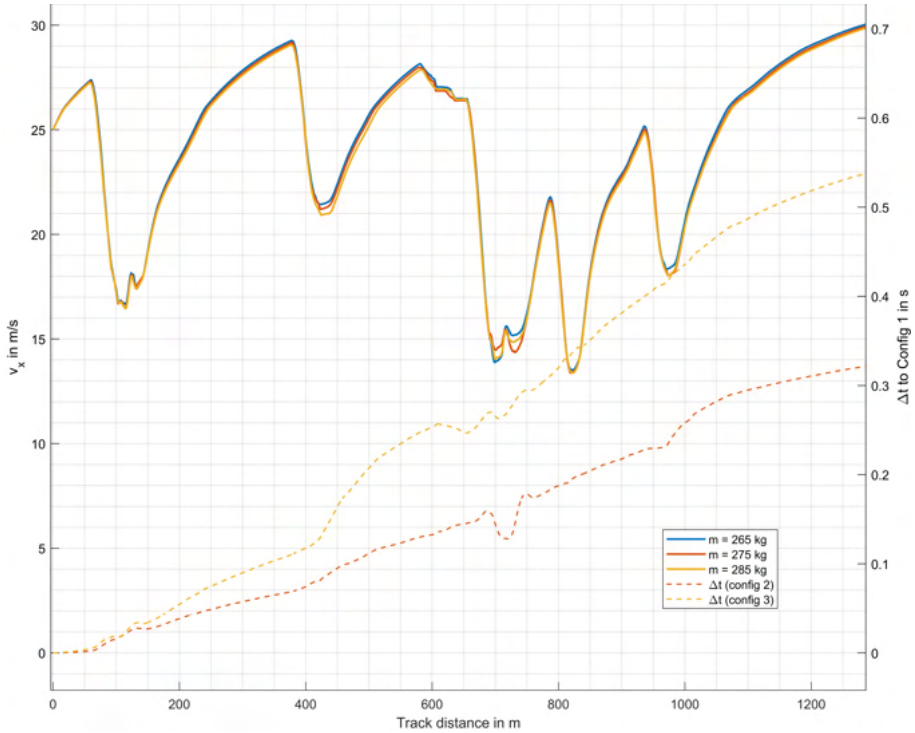

Source: Created by the author

Figure 69 – Acceleration profile comparison - Interlagos Circuit

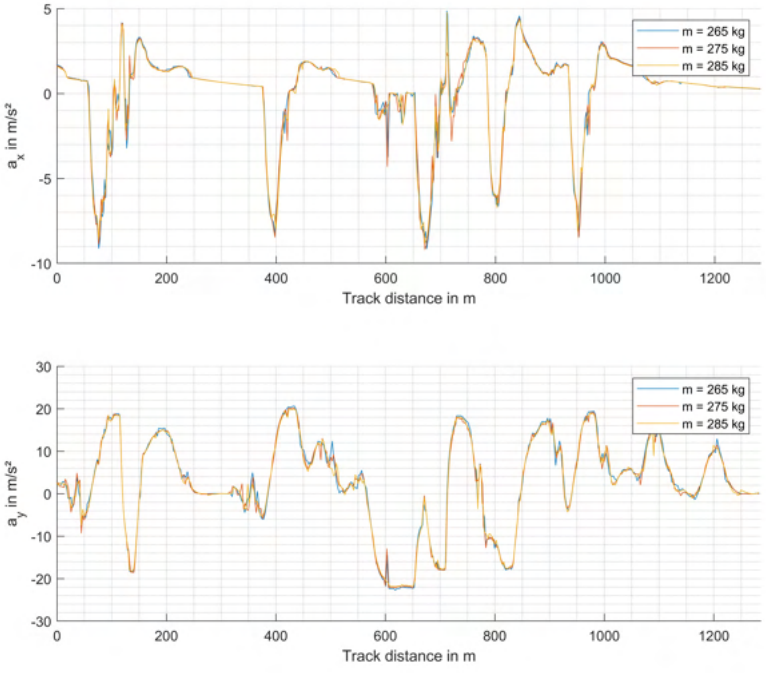

Source: Created by the author

Figure 70 – 3D speed visualization - Interlagos Circuit

Source: Created by the author

Note: The track layout is presented in gray, in 2D. The higher the curve, the faster the vehicle was at that point of the circuit

B.4 Circuit of Hockenheim

B.4.1 Evaluation of the effect of the aerodynamic package - Hockenheim Circuit

Figure 71 – Trajectory comparison - Hockenheim Circuit

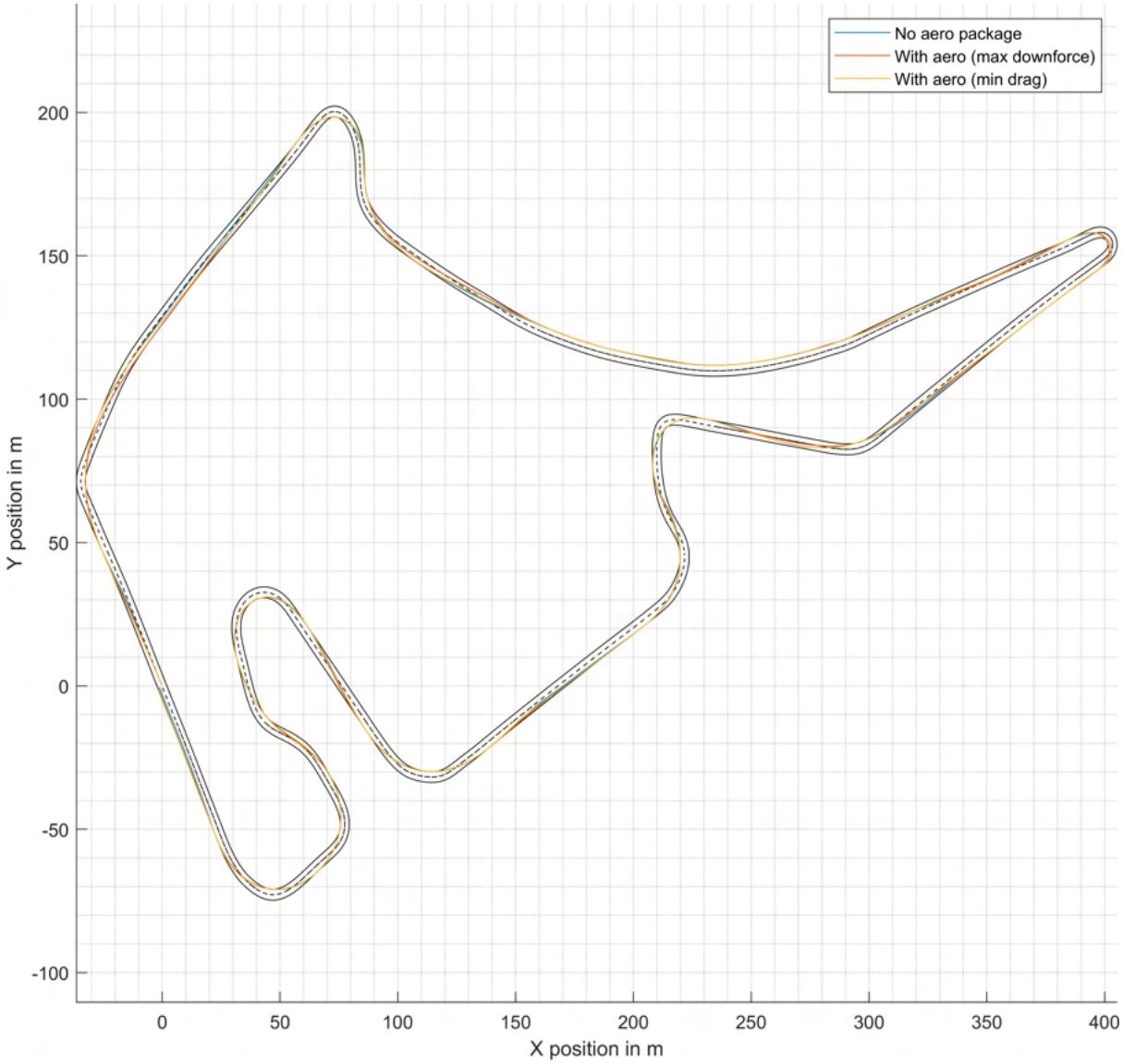

Source: Created by the author.

Figure 72 – Speed profile comparison - Hockenheim Circuit

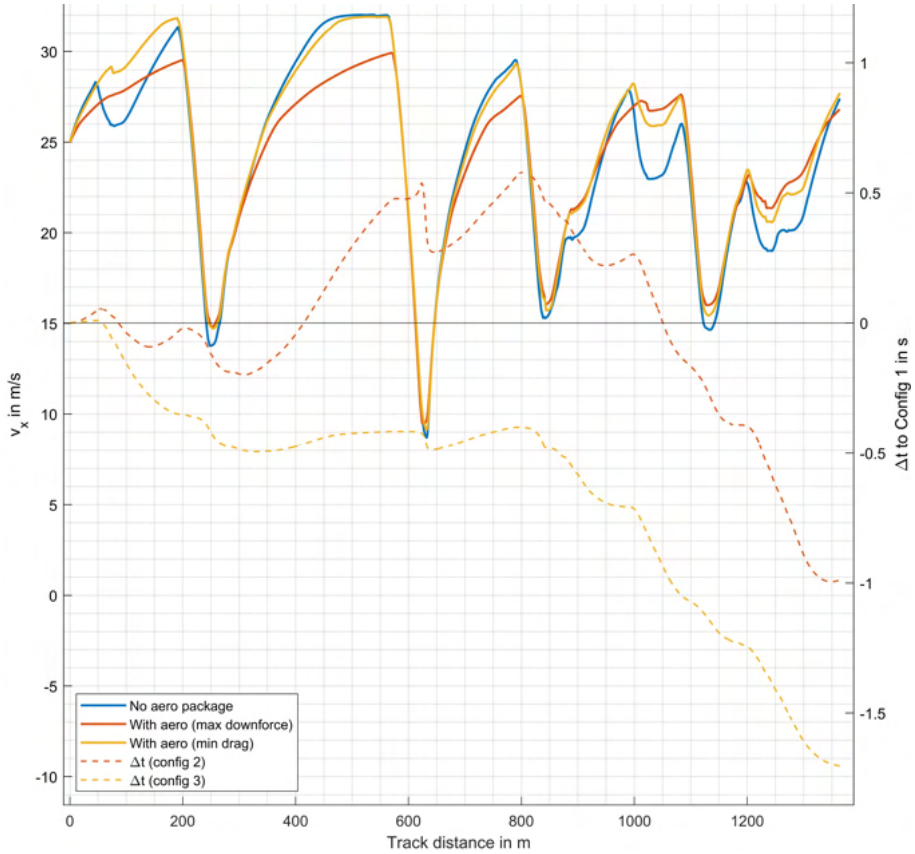

Source: Created by the author

Figure 73 – Acceleration profile comparison - Hockenheim Circuit

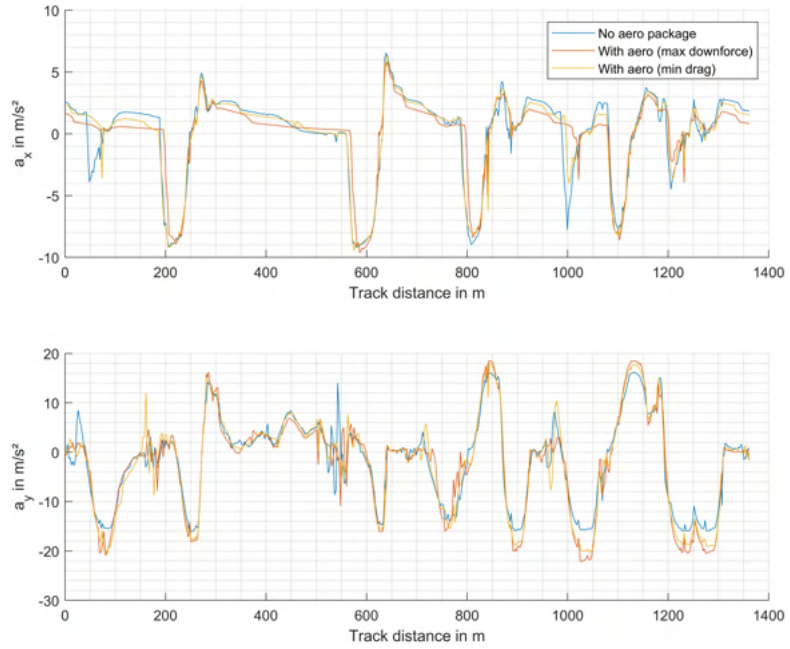

Source: Created by the author

Figure 74 – 3D speed visualization - Hockenheim Circuit

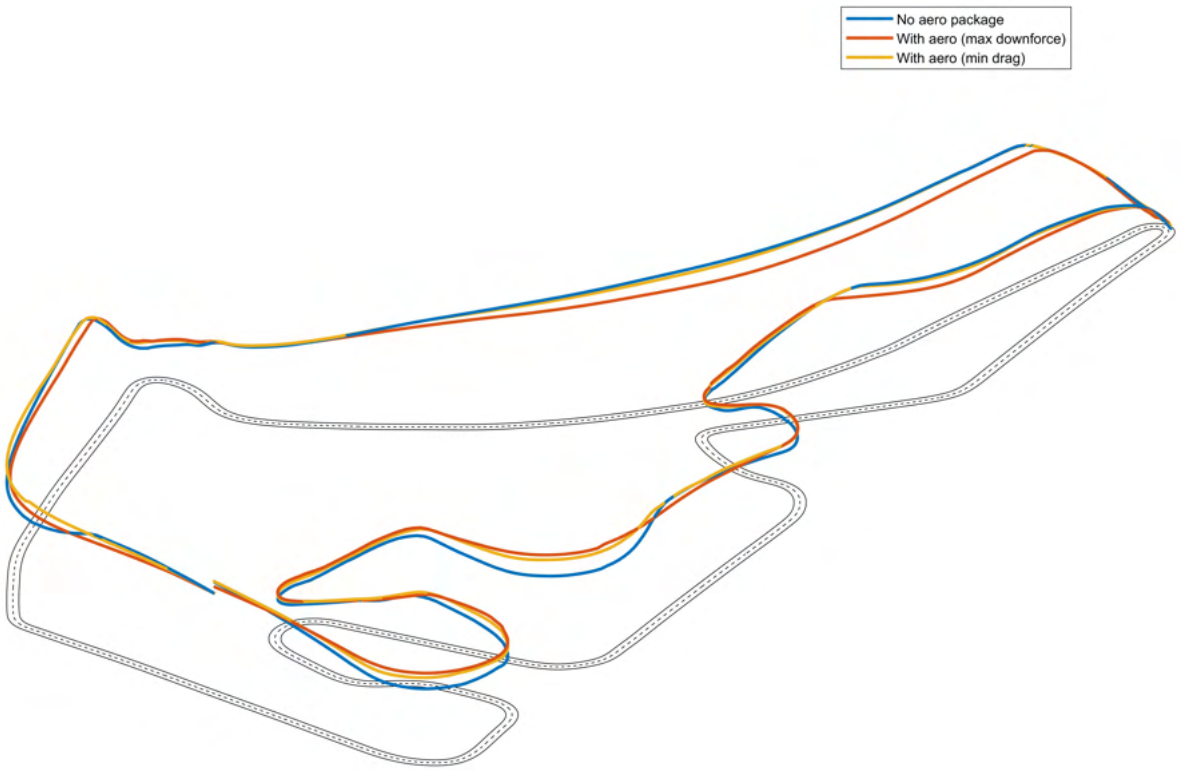

Source: Created by the author

Note: The track layout is presented in gray, in 2D. The higher the curve, the faster the vehicle was at that point of the circuit

B.4.2 Evaluation of the effect of the mass variation - Hockenheim Circuit

Figure 75 – Trajectory comparison - Hockenheim Circuit

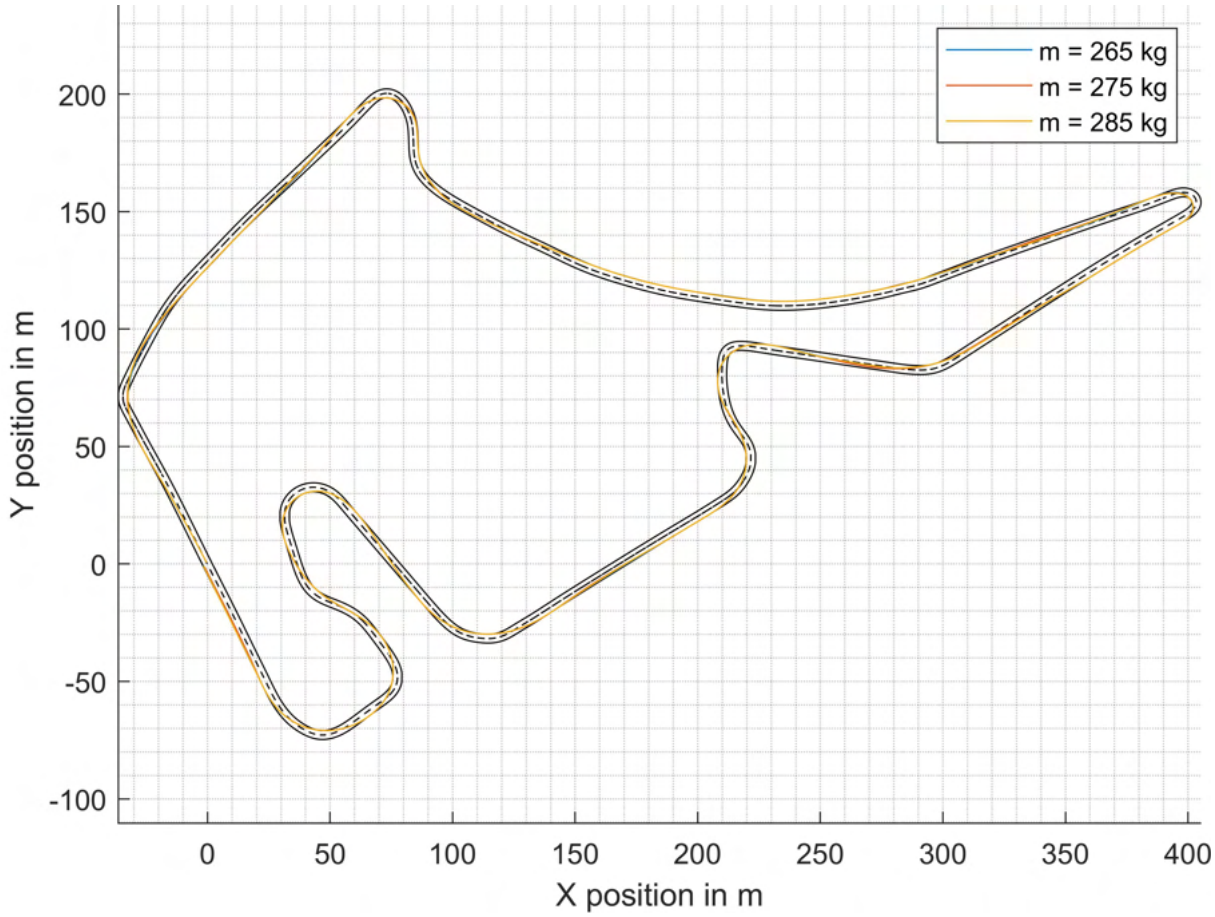

Source: Created by the author.

Figure 76 – Speed profile comparison - Hockenheim Circuit

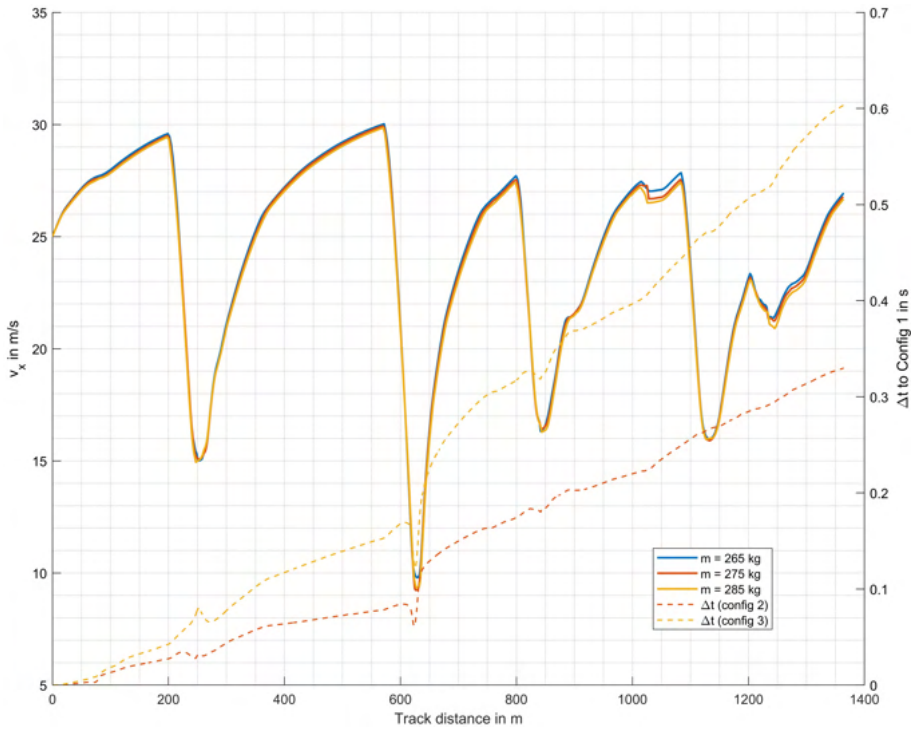

Source: Created by the author

Figure 77 – Acceleration profile comparison - Hockenheim Circuit

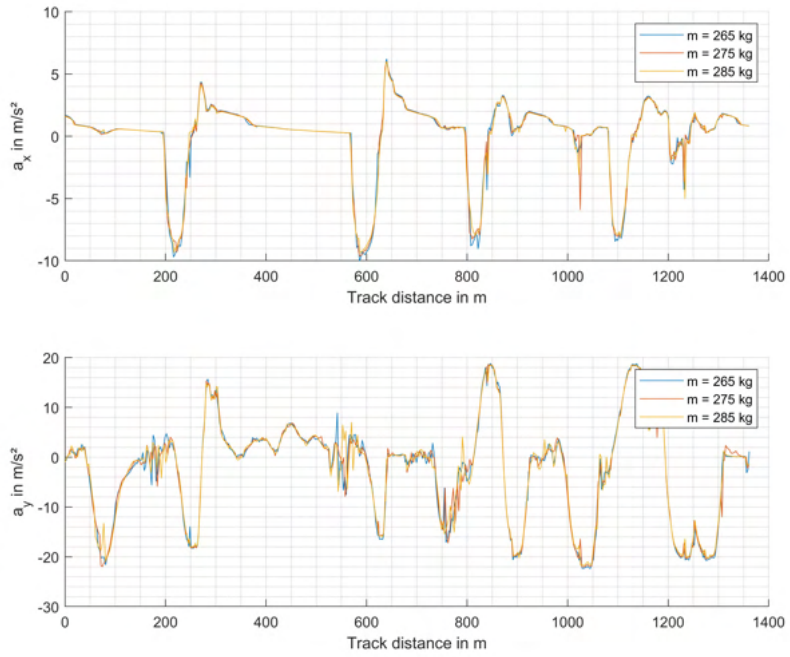

Source: Created by the author

Figure 78 – 3D speed visualization - Hockenheim Circuit

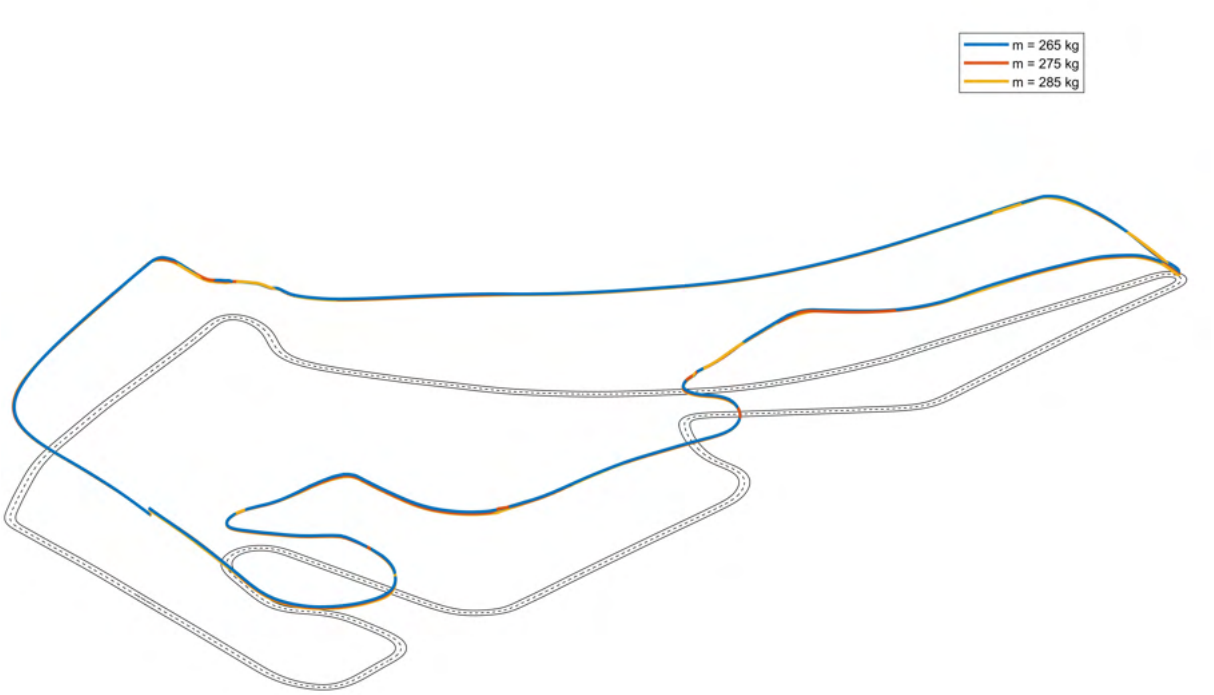

Source: Created by the author

Note: The track layout is presented in gray, in 2D. The higher the curve, the faster the vehicle was at that point of the circuit